On the Design of Optimal Noise Matching Networks for a Class of Multi-Mode Antennas

by

Raven Jon Kenned

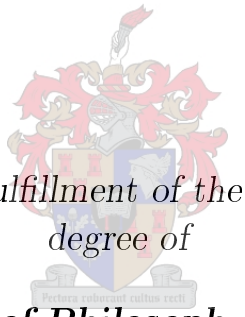

Thesis presented in fulfillment of the requirements for the degree of

Doctor of Philosophy (PhD)

in the Faculty of Engineering at Stellenbosch University

Supervisor: Prof P. Meyer

December 2019

The financial assistance of the National Research Foundation (NRF) towards this research is hereby acknowledged. Opinions expressed and conclusions arrived at, are those of the author and are not necessarily to be attributed to the NRF.

Declaration

By submitting this dissertation electronically, I declare that the entirety of the work contained therein is my own, original work, that I am the sole author thereof (save to the extent explicitly otherwise stated), that reproduction and publication thereof by Stellenbosch University will not infringe any third party rights and that I have not previously in its entirety or in part submitted it for obtaining any qualification.

Date: ..... December 2019 .....

Abstract

On the Design of Optimal Noise Matching Networks for a Class of Multi-Mode Antennas

R. J. Kenned

Department of Electrical and Electronic Engineering,
University of Stellenbosch,
Private Box X1, Matieland 7602.

Dissertation: PhD

December 2019

In modern times, Multiple-Input-Multiple-Output (MIMO and Multiple-Input-Single-Output (MISO receivers have commonly been implemented using coupled antenna arrays. This holds many advantages, including but not limited to, increased channel capacity, decreased mechanical size and weight, ease of operation and maintenance and reduced cost. A large body of theory exists on the properties and effects of mutually coupled radiating structures and the differences exhibited compared to single radiating structures.

This project investigates the use of impedance matching to achieve improvements in the output Signal-to-Noise Ratio of such coupled antenna arrays as they are scanned over angle. As an array is scanned over angle, the optimal source impedance for noise matching will vary. This project defines an approximation method for the varying optimal impedance, chooses fixed points either based on the varying impedance or coverage of the surface area of the Smith chart, and considers previously presented methods in literature for optimum impedance selection. The calculated performance is then numerically optimized. The methods are applied to a novel Quad Mode Antenna as well as a standard Four Monopole Array as control, so that conclusions on the SNR improvement ability of the Quad Mode Antenna can be drawn.

In order to perform the approximation and numerical optimization, refinements to the theoretical models available in literature were made and a software based model constructed in MATLAB. A simulated model in ADS was also made to serve as confirmation of the values calculated by the refined

model. The models are seen to agree with each other.

The degree of similarity of receiver responses over implementation criteria for a given antenna array is quantitatively and qualitatively discussed at the hands of the Structural Similarity Index, an image processing technique. Secondary considerations for the selection of a matching criteria is discussed. Conclusions on the degree to which the Quad Mode Antenna lends itself to SNR improvement are drawn at the hand of the comparative improvements in the Four Monopole Array. Conclusions on the improvement of output SNR through the proposed methods are also drawn and discussed subject to the two cases for which the methods were implemented.

Uittreksel

Aangaande die Ontwerp van Optimale Ruis Aanpassingsnetwerke vir 'n Klas van Multi-Modus Antennas

("On the Design of Optimal Noise Matching Networks for a Class of Multi-Mode Antennas")

R. J. Kenned

Department van Elektriese en Elektroniese Ingenieurswese,
Universiteit van Stellenbosch,
Privaatsak X1, Matieland 7602.

Proefskrif: PhD

Desember 2019

In moderne tye word MIMO en MISO ontvangers alom deur gekoppelde antenna samestellings geimplementeer. Hierdie implementasie behels verskeie voordele, insluitend verhoogde kanaal kapasiteit, verlaagde megansiese grootte en gewig, maklikheid van operasie en onderhoud en verlaagde koste. 'n Beduidende hoeveelheid teorie bestaan aangaande die eienskappe en effek van wedersyds gekoppelde stralende strukture en die verskille wat dit toon teenoor enkelstaande stralende strukture.

Hierdie projek ondersoek die gebruik van impedansie aanpassing om verbetering van die uittree Sein-tot-Ruis verhouding van sulke gekoppelde antenna samestellings te bereik, soos dit oor hoek geskandeer word. Soos die samestelling oor hoek geskandeer word sal die optimale bronimpedansie vir ruis aanpassing varieer. Hierdie projek definieer 'n benaderingsmetode vir die varierende optimale impedansie, kies vaste punte eerder gebasseer op die varierende impedansie of dekking van die oppervlakarea van die Smithkaart en oorweeg voorheen voorgestelde metodes in literatuur vir optimale impedansie seleksie. Die berekende gedrag word dan numeries geoptimiseer. Die metodes word toegepas op 'n nuwe "Quad Mode Antenna" sowel as 'n standaard "Four Monopole Array" as kontrole, sodat gevolgtrekkings oor die SNR verbeteringsvermo'e van die "Quad Mode Antenna" getrek kan word.

In orde om die benadering en numeriese optimisering uit te voer was verfynings aan die beskikbare teoreties modelle bygebring en ‘n sagtewaremodel in MATLAB geskep. ‘n Gesimuleerde model was ook in ADS geskep om as bevestiging te dien vir die waardes bereken deur die verfynde model. Die modelle word gesien om ooreen te stem met mekaar.

Die graad van eendersheid tussen die ontvanger response oor implementasie kriteria vir ‘n gegewe antenna samestelling word kwantitatief en kwalitatief bespreek aan die hand van die “Structural Similarity Index”, ‘n beeldprosesseringstegniek. Sekondêre oorwegings vir die seleksie van aanpassingskriteria word bespreek. Gevolgtrekkings aangaande die graad waartoe die “Quad Mode Antenna” dit self aan SNR verbetering toeleen word getrek aan die hand van ooreenstemmende verbeteringe vir die “Four Monopole Array”. Gevolgtrekkings aangaande die verbetering van uittree SNR deur die voorgestelde metodes word ook getrek en bespeek, onderhewig aan die twee gevalle waarop die metodes geimplementeer is.

Acknowledgements

I would like to express my sincere gratitude to the following people and organisations:

- To God, who carried me through it all
- The NRF, for the financial assistance
- SAAB Grintek Defence, who waited patiently for me to do a full time postgradute degree
- Professor Petrie Meyer, my supervisor who assisted, encouraged and supported me so much
- The lecturers of the Electric and Electronic Engineering department of the University of Stellenbosch, who were always willing to help and share knowledge
- My Stellenbosch University Radar Lab labmates, who were patient and welcoming and supportive at all times
- My family, for being there for me and loving me unconditionally
- Peter-Luke Benson, who took me into his home when I was finishing the writing of this thesis
- Brandt Klopper, for many afternoons of discussions on ideas and problems
- Keshav Sewraj, who made sure I got out of the radar lab every now and then

Dedications

This dissertation is dedicated to my mother, who believed in me until her dying day, and my father, who was always there supporting me

Contents

List of Figures

List of Tables

Nomenclature

Constants

$k_B = 1.38064852 \times 10^{-3}\,m^2kg/s^2K$
$\varepsilon_0 = 8.85418787 \times 10^{-12}\,F/m$
$\mu_0 = 4\pi \times 10^{-7}\,H$
$c_0 = 2.99792458 \times 10^{8}\,m/s$

Variables

ε_r	Relative permittivity	[ ]
μ_r	Relative permeability	[ ]
ω	Angular frequency	[rad/s]
f	Temporal frequency	[Hz]
θ	Elevation scan angle	[deg]
ϕ	Azimuth scan angle	[deg]
Z	Impedance	[Ω]
Y	Admittance	[S]
V	Electric potential difference	[V]
I	Electric current strength	[A]
P	Electric signal power	[W]
SNR	Signal to Noise Ratio	[ ]
F	Noise figure	[ ]

Vectors and Matrices

$[\tilde{\boldsymbol{v}}]$	Voltage excitation vector
$[\tilde{\boldsymbol{w}}]$	Beamformer weights vector
$[R]$	Voltage correlation matrix
$[S]$	Scattering parameter matrix
$[Z]$	Impedance parameter matrix
$[Y]$	Admittance parameter matrix

Chapter 1

Introduction

1.1 Background

In the modern scientific landscape, focus has fallen upon the implementation of large antenna arrays instead of singular, massive structures, as arrays have many advantages over their singular counterparts [1]-[2]. The radiation and receiving properties of antenna arrays have been widely investigated [3] and have become well known and commonplace for electronic engineering use. Due to the fact that many small elements can be combined to form a large receiver, the need for massive structures requiring enormous machinery and support structures, that are heavy and difficult to operate, has diminished. The cost of many, small elements can also be controlled better than that of one large element. The benefits seem in abundance. It is however so, that multiple radiating elements placed in proximity to each other will experience mutual coupling that has to be accounted for.

This opens a complete field of study into the effect that mutual coupling has on the properties of radiating structures, such as antenna arrays, [4], [5]. It is imperative to attempt to quantify the differences between an uncoupled element and its coupled counterpart as there are similarities but also subtle differences. Even though the differences may be small, the margin for error in the calculations is even smaller, considering the scale of the quantities that are concerned.

A considerable amount of effort has been spent in literature on describing and quantifying the effects of coupling, and the body of knowledge is sufficient to describe the effects of coupling well enough that engineers can have an understanding of the potential impact of coupling on various system properties, considerations and applications. These include among others, active element beam pattern, antenna element terminal phase deviation, directivity of antenna arrays, self- and mutual impedance, decorrelation of elements for MIMO systems, practical techniques for multiport coupling network design and

loss of visibility in interferometic radiometers due to coupling, linear multiport network noise analysis, as well as techniques to mitigate the effects to a certain extent[6]-[10]. An area of research which has in recent years gained much interest, is that of the influence of mutual coupling on the noise performance of antenna arrays. In uncoupled systems, well-developed design techniques and analysis theory exist. For coupled systems however, available theory assumes many approximations and idealities in order to make the problems tractable. It has lately, especially in astronomy projects such as the Square Kilometer Array (SKA), become of utmost importance that extreme measures are taken to ensure a system noise performance that adheres to strict limitations, as system sensitivity becomes crucial. This necessitates that new models and design techniques be created for noise analysis and mitigation.

Because of the ambiguities and uncertainties in the analysis, description and mitigation of system noise for coupled systems, a significant amount of work has been done in order to improve the understanding of such system properties and developing techniques to aid the synthesis and design of systems which consider noise performance an important outcome. The work done on the topic of multiport noise formulation through the use of noise matrices go as far back as 1959, [11] by Haus and Adler, who proposed an impedance matrix formulation as well as a lossless impedance matrix transformation formulation. They also set forth an impedance formulation for the characteristic-noise matrix and developed a canonical representation of linear noisy networks and transformation methods between matrix forms. Lastly, Haus and Adler focused on the noise measure of a linear network and proposed a network realization of the optimum amplifier system noise performance. The work done by Haus and Adler approached the topic in terms of exchangeable powers between network ports.

Wedge and Rutledge implemented wave techniques for the measurement and modeling of noise in a system in 1992, [12]. They also discussed the advantages of using noise waves to characterize the noise behaviour of a system. Their work calculated the network correlation matrices on both component and the overarching network level and discussed relations to two-port Figures of Merit and scattering parameters and transformations to traditional representations for noise measurement. This research also focused on presenting parameters for noise modeling specifically for applications using MESFET and HEMT transistors, relating noise wave parameters directly to the scattering matrix of such a transistor, given by its circuit model parameters. Wedge and Rutledge presented a two-port to three-port conversion of the noise wave correlation matrix, necessary for improving the equivalent circuit of a device through the modeling of stray capacitance, lead resistance and inductance. The theoretical, circuit model calculated, and measured optimum noise reflection coefficients, were compared between 2 GHz and 18 GHz as well as the minimum noise fig-

ure and noise resistance parameters. A noise wave method measurement was performed to measure MESFET transistor noise parameters, and compared to the parameters obtained using a source-pull tuner measurement. Wedge and Rutledge discussed the advantages of the noise wave measurement method, including the fact that the system of equations is over determined, which leads to advantages in statistical analysis.

Randa, in 2001, working on noise characterization of multiport amplifiers, adressed the definition and measurement of the device noise figure and relevant parameters to charactierize multiport devices, with a specific view on differential amplifiers. Randa proposed that a noise matrix parameterization seems the most practical method for characterising a device in terms of noise. The research done by Randa defined an output port noise figure, and related it to the noise matrix and scattering parameters of the device. Furthermore, Randa also investigated the correlations between noise waves with different inputs and the determining of the signal-to-noise ratio degradation factor (SNR) using a special choice of input correlation function [13]. Randa considered in detail the case of a three-port differential amplifier and the case of a four-port mixed-mode amplifier, both with reflectionless terminations and uncorrelated incident noise.

Weem and Popović set forth a method, in 2001, for determining analytically the noise coupling in a phased array using the active reflective coefficient [14], showing that the noise coupling is related explicitly to the scan angle dependent active reflection coefficient. They subsequently used this to calculate the noise coupling from the scattering parameters and noted that it can be used in the design of a phased array receiver. They used a Method of Moments (MoM) solver to practically calculate the scattering matrix of a 49 (7×7) element half wave dipole array, with an element spacing of $0.55\lambda_0$ at 1 GHz. Weem and Popović experimentally, for the aforementioned array, determined the maximum amount of coupling that can be allowed in the system that would not exceed 50% more noise power than expected for an analogous uncoupled array, as a Figure of Merit (FoM). They note that the resultant magnitude of the reflection coefficient is dependent on the amplifier gain and for Low Noise Amplifiers (LNA) with higher gains, the reflection coefficient magnitude would be significantly lower than they achieved. Weem and Popvić also note that they calculated the scan angle active reflection coefficient for a spacing of λ_0 and found a much reduced noise coupling between array elements. They recommended considering using larger element spacings, while keeping in mind the reduced scan angle coverage due to grating lobes such a selection would yield.

Work done by Warnick and Jensen on mutually coupled receiving arrays have focused on various different inherent properties of mutually coupled systems.

This work, done in 2005, in particular investigated the effects of mutual coupling on interference mitigation [15]. The coupling between elements was shown to be largest around an element spacing of $0.5\lambda_0$. Various matching networks were investigated and their effects on the array Q factor and array noise performance graphically compared, with the array Q factor defined as the numerical measure of the degree of superdirectivity of an array. This work provided a rigorous mathematical description of noise contributions in the receiver system. In 2007, Warnick and Jensen implemented the desired interference mitigation through optimal noise matching in coupled arrays [16], showing that classical two-port noise theory can be extended to the multiport case and that techniques and approaches for the two-port case can be used, if the N-channel array system is decoupled and isolated. Multiport noise optimization is done under the assumption of identical channel optimum reflection coefficients. Warnick and Jensen showed graphically that decoupling the receiver channels of a two-channel array leads to orthogonal receiver patterns and further proposed that the output noise of the array can be minimized by reflecting the output port reverse noise waves with proper phase, such that the correlated parts of the partially correlated forward and reverse noise waves cancel. As the reverse noise waves would couple to the other array elements, if allowed, Warnick and Jensen proposed that to minimize such noise, the array channels must be decoupled, using a matching network, to achieve optimal noise performance.

In 2007, Maaskant and Woestenburg investigated applying the active antenna impedance to a two-channel, phase scanned receiving dipole antenna array in order to achieve noise matching [17], showing the change in noise performance due to the scan angle dependency of the phase scanned array active optimum noise reflection coefficient. It was shown in their work that very large minimum to maximum noise temperature differences can arise due to the reflection coefficient mismatch, even when a match is designed to equal the optimum reflection coefficient at a certain scan angle. They furthermore showed that as the scan angle changes, the reflection coefficient moves in a circle on the Smith chart around the port self reflection coefficient. Their work also showed the variance in the receiving cross section and receiver sensitivity as the array scan angle is varied.

In 2009, Warnick, Woestenburg, Belostotski and Russer also attempted to minimize the effective noise power in a receiving array for phase scanned antenna arrays [18], presenting a theoretical framework for determining the optimal reflection coefficient for multiport noise matching to achieve maximum signal to noise ratio analytically, using both beamforming and non-beamforming applications. From the results of the beam equivalent receiver noise temperature for a two-element and five-element array investigated, the active impedance matching technique was shown to be less efficient as the number of array ele-

ments increased. In this work, Warnick, Woestenburg, Belostotski and Russer also showed that if the beamformer coefficients are of unequal magnitude, the center point of the circle that defines the active reflection coefficient over scan angle on the Smith chart shifts away from the array element self reflection coefficient, s_{nn}.

In 2015, Prinsloo proposed a multi-mode antenna excited through a multiconductor feed to achieve near-hemispherical field of view coverage [19]. Prinsloo presented three multi-mode antenna designs: one dual mode antenna and two quad mode antennas (QMA). Generalized transformations for the calculation of multi-mode S-parameters and radiated far-fields were derived and an equivalent network representation for active multi-mode antennas presented, which related the multi-mode signal and noise response of low noise amplifiers to two port amplifier S-parameters and noise parameters. In 2015, Prinsloo, Meyer, Maaskant and Ivashina also presented measurements to validate the far-field radiation pattern and co-polar gain of each mode [20]. Conclusions were drawn on the complementary nature of the orthogonal excitation modes to achieve near-hemispherical field of view coverage.

In 2016, Ivashina, Redkina, Maaskant and Prinsloo presented a numerical study on beam-steering arrays of multi-mode antennas [21]. This study investigated the modification of performance for multi-mode antennas in mutually coupled dense regular arrays with regards to maximum scan range and bandwidth. From the comparison with the final results presented for sparse and irregular arrays, the favorable array environment for mutually coupled multi-mode antenna arrays is concluded to be the sparse, irregular environment.

In 2014 and 2015 Dobrowolski performed noise characterization of multiport networks which utilize mixed, common and differential modes to present a noise wave approach to describe analytical relations between input port noise correlations and relation between output port noise figure and the noise matrix and scattering parameters of a multiport network, [22], [23]. Dobrowolski presented a modified reflection coefficient representation which combines common mode, differential mode and single ended reflection coefficients into the reflection coefficient matrix, which he related to the device scattering parameters, and used it to develop the formulation of the noise figure and Signal-to-Noise ratio (SNR) specifically for differential ports. He then reformulated the noise figure and SNR in terms of the intrinsic noise correlation matrix instead of reflection coefficients.

In 2017, Vaezi, Abdipour, Mohammadi and Ghannouchi investigated the effect of backward crosstalk at the output of power amplifiers in MIMO transmitters [24]. They showed that mutual coupling among the antenna elements of the MIMO receiver affects the behaviour of the power amplifiers and thus proposed

a novel non-linear behavioural model based on a generalized memory polynomial. They also showed that digital predistortion algorithms can compensate for the non-linearities and crosstalk effects in the MIMO transmitter. Experimental verification was done and the results compared to linearized SISO models. The proposed models showed improvements in the measured error power spectra.

In 2018, Hausmair, Landin, Gustavsson, Fager and Eriksson proposed a digital predistortion technique to compensate for power amplifier non-linearity, antenna crosstalk and impedance mismatches in MIMO transmitters, [25]. A linear model shared by all transmit paths was implemented to reduce complexity and increase scalability. Least-Square estimation techniques were implemented on the output measurements of the power amplifiers to determine all necessary information of the dual-input digital predistortion and crosstalk mismatch models. Through experimental validation it was confirmed that similar results to existing predistortion techniques was achieved with lower complexity.

1.2 Proposed Contributions

While noise theory is a mature subject, the current popularity of arrays has generated significant new contributions as discussed. However, noise design for multi-mode antennas is still largely an unexplored field. This project aims to quantize and mitigate the effect of noise in coupled antenna arrays, with specific attention to multi-mode systems. This is done through optimization methods in the selection and implementation of noise matching networks and beamforming methods. The noise matching networks limit noise coupling between array channels or maximize signal coupling to achieve optimum output SNR, while beamforming methods focus on maximizing signal integrity. The project aims to remove the constraints created by assumptions of identical ideal components in order to generalize solutions. In order to achieve the goals of the project, it is necessary to refine the existing models for coupled array receivers so that the output response can be directly numerically optimized in terms of the receiver circuit parameters. The improved models are then applied to design optimum noise matching networks for the QMA antenna.

The following are the main contributions presented in this dissertation.

- A design of optimum noise matching networks for the QMA
- Improved noise-matching design approaches for non-ideal, coupled antenna arrays using analytical and numerical optimization methods

- An improved receiver model for coupled arrays which utilizes non-identical amplifiers and non-identical, non-ideal radiating elements that can be numerically optimized
- Construction of a software based receiver model for non-ideal, coupled antenna arrays with non-identical amplifiers

1.2.1 QMA Optimum Noise Matching Network

The current noise design approach for the QMA assumes fixed matching to the self-impedance of each antenna. This dissertation presents an improved design by investigating the active impedance of the QMA as the angle of arrival for an incident signal is varied. The achieved output SNR of the QMA is numerically optimized to achieve optimum noise matching.

1.2.2 Source Impedance Matching Criteria and Methods

The active impedance of each channel of a scanned array can change to a large degree as a function of scan angle and changes can affect both the magnitude and phase. It is thus impossible to avoid sub-optimal performance over scan angle. There is thus room to investigate approaches which start with the optimal active impedance over angle and look at ways to approximate it to a single value or achieve a compromise that exhibits favorable output behavior. Here, a detailed investigation of possible matching strategies is presented, including a new set of averaged impedance values.

1.2.3 Refined Circuit Model

This contribution generalizes the receiver model so that no assumptions are made with regards to the values of the elements of the receiver circuit. In doing so greater design freedom is afforded. Furthermore, the model is formulated in terms of impedances and admittances, which are easy to model and can be directly optimized numerically. Impedances and admittances are closely related to inductors and capacitors, which are fundamental circuit components. Describing the receiver in terms of fundamental building blocks opens up the way for techniques from other fields of circuit design to be used.

1.2.4 Software Based Model

Software based models are necessary in order to numerically optimize the large sets of data and evaluate and compare the predicted results. It is also required that a control software model be implemented in premium circuit simulation software to confirm results.

1.3 Dissertation Outline

The layout of this dissertation to address the problem as stated will be as follows:

Chapter 2 begins by describing the necessary underlying theory of impedance matching and the fundamentals of noise theory and SNR. For the SNR analysis, the response of a receiver circuit is split into the cases of a signal of interest in the absence of interference, and the case of a noise signal in the absence of a signal of interest. The cases are then combined for the full response. Chapter 2 then continues to present the receiver models used as the basis for the analysis of the problem. First a rudimentary model is presented that describes the noise response directly in terms of circuit admittances for multiple loads. Thereafter, a more complex receiver that implements impedance matching and beamforming is presented. The concept of transformation matrices to refer excitations to different nodes of a receiver are also introduced. The presented model describes the response in terms of scattered waves and not circuit impedances and admittances, which is desirable for optimation however. Thirdly, chapter 2 presents techniques for the modeling of the active impedance and techniques that implement source matching for the varying active impedance in scanned receivers. Lastly, the theory of the optimum SNR beamformer is presented.

Chapter 3 begins with refinements to the signal and noise response models through the use of auxilliary equations to construct general, non-identical N-channel responses in terms of transformation matrices. The models are presented for receivers that are impedance matched and beamformed, directly in terms of circuit impedances and admittances. Chapter 3 then also presents a verification model implemented in software for the analysis of the receiver responses. A comparison between the results from the theoretical model and simulated model are presented and implementation differences are discussed.

Chapter 4 discusses the active impedance for both the signal and noise excited cases and discusses properties and characteristics of the active impedance and corresponding active reflection coefficient magnitude. After the discussion on the active impedance, chapter 4 then presents the techniques that this project proposes for the initial solution as the criteria for impedance matching in addition to the techniques discussed in chapter 2.

Chapter 5 focuses on the implementation of the modeling, design and optimization techniques on a novel Quad Mode Antenna. Firstly, the determining of the network parameters for the receiver is presented. The active impedance of the receiver is then calculated and discussed. The criteria and techniques presented in chapters 2 and 4 are applied and discussed. Numerical optimiza-

tion of the results achieved using the best performing of the methods presented is then implemented and discussed. An image processing technique is then presented, discussed and used to quantify and qualitatively compare the degree of change introduced to the receiver by performing matching. Lastly the output results for all criteria investigated are comparatively presented and the characteristics of the Quad Mode Antenna noted.

In chapter 6 a control antenna is presented. A standard Four Monopole Array is designed so a comparison of the results achieved on the novel Quad Mode Antenna can be drawn. As in chapter 5 the parameters are determined and the criteria and techniques applied. The resulting output SNR performance is then presented and the characteristics of the Four Monopole Array noted.

Chapter 7 discusses the similarity of the results achieved for a given antenna array case in chapters 5 and 6 and then subsequently discusses the need for secondary criteria for the selection of an implementation. At the hand of the secondary criteria, a selection of implementation is made for both antenna cases. Conclusions are then drawn on the performance of the proposed methods as observed for the two antenna arrays investigated.

Chapter 8 presents an evaluation of the proposed contributions of this project.

Chapter 2

Noise Modeling in Receivers

Various noise models have been proposed for multi-antenna receivers, as discussed in the previous chapter. Here, a short overview of each will be given. The chapter will end with a description of the current state of the art algorithms for noise matching in antenna arrays.

2.1 Fundamentals of Noise Theory and SNR

The formulation of the fundamentals of noise theory will be illustrated at the hand of a simple two-element array together with two low-noise amplifiers, each terminated with a load impedance. The array is modelled by its S-matrix and an impressed voltage vector, while the low-noise amplifiers are modelled as an input impedance and output impedance, with an output voltage dependent on the LNA input voltage applied at the LNA ouput, together with two correlated noise sources. The noise sources consist of a noise voltage, e_n and noise current source, i_n. The receiver model is shown in figure 2.1.

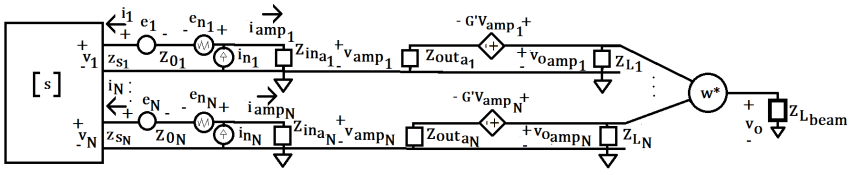

Figure 2.1: Receiver model circuit diagram without matching network

2.1.1 Receiver Signal Response

Using standard circuit theory, the signal voltages at the ports of the antenna array, v_m can be determined in terms of the impressed voltages e_m, the array scattering parameters, $[S]$, the characteristic impedances Z_{0_m}, the input impedances Z_{s_m} and the load input impedances Z_{in_a}, with all noise sources zero, as

$$v_m = \sum_{k=1}^{N} \sqrt{\frac{\Re\{Z_{0_m}\}}{\Re\{Z_{0_k}\}}} \left(\frac{Z_{s_m}}{Z_{s_m} - {Z_{0_m}}^*}\right)\left(\frac{Z_{s_k} + Z_{0_k}}{Z_{s_k} + Z_{in_{a_k}}}\right) s_{mk} e_k \tag{2.1}$$

In general the ports of any given device are referenced to the same characteristic impedance, causing the square root parts of 2.1 to collapse to 1. In the receiver model as shown in figure 2.1, the LNA input impedance of the m-th channel, $Z_{in_{am}}$ is reciprocal to its admittance, [26], defined in terms of the 2×2 LNA admittance matrix, and the amplifier load admittance, $Y_{L_m} = 1/Z_{L_m}$ as

$$Y_{in_{am}} \triangleq y_{11} - \frac{y_{12_{amp}} y_{21_{amp}}}{y_{22_{amp}} + Y_{L_m}} \tag{2.2}$$

In the absence of noise, ie. with $e_n = i_n = 0$ for each channel, the average signal power at the input of the LNA of the m-th channel, $P_{s_{av_m}}$ is given by the real part of the apparent power.

$$\begin{aligned} P_{s_{av_m}} &= \frac{1}{2}\Re\{v_{amp} {i_{amp}}^*\} \\ &= \Re\left\{\frac{1}{2{Z_{in_{am}}}^*}(v_m - e_m)(v_m - e_m)^*\right\} \\ &= \Re\left\{\frac{1}{2{Z_{in_{am}}}^*}|v_m - e_m|^2\right\} \end{aligned} \tag{2.3}$$

The output of the LNA can be modeled as the load impedance Z_{L_m} with a dependent voltage $v_{o_{amp_m}}$ over it, as shown in figure 2.2.

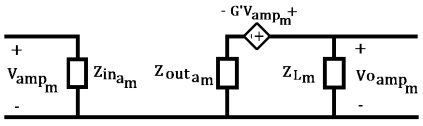

Figure 2.2: LNA output voltage dependent on input voltage

The dependent output voltage $v_{o_{amp_m}}$ is given, with $G'_m = \frac{Z_{out_{a_m}} + Z_{L_m}}{Z_{L_m}} G_{v_m}$, in terms of the LNA S-parameters, input impedance and load impedance as

$$\begin{aligned} v_{o_{amp_m}} &= \frac{Z_{L_m}}{Z_{L_m} + Z_{out_{a_m}}} G'_m v_{amp_m} \\ &= G_{v_m} v_{amp_m} \\ &= \frac{Z_{L_m}}{Z_{in_{a_m}}}\left(\frac{Z_{in_{a_m}} + Z_0}{Z_{L_m} + {Z_0}^*}\right) s_{21_{amp}} v_{amp_m} \end{aligned} \tag{2.4}$$

At the output of the LNA, the signal power is given by

$$\begin{aligned} P_{s_{beam_m}} &= \Re\{G_{p_m} P_{s_{av_m}}\} \\ &= \Re\left\{ \frac{Z_{L_m}}{Z_{in_{a_m}}} \left| \frac{Z_{in_{a_m}} + Z_0}{Z_{L_m} + Z_0{}^*} \right|^2 |s_{21}|^2 P_{s_{av_m}} \right\} \end{aligned} \tag{2.5}$$

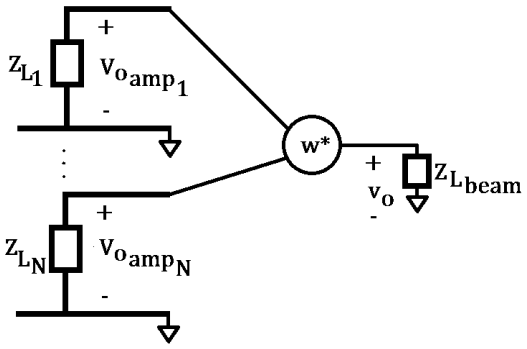

Figure 2.3: Amplifier outputs fed into beamformer

The amplifier output voltages for each of the N channels is then fed into a beamformer with weights given by $[\tilde{\boldsymbol{w}}]$ as shown in figure 2.3 so that the beamformer output voltage is given by

$$v_o = [\tilde{\boldsymbol{w}}]^\dagger [\tilde{\boldsymbol{v}}_{\boldsymbol{o_{amp}}}] \tag{2.6}$$

The notation $[\tilde{\boldsymbol{x}}]$ indicates that x is a vector. The signal power at the output of the beamformer can then be determined as shown in 2.7 with † denoting the complex conjugate transponent operation, $\overline{X}$ denoting the expected value of X and $[R_{beam}]$ being the beamformer input signal voltage correlation matrix.

$$\begin{aligned} P_{s_{out}} &= \frac{1}{2}\Re\{v_o {i_o}^*\} \\ &= \Re\left\{ \frac{1}{2Z_{L_{beam}}{}^*} [\tilde{\boldsymbol{w}}]^\dagger [\tilde{\boldsymbol{v}}_{\boldsymbol{o_{amp}}}] [\tilde{\boldsymbol{v}}_{\boldsymbol{o_{amp}}}]^\dagger [\tilde{\boldsymbol{w}}] \right\} \\ &= \Re\left\{ \frac{1}{2Z_{L_{beam}}{}^*} [\tilde{\boldsymbol{w}}]^\dagger [R_{beam}] [\tilde{\boldsymbol{w}}] \right\} \end{aligned} \tag{2.7}$$

2.1.2 Receiver Noise Response

A noisy LNA can be modeled as a noiseless two port cascaded with a noise voltage and noise current source, referred to the input port of the LNA. The mean-squared values of the uncorrelated LNA noise voltage and current sources for the m-th channel are given by 2.8 and 2.9, with Boltzmann's constant k_B,

temperature T and noise bandwidth B. R_n and G_n are device dependent scaling factors, called the noise resistance and conductance, respectively.

$$\overline{|e_{n_m}|^2} = 4k_BTBR_{n_m} \tag{2.8}$$

$$\overline{|i_{u_m}|^2} = 4k_BTBG_{n_m} \tag{2.9}$$

The noise voltage and current sources are correlated in general. The noise current source can be written as the sum of a correlated and uncorrelated part.

$$\begin{aligned} i_n &= i_u + i_c \\ &= i_u + Y_c e_n \end{aligned} \tag{2.10}$$

The correlation admittance Y_c and noise conductance G_n can be shown to be dependent on the LNA noise parameters, [27], F_{min}, R_n and $Z_{s_{opt}}$ as

$$\begin{aligned} G_n &= R_n({G_{s_{opt}}}^2 - {G_c}^2) \\ G_c &= \frac{F_{min} - 1}{2R_n} - G_{s_{opt}} \\ B_c &= -B_{s_{opt}} \\ Y_c &= G_c + jB_c \end{aligned}$$

The expected value of the LNA input port noise power for the m-th channel is then given by equation 2.11. The coupled terms of the noise power are contained in the array port noise voltage term v_{n_m}, which can be calculated using equation 2.1 with the equivalent noise voltage source $e_{n_{eq_m}} = e_{n_m} + Z_{in_{a_m}} i_{n_m}$.

$$\begin{aligned} P_{n_{amp_m}} &= \frac{1}{2}\Re\{\overline{v_{n_{amp_m}} {i_{n_{amp_m}}}^*}\} \\ &= \Re\Big\{\frac{1}{2{Z_{in_{a_m}}}^*}\,\overline{|v_{n_{amp_m}}|^2}\Big\} \\ &= \Re\Big\{\frac{1}{2{Z_{in_{a_m}}}^*}\,\overline{|v_{n_m} + e_{n_m}|^2}\Big\} \\ &= \Re\Big\{\frac{1}{2{Z_{in_{a_m}}}^*}\Big(\overline{|v_{n_m}|^2} + 2\Re\{\overline{v_{n_m} {e_{n_m}}^*}\} + \overline{|e_{n_m}|^2}\Big)\Big\} \end{aligned} \tag{2.11}$$

At the output of the LNA, in terms of the amplifier power gain, G_{p_m}, the beamformer input noise power has an expected value of

$$\begin{aligned} P_{n_{beam_m}} &= \Re\{G_{p_m} P_{n_{amp_m}}\} \\ &= \Re\Big\{\frac{Z_{L_m}}{Z_{in_{a_m}}}\Big|\frac{Z_{in_{a_m}} + Z_0}{Z_{L_{amp_m}} + {Z_0}^*}\Big|^2 |s_{21}|^2 P_{n_{amp_m}}\Big\} \end{aligned} \tag{2.12}$$

The beamformer input noise voltage correlation matrix is then determined and the expected value of the beamformer output noise power can then be calculated, using the beamformer output noise voltage and current, v_{n_o} and i_{n_o} respectively, as

$$\begin{aligned} P_{n_{out}} &= \frac{1}{2}\Re\{\ \overline{v_{n_o} {i_{n_o}}^*}\} \\ &= \Re\Big\{\frac{1}{2{Z_{L_{beam}}}^*}\ \overline{|v_{n_o}|^2}\Big\} \\ &= \Re\Big\{\frac{1}{2{Z_{L_{beam}}}^*}[\tilde{\boldsymbol{w}}]^\dagger\overline{[\tilde{\boldsymbol{v}}_{\boldsymbol{o_{amp_n}}}][\tilde{\boldsymbol{v}}_{\boldsymbol{o_{amp_n}}}]^\dagger}[\tilde{\boldsymbol{w}}]\Big\} \\ &= \Re\Big\{\frac{1}{2{Z_{L_{beam}}}^*}[\tilde{\boldsymbol{w}}]^\dagger[R_{n_{beam}}][\tilde{\boldsymbol{w}}]\Big\} \end{aligned} \tag{2.13}$$

The SNR can then be determined at any point in the circuit model using the signal and expected noise powers as

$$SNR_{node} = \frac{P_{s_{node}}}{P_{n_{node}}}$$

With the SNR known, the noise figure of any component can be determined by taking the ratio of the input SNR to the output SNR,

$$F = \frac{SNR_i}{SNR_o}$$

2.2 Current-Based Receiver Circuit Model

For multi-port networks, the formulation in the previous section becomes cumbersome and other, matrix-based methods exist. The first of these is a current based nodal representation of the multi-port receiver [28]. Figure 2.4 shows the circuit diagram of the nodal receiver model for an array with n_R elements. In the diagram, the m-th channel port current is given by I_m. i_m represents the complex amplitudes of the thermal noise current generators. Y_{Lm} and i_{Lm} represent the m-th channel receiver load input admittance, generally a LNA, and the thermal noise current generated by the m-th channel load respectively.

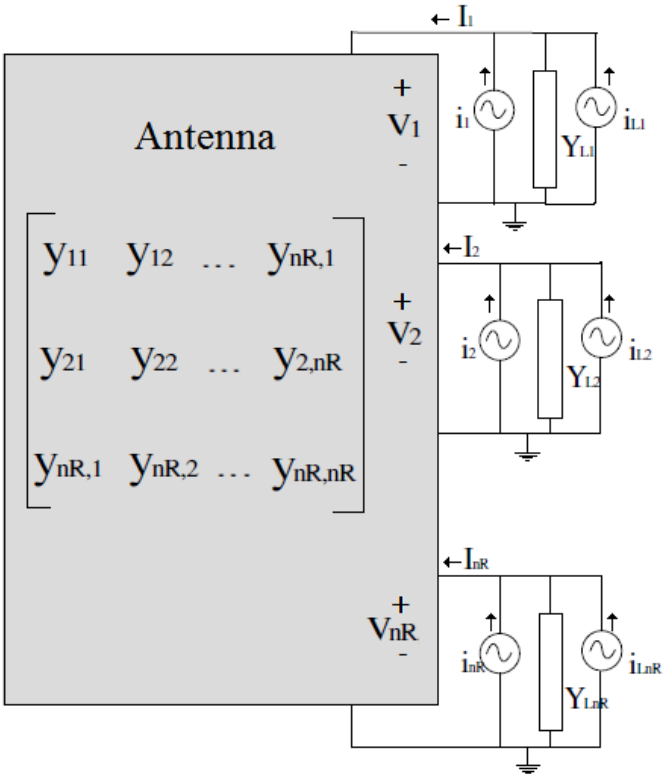

Figure 2.4: Current based nodal receiver model circuit diagram

The currents into and the voltages across each node of the receiver are given by

$$[I] = \begin{bmatrix} i_{L1} + i_1 - Y_{L1}V_1 \\ i_{L2} + i_2 - Y_{L2}V_2 \\ \vdots \\ i_{Ln_R} + i_{n_R} - Y_{Ln_R}V_{n_R} \end{bmatrix}$$

$$[V] = \begin{bmatrix} V_1 \\ V_2 \\ \vdots \\ V_{n_R} \end{bmatrix}$$

With the unity identity vector $[U]$, the admittance matrix for identical loads

Y_L is given by

$$[Y + Y_L U] = \begin{bmatrix} y_{11} + Y_L & y_{12} & \cdots & y_{1n_R} \\ y_{21} & y_{22} + Y_L & \cdots & y_{2n_R} \\ \vdots & \vdots & \ddots & \vdots \\ y_{1n_R} & y_{2n_R} & \cdots & y_{n_R n_R} + Y_L \end{bmatrix}$$

In order to determine the receiver total noise power, the noise correlation matrix is needed. With T the antenna temperature, k_B the Boltzmann constant and $\dagger$ denoting the transpose of the complex conjugate, the per frequency bandwidth unit noise correlation matrix of the receiver is determined as follows. The noise current generators are partially correlated for a reciprocal mutually coupled array and the expected values of the products of the noise currents are given, from Twiss's theorem, by

$$\begin{aligned} \overline{i_j i_k^*} df &= 2k_B T(y_{jk} + y_{jk}^*) df \\ \overline{i_{L_j} i_k^*} &= 0 \\ \overline{i_{L_j} i_{L_k}^*} &= 0, \quad j \neq k \end{aligned}$$

The noise correlation matrix is then given by

$$\begin{aligned} [N] &= \frac{1}{2}(Y_L + Y_L^*)\overline{[V][V]^\dagger} \\ &= \frac{1}{2}(Y_L + Y_L^*)[Y + Y_L U]^{-1}\overline{[I][I]^\dagger}\left[[Y + Y_L U]^{-1}\right]^\dagger \end{aligned}$$

Using the definition of $[I]$ together with the expected values of the products of the noise currents, it can then be shown that

$$\begin{aligned} \overline{[I][I]^\dagger} &= \begin{bmatrix} i_1 i_1^* + i_{L_1} i_{L_1}^* & i_1 i_2^* & \cdots & i_1 i_{n_R}^* \\ i_2 i_1^* & i_2 i_2^* + i_{L_2} i_{L_2}^* & \cdots & i_2 i_{n_R}^* \\ \vdots & \vdots & \ddots & \vdots \\ i_{n_R} i_1^* & i_{n_R} i_2^* & \cdots & i_{n_R} i_{n_R}^* + i_{L_{n_R}} i_{L_{n_R}}^* \end{bmatrix} \\ &= 2k_B T \begin{bmatrix} y_{11} + y_{11}^* + Y_L + Y_L^* & y_{12} + y_{12}^* & \cdots & y_{1n_R} + y_{1n_R}^* \\ y_{21} + y_{21}^* & y_{22} + y_{22}^* + Y_L + Y_L^* & \cdots & y_{2n_R} + y_{2n_R}^* \\ \vdots & \vdots & \ddots & \vdots \\ y_{n_R 1} + y_{n_R 1}^* & y_{n_R 2} + y_{n_R 2}^* & \cdots & y_{n_R n_R} + y_{n_R n_R}^* + Y_L + Y_L^* \end{bmatrix} \end{aligned} \tag{2.14}$$

Substituting $\overline{[I][I]^\dagger}$ back into $\overline{[V][V]^\dagger}$ then leads to the per unit bandwidth noise correlation matrix given by

$$[N] = k_B T(Y_L + Y_L^*)[Y + Y_L U]^{-1}\left[[Y + Y_L U] + [Y + Y_L U]^*\right]\left[[Y + Y_L U]^{-1}\right]^\dagger \tag{2.15}$$

For a given noise bandwidth B and input signal current vector, $[I_{sig}]$, the receiver SNR at the loads is then given by [28]

$$SNR = \frac{\text{trace}(\frac{R_L}{2}[I_{sig}][I_{sig}]^\dagger)}{\int_B \text{trace}([N])df} \tag{2.16}$$

2.3 Wave-Based Receiver Circuit Model

Another N-port model is based on wave-descriptions as presented in [16]. Figure 2.5 shows a wave based receiver model fed into a beamformer.

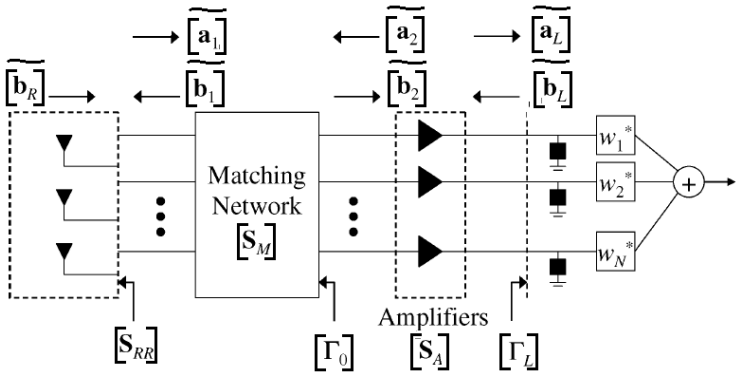

Figure 2.5: Wave based model with outputs fed to a beamformer circuit diagram

Supposing that $[\tilde{\boldsymbol{v}}_{\boldsymbol{s}}]$ and $[\tilde{\boldsymbol{v}}_{\boldsymbol{n}}]$ are the open circuit signal and noise voltages excited by external sources at the terminals of the antenna, which give rise to the forward and reverse traveling voltage waves $[\tilde{\boldsymbol{a}}_{\mathbf{1}}]$ and $[\tilde{\boldsymbol{b}}_{\mathbf{1}}]$ as well as the corresponding noise voltage waves, the open circuit signal and noise correlation matrices are given by

$$[\hat{R}_s] = \overline{[\tilde{\hat{\boldsymbol{v}}}_{\boldsymbol{s}}][\tilde{\hat{\boldsymbol{v}}}_{\boldsymbol{s}}]^{\dagger}}$$
$$[\hat{R}_n] = \overline{[\tilde{\hat{\boldsymbol{v}}}_{\boldsymbol{n}}][\tilde{\hat{\boldsymbol{v}}}_{\boldsymbol{n}}]^{\dagger}}$$

The † denotes the transpose of the complex conjugate. The amplifier S-parameters are given by $[S_A]$ and the antenna array S-parameters by $[S_{RR}]$. The matching network S-parameters are given by a block matrix of the form

$$[S_M] = \begin{bmatrix} [S_{11}] & [S_{12}] \\ [S_{21}] & [S_{22}] \end{bmatrix}$$

The matrices $[G_0]$ and $[Q]$ are then defined as in equations 2.17 and 2.18

$$[G_0] = \frac{1}{2Z_0^{\frac{1}{2}}}[S_{21}]\big[[I] - [S_{RR}][S_{11}]\big]^{-1}\big[[I] - [S_{RR}]\big] \tag{2.17}$$

$$[Q] = Z_0^{\frac{1}{2}}\big[[I]+[\Gamma_L]\big]\Big[\big[[I]-[\Gamma_0][S_{A,11}]\big][S_{A,21}]^{-1}\big[[I]-[S_{A,22}][\Gamma_L]\big]-[\Gamma_0][S_{A,12}][\Gamma_L]\big]\Big]^{-1} \tag{2.18}$$

$[G_0]$ relates the open-circuit voltage responses to the voltages at the amplifier inputs and $[Q]$ relates the voltages at the amplifier inputs to the output loads.

In both equations 2.17 and 2.18, $[\Gamma_0]$ is the scattering matrix seen looking into the matching network section from the amplifier input ports. The voltages over the amplifier terminations are then given in terms of the open circuit loaded response, $[\tilde{\hat{\boldsymbol{v}}}]$ and the forward and reverse traveling noise voltage waves, $[\tilde{\boldsymbol{a}}_{\boldsymbol{\eta}}]$ and $[\tilde{\boldsymbol{b}}_{\boldsymbol{\eta}}]$ respectively, as

$$[\tilde{\boldsymbol{v}}_{\boldsymbol{L}}] = [Q]\big[[G_0][\tilde{\hat{\boldsymbol{v}}}] + [\Gamma_0][\tilde{\boldsymbol{b}}_{\boldsymbol{\eta}}] - [\tilde{\boldsymbol{a}}_{\boldsymbol{\eta}}]\big]$$

In a noisy component represented by scattering matrix $[s]$, the reverse traveling waves are given as the sum of the reflected forward traveling waves and the noise waves emanating from the component, [12], as shown for a two-port element in figure 2.6.

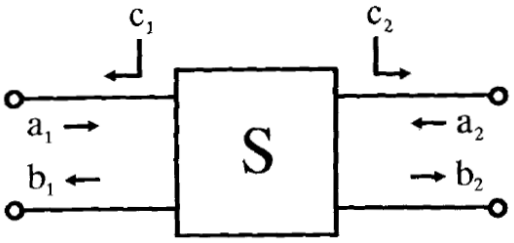

Figure 2.6: Two port circuit element with forward, reverse and noise waves

The noise waves contribute to the scattered waves as

$$\begin{bmatrix} b_1 \\ b_2 \end{bmatrix} = \begin{bmatrix} s_{11} & s_{12} \\ s_{21} & s_{22} \end{bmatrix} \begin{bmatrix} a_1 \\ a_2 \end{bmatrix} + \begin{bmatrix} c_1 \\ c_2 \end{bmatrix}$$

The signal, external and LNA noise correlation matrices are given by the equations

$$[R_s] = [Q][G_0][\hat{R}_s][G_0]^\dagger[Q]^\dagger \tag{2.19}$$

$$[R_n] = [Q][G_0][\hat{R}_n][G_0]^\dagger[Q]^\dagger \tag{2.20}$$

$$[R_{LNA}] = k_B B[Q][\hat{R}_\eta][Q]^\dagger \tag{2.21}$$

$$[R_\eta] = T_\alpha[I] + T_\beta[\Gamma_0][\Gamma_0]^\dagger - T_\gamma[\Gamma_0] - T_\gamma^*[\Gamma_0]^\dagger \tag{2.22}$$

In equation 2.22, T_α T_β and T_γ are the noise wave parameters in units of Kelvin, [29], given by

$$T_\alpha = \frac{1}{2k_B B}\overline{|a_\eta|^2} = T_0[Z_0 G_u + R_n Y_0(1 + Z_0^2|Y_c|^2 + 2Z_0 G_c)]$$

$$T_\beta = \frac{1}{2k_B B}\overline{|b_\eta|^2} = T_0[Z_0 G_u + R_n Y_0(1 + Z_0^2|Y_c|^2 - 2Z_0 G_c)]$$

$$T_\gamma = \frac{1}{2k_B B}\overline{a_\eta^* b_\eta} = T_0[-Z_0 G_u + R_n Y_0(1 - Z_0^2|Y_c|^2) - j2R_n B_c]$$

For identical amplifiers the optimal scattering coefficient seen looking into the matching section from the amplifier inputs, $[\Gamma_0] = \Gamma_{opt}[I]$ and Γ_{opt} can be shown to be given in terms of the LNA noise temperature parameters as

$$\Gamma_{opt} = \frac{T_\alpha + T_\beta \pm \sqrt{(T_\alpha + T_\beta)^2 - 4|T_\gamma|^2}}{2T_\gamma} \tag{2.23}$$

The output SNR is then given by the ratio

$$SNR = \frac{[\tilde{\boldsymbol{w}}]^\dagger [R_s][\tilde{\boldsymbol{w}}]}{[\tilde{\boldsymbol{w}}]^\dagger \big[[R_n] + [R_{LNA}]\big][\tilde{\boldsymbol{w}}]}$$

2.4 Active Impedance Modeling

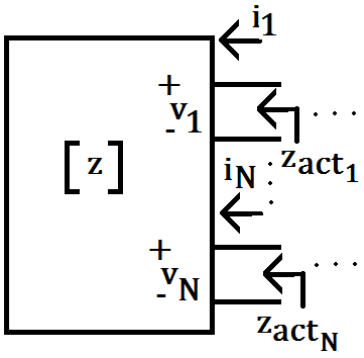

Figure 2.7: The active impedances of a general N-port array

In general, for an N-port array as shown in figure 2.7, the active impedance of a coupled receiver channel, seen looking into the port of the channel, is defined as the ratio of the voltage across the port to the input current at the port. For the coupled antenna, [30], the voltage across the terminals of any port is given by the product of the impedance matrix, which includes the mutual impedance, and the current vector of all the ports. The active impedance of the m-th channel then becomes

$$\begin{aligned} Z_{act_m} &= \frac{V_m}{I_m} \\ &= \frac{I_1 Z_{m1} + I_2 Z_{m2} + \cdots + I_N Z_{mN}}{I_m} \\ &= \sum_{n=1}^{N} \frac{I_n}{I_m} Z_{mn} \end{aligned} \tag{2.24}$$

To calculate the active impedance simultaneously for all channels, the matrix form is given, with $[I_{diag}]$ the diagonal matrix of the port currents, by

$$[Z_{act}] = [I_{diag}]^{-1}[Z][I] \tag{2.25}$$

Equivalently, the active impedance can also be determined by taking the per element inverse of the active admittance given by

$$[Y_{act}] = [V_{diag}]^{-1}[Y][V] \tag{2.26}$$

In a receiver with a beamformer present, the active impedance can alternatively be shown to exhibit a beamforming coefficient dependency, [18], and be given by

$$Z_{act_m} = \frac{1}{\omega^*_{oc,m}} \sum_{n=1}^{M} \omega^*_{oc,n} Z_{Ant,nm} \tag{2.27}$$

In this formulation, $\omega_{oc,m}$ is the m-th channel beamformer coefficient referred to the antenna ports.

The active impedance is dependent on the ratio of excitations applied to each port of an array, or by reciprocity, the ratio of excitations received by each element of an array. Through beamforming or the spatial scanning of an antenna, the ratios can vary as an array is operated. For each combination of excitations, a different active impedance value can be calculated. The degree of variance is dependent not only on the excitation ratios, but also the mutual coupling between array elements. For coupled receiver design, the active impedance is thus a quantity of great importance. Any design consideration which is reliant on the source impedance is affected by the variation of the active impedance. Examples include, but are not limited to, noise matching for low noise amplifiers, gain matching for high gain amplifiers, amplifier stability design and regulation of power consumption by the array through current control. In high sensitivity systems, such as radio interferometers, mismatches that occur due to a varying source impedance can have catastrophic effects on system performance if not designed for or mitigated.

2.5 Matching Criteria for Optimal Noise Performance

2.5.1 Active Impedance at Given Angle

The propagation paths of noise waves in a phased antenna array, shown in figure 2.8, [17], can be represented using the active reflection coefficients of each channel of the array.

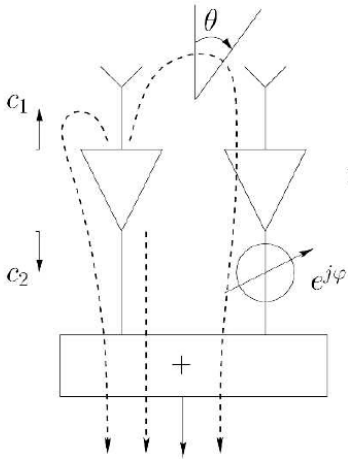

Figure 2.8: Propagation paths of noise waves an a phased antenna array

The total noise wave at the beamformer output, with beamforming coefficients of unity for each channel, as in figure 2.8 is then given by

$$\begin{aligned} c_{tot} &= \text{Direct Part } + \text{Coupled Part } + \text{Reflected Part} \\ &= c_2 + c1 S_{21}^{ant} S_{21}^{LNA} e^{j\phi} + c_1 S_{11}^{ant} S_{21}^{LNA} \\ &= c_2 + c_1 S_{21}^{LNA} \left(S_{11}^{ant} + S_{21}^{ant} e^{j\phi} \right) \\ &= c_2 + c_1 S_{21}^{LNA} \Gamma_{act}^{1}(\phi) \end{aligned}$$

For an N-channel linear phase scanned array, [31], the phase difference between adjacent channels is given by $\phi = kd\sin(\theta)$, with k the wavenumber and d the linear distance between antenna elements. The active reflection coefficient term of the m-th channel is then seen to be given by

$$\Gamma_{act}^{m}(\phi) = \sum_{n=1}^{N} S_{nm}^{ant} e^{j(m-n)\phi} \tag{2.28}$$

Using the active reflection coefficient, as defined in equation 2.28, the channels of the array can be decoupled as shown in figure 2.9.

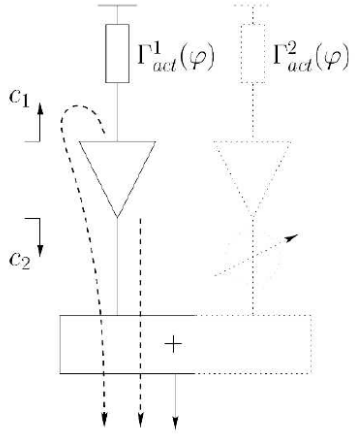

Figure 2.9: Equivalent decoupled array channel representation using the active reflection coefficient

The active reflection coefficient can be plotted on the Smith chart, and for the two channel case is seen to move along a circle of constant radius S^{ant}_{mn} around the point S^{ant}_{mm} as shown in figure 2.10, [17].

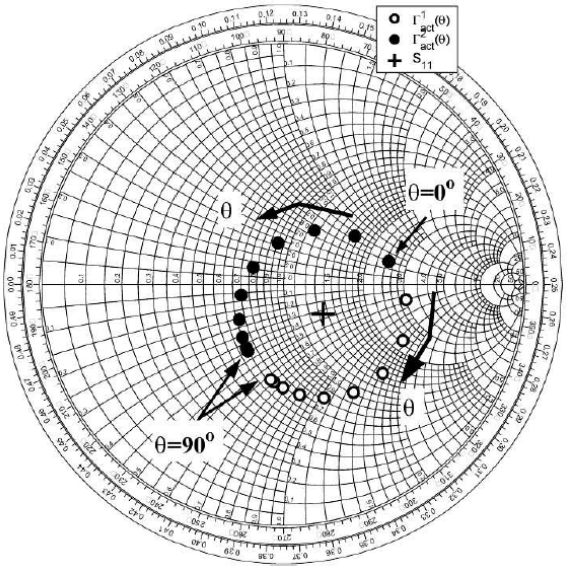

Figure 2.10: Two channel phased array active impedance plotted on the Smith chart

If noise matching networks are designed for each channel to transform Γ_{act} at θ_0 to the optimum noise reflection coefficient of the LNA, $\Gamma_{s_{opt}}$, the LNA can then be noise matched at the angle θ_0. For each channel, the decoupled channel circuit with the new equivalent LNA, consisting of the original LNA and matching network, is then shown in figure 2.11, [17].

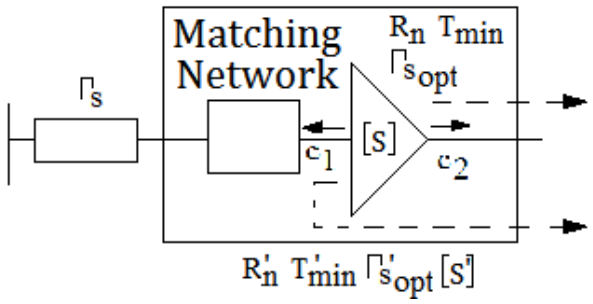

Figure 2.11: Decoupled channel after noise matching to angle θ_0

The receiver temperature of the equivalent LNA is given in terms of the LNA noise parameters with $\Gamma_s = \Gamma_{act}$ by the equation

$$T_{LNA} = T'_{min} + \frac{4T_0 R'_n}{Z_0} \frac{|\Gamma_s - \Gamma'_{s_{opt}}|^2}{|1 + |\Gamma'_{s_{opt}}|^2 (1 - |\Gamma_s|^2)} \tag{2.29}$$

Figure 2.12 ,[17], shows how the noise temperature of a typical receiver varies over scan angle θ_0.

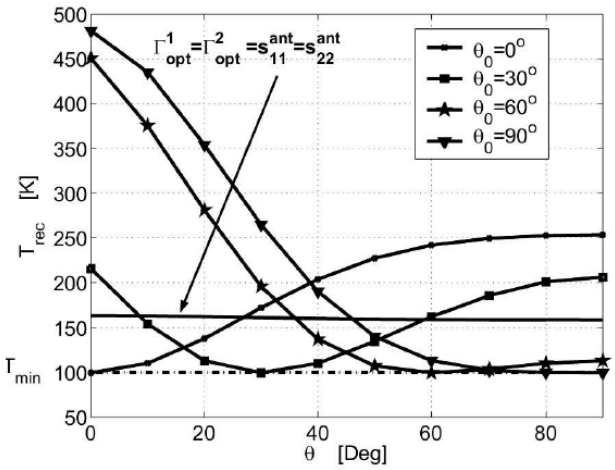

Figure 2.12: Noise temperature of receiver as θ varies, for given angles of θ_0

It can be seen from figure 2.12 that the choice of θ_0 influences both the maximum LNA noise temperature as well as the gradient of the noise temperature curve, and thus the bandwidth of the noise match.

2.5.2 Self-Impedance Matching

As the active impedance of a scanned array varies as the array is scanned, the noise matching efficiency will also vary as the array is scanned. The amount

of variation can be shown,[32], to be proportional to the element separation in wavelengths. Increasing the distance between elements reduces the coupling and thus the degree to which the active impedance varies. As seen in figure 2.13,[32], for the three dipole array as shown in figure 2.14, the magnitude and phase of the active reflection coefficient increasingly tracks that of S_{mm} as the element separation increases.

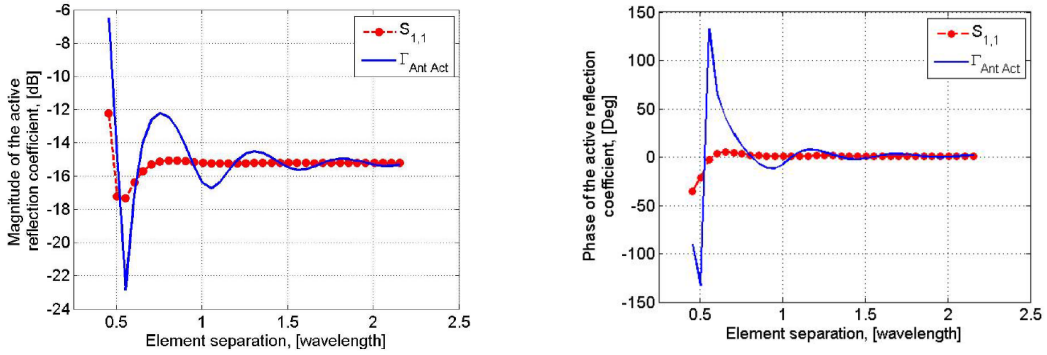

(a) Magnitude (b) Phase

Figure 2.13: Active reflection coefficient and S_{mm} magnitude and phase as element separation varies

Considering the three channel phase scanned array as shown in figure 2.14,[32], where the active reflection coefficient is calculated as in equation 2.28, the active reflection coefficients per channel are plotted on the Smith chart in figure 2.15,[32].

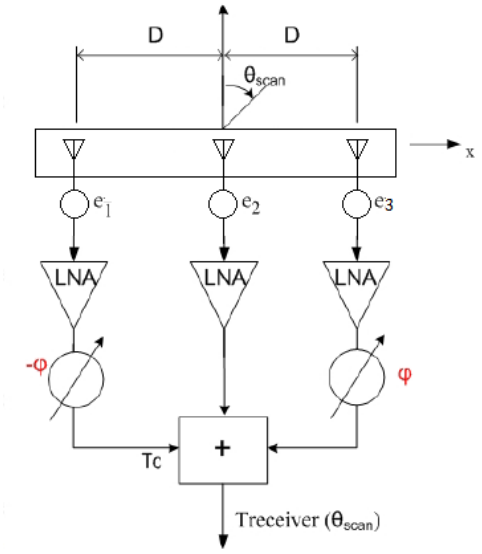

Figure 2.14: Three dipole phased antenna array

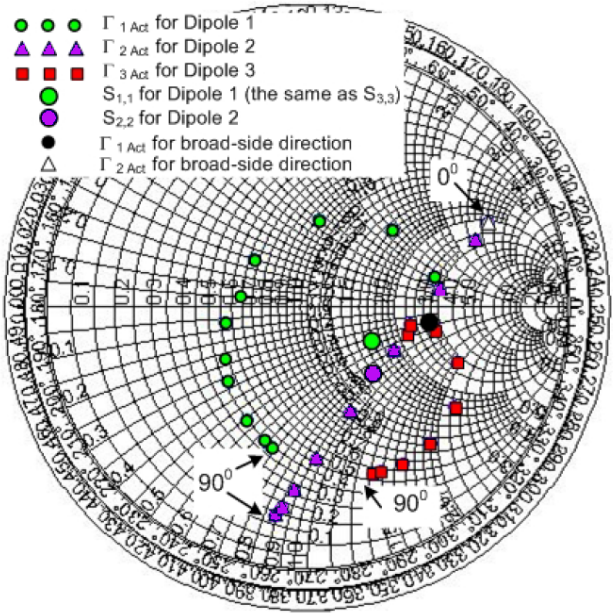

Figure 2.15: Active reflection coefficient per channel plotted for three dipole array, for a scan angle of $\theta \in [0°, 90°]$ at one frequency

One of the most standard ways of matching design for arrays is to transform the self-reflection, S_{mm}, to the optimum noise source reflection coefficient for each channel, as shown in figure 2.16.

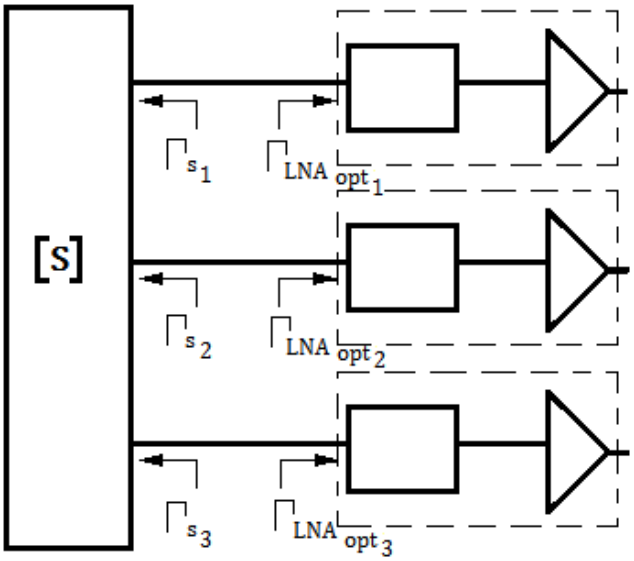

Figure 2.16: Transformation of LNA optimum noise source reflection coefficient

For the three dipole example, the resulting receiver noise temperature is shown in figure 2.17 for different scan angles,[32]. The receiver noise temperature is determined using equation 2.29.

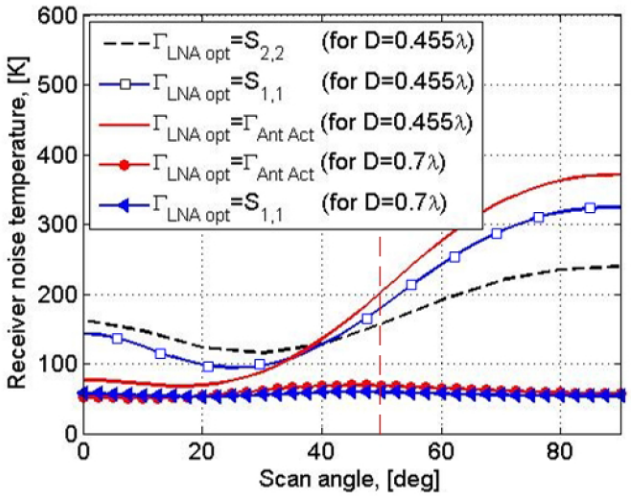

Figure 2.17: Receiver noise temperature for different $\Gamma_{s_{opt}}$ over scan angle

It can be seen from figure 2.17 that for small element separations, over certain angles matching to the array channel input reflection coefficient, S_{mm}, can produce better results than matching to the active reflection coefficient at broadside, while for large element separations, the resulting receiver noise temperature is approximately equal when matching to either Γ_{act} or S_{mm}.

2.5.3 Multibeam Average Noise Optimization

Matching to the active impedance will minimize the receiver noise temperature for a given beam in the antenna field of view. If the field of view is spanned by a number of beams, P, each constructed using beamformer coefficients $[\tilde{\boldsymbol{w}}^p]$, [18], the average beam equivalent noise temperature is defined as

$$T_{av} = \frac{1}{P}\sum_{p=1}^{P} T_{rec}^{p} \tag{2.30}$$

The receiver noise temperature T_{rec} for a given beam for an M channel receiver can be shown to be given in terms of the LNA noise parameters T_{min}, R_n, Y_{opt}, with $w_{oc,m}$ and $R_{act,m}$ the open circuit referred beamformer coefficients and

real part of the active impedance for the m-th channel respectively, as

$$T_{rec} = T_{min} + T_0 \frac{\sum_{m=1}^{M} |w_{oc,m}|^2 R_{c,m}}{\sum_{m=1}^{M} |w_{oc,m}|^2 R_{act,m}} \tag{2.31}$$

Where for the m-th channel, with $R_{n,m}$ the m-th channel noise resistance, R_c is given by

$$R_{c,m} = R_{n,m}|Z_{act,m}|^2|Y_{act,m} - Y_{opt,m}|^2$$

Inserting equation 2.31 into equation 2.30 leads to

$$T_{av} = T_{min} + \frac{T_0}{P} \sum_{p=1}^{P} \frac{\sum_{m=1}^{M} |w_{oc,m}^p|^2 R_{c,m}^p}{\sum_{m=1}^{M} |w_{oc,m}^p|^2 R_{act,m}^p} \tag{2.32}$$

Differentiating equation 2.32 with respect to $Y_{opt,m}^*$ and setting the partial derivative $\frac{\partial T_{av}}{\partial Y_{opt,m^*}} = 0$ to minimize T_{av}, the multibeam average noise optimal admittance is then given by

$$Y_{opt,m} = \frac{\sum_{p=1}^{P} |w_{oc,m}^p|^2 Z_{act,m}^{p*}}{\sum_{p=1}^{P} |w_{oc,m}^p|^2 |Z_{act,m}^p|^2} \tag{2.33}$$

Using this optimum admittance as a noise matching criteria minimizes the average beam equivalent receiver noise temperature over the P beams constructed by the beamformer weights $[\tilde{\boldsymbol{w}}^p]$. Equation 2.33 can be seen to be directly dependent on the beamformer weights and therefore a beamformer like the maximum SNR beamformer, which is dependent on the matching criteria, cannot be used as there is circularity in determining the parameters. The multibeam average noise optimum admittance can instead be calculated using a different beamforming scheme, such as the conjugate field match (CFM) beamformer, given by

$$[\tilde{\boldsymbol{w}}_{\boldsymbol{oc}}] = [\tilde{\boldsymbol{v}}_{\boldsymbol{sig,oc}}(\boldsymbol{\Omega_s})]$$

The multibeam average optimum receiver noise temperature for a five dipole array steered over angle is shown against the receiver temperatures obtained when matching to either the self impedance or active impedance in figure 2.18, [18].

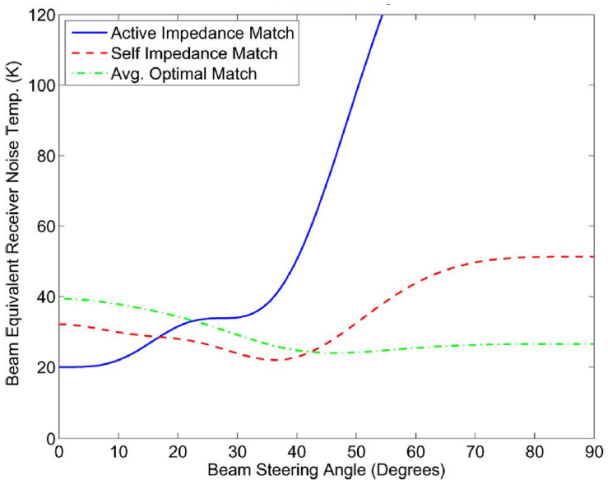

Figure 2.18: Five dipole array receiver noise temperature for the multibeam average optimum vs self impedance and active impedance matching

2.6 Beamformer

For a receiver system, the FoM of interest is not always the noise temperautre of each channel LNA. In many cases the total receiver SNR is of higher importance, as varying levels of noise can be acceptable if the signal of interest is large enough. In order to construct a single output signal, the outputs of each LNA of a receiver are fed into a beamformer. Beamformers act as spacial filters and it is possible that through the choice of beamformer coefficients, the SNR of the received signal can drop to zero, for example, by either scanning into a region with a high power noise source, or through scanning into an area where none of the signal of interest is received by the receiver. Both the signal of interest and any interfering noise signal are subject to weighting via the beamformer. It is thus important to achieve a balance between the signal and noise inputs in order to maximize the SNR. Maximizing the beamformer output SNR is suboptimal in terms of achieving maximum signal gain however. The signal received by an array can be written as the sum of a signal of interest, $[\tilde{\boldsymbol{v}}_{\boldsymbol{s}}]$ and some interfering signal $[\tilde{\boldsymbol{v}}_{\boldsymbol{\eta}}]$ [33]. The signal to noise ratio at the output of the beamformer with coefficients $[\tilde{\boldsymbol{w}}]$ is then given by

$$SNR = \frac{\overline{|[\tilde{\boldsymbol{w}}]^{\dagger}[\tilde{\boldsymbol{v}}_{\boldsymbol{s}}]|^2}}{\overline{|[\tilde{\boldsymbol{w}}]^{\dagger}[\tilde{\boldsymbol{v}}_{\boldsymbol{\eta}}]|^2}} = \frac{[\tilde{\boldsymbol{w}}]^{\dagger}[R_s][\tilde{\boldsymbol{w}}]}{[\tilde{\boldsymbol{w}}]^{\dagger}[R_\eta][\tilde{\boldsymbol{w}}]} \tag{2.34}$$

Where $[R_s]$ and $[R_\eta]$ represent the signal and noise correlation matrices respectively. Maximizing equation 2.34 with respect to $[\tilde{\boldsymbol{w}}]$ leads to

$$[R_\eta]^{-1}[R_s][\tilde{\boldsymbol{w}}] = \lambda_{max}[\tilde{\boldsymbol{w}}]$$

$$\lambda = \frac{[\tilde{\boldsymbol{w}}]^{\dagger}[R_s][\tilde{\boldsymbol{w}}]}{[\tilde{\boldsymbol{w}}]^{\dagger}[R_\eta][\tilde{\boldsymbol{w}}]}$$

As λ is the SNR, the eigenvector of the largest magnitude eigenvalue solves the optimization problem. For $[R_s] = \overline{[\tilde{\boldsymbol{v}}_{\boldsymbol{s}}][\tilde{\boldsymbol{v}}_{\boldsymbol{s}}]^{\dagger}}$, the weights of the maximum SNR beamformer reduce to

$$[\tilde{\boldsymbol{w}}] = [R_{\eta}]^{-1}[\tilde{\boldsymbol{v}}_{\boldsymbol{s}}] \tag{2.35}$$

Chapter 3

Refinements to Circuit Model Solution

In chapters 1 and 2, an overview was given on currently used system models for noisy antenna arrays. All of these models however include some simplifications or assumptions in order to obtain elegant formulations. When working with completely different radiating elements in one array, such as the case for many multi-mode antennas, many of these assumptions can no longer be made. This chapter presents a noise-signal model for a system which can include non-identical antennas as well as non-identical matching networks and LNAs. For verification purposes, both a matrix-based mathematical model and an ADS simulation model are developed.

3.1 Full Circuit System Noise Model

The working of a receiver system can be split into two response models, one model describing the response of the system to an incoming voltage signal in the absence of noise, the other describing the response of the system to the expected noise sources generated by lossy components in the system and external noise sources. These two responses can then be considered as orthogonal responses to determine and design the performance of the system.

In the model proposed here, four second order matching sections, as shown in figure 3.1, are used. To enable exact equations, closed form expressions are derived for each option. The noise model should consider noise contributions from the antenna array source as well as the amplifying section for each matching network topology in a noisy environment. Each of the matching topologies will be considered and a description derived for the Signal-no-Noise and Noise-no-Signal responses of the receiver system. Criteria for the selection of topology will also be given.

A significant advantage of the improved model is the availability of signal voltages and noise voltages at each node in the receiver, so that the SNR and Noise Figure can be analytically determined at each point.

The model also allows for non-identical, non-ideal receiver channels with regards to matching sections, LNAs and loads.

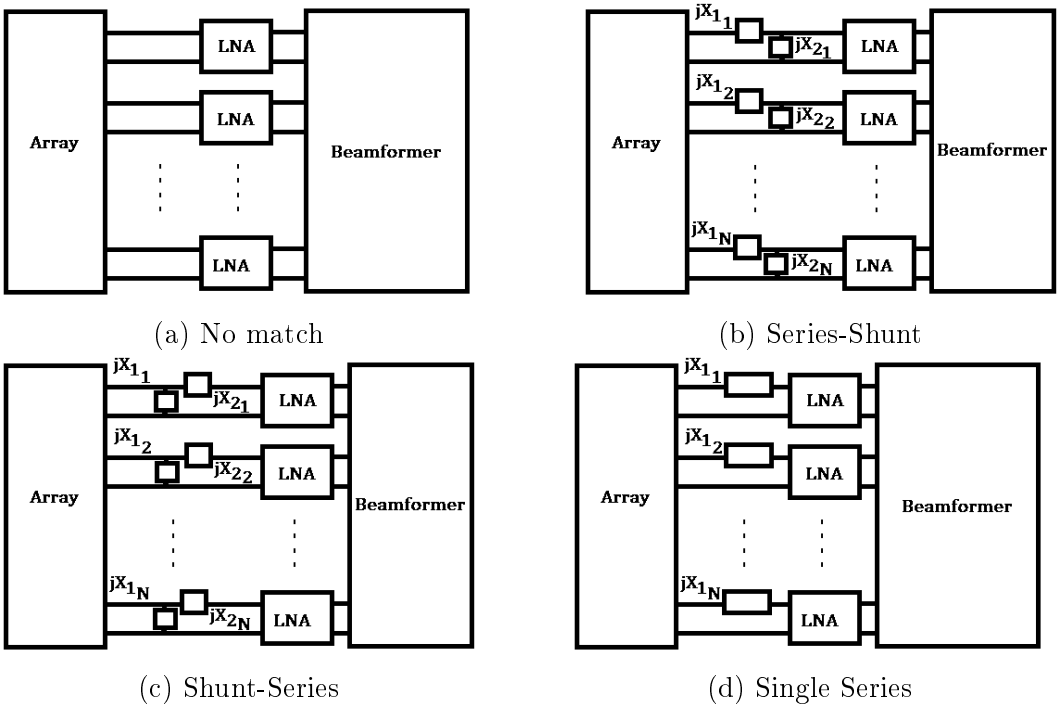

(a) No match

(b) Series-Shunt

(c) Shunt-Series

(d) Single Series

Figure 3.1: Four topologies for matching networks in receiver

The elements of all the matching networks for each channel of the receiver will be designated by diagonal matrices $j[X_{k_d}] = j[B_{k_d}]^{-1}$, where $k = 1$ indicates the element on the antenna side and $k = 2$ indicates the element on the LNA side, as shown in figure 3.1. Subscript m indicates the receiver channel. The diagonal matrices are given by

$$j[X_{k_d}] = j\begin{bmatrix} X_{k_1} & 0 & 0 & \dots & 0 \\ 0 & X_{k_2} & 0 & \dots & 0 \\ 0 & 0 & X_{k_3} & \dots & 0 \\ \vdots & \vdots & \vdots & \ddots & \vdots \\ 0 & 0 & 0 & \dots & X_{k_N} \end{bmatrix}$$

$$j[B_{k_d}] = j\begin{bmatrix} B_{k_1} & 0 & 0 & \dots & 0 \\ 0 & B_{k_2} & 0 & \dots & 0 \\ 0 & 0 & B_{k_3} & \dots & 0 \\ \vdots & \vdots & \vdots & \ddots & \vdots \\ 0 & 0 & 0 & \dots & B_{k_N} \end{bmatrix} = j[X_{k_d}]^{-1}$$

3.1.1 Signal Response Transformaton Matrices for Array with or without Matching Network

For the signal-no-noise case, the noise voltage source is short circuited and the noise current source is open circuited in each channel. The external noise voltage and the array ohmic noise voltage sources are also shorted. With reference to figure 3.2, this corresponds to

$$\begin{aligned} e_{n_m} &= 0 \\ i_{n_m} &= 0 \\ e_{n_{ext_m}} &= 0 \\ e_{n_{ohmic_m}} &= 0 \quad \forall \quad m \in [1, \cdots, N] \end{aligned}$$

One of three topologies for the matching network, or no matching network, is then used. It is necessary to specify that each channel of the receiver has a matching section of the same topology as all the others, even if the stub reactances are allowed to differ. The signal and noise voltage models are then determined as shown in sections 3.1.1 and B.1.

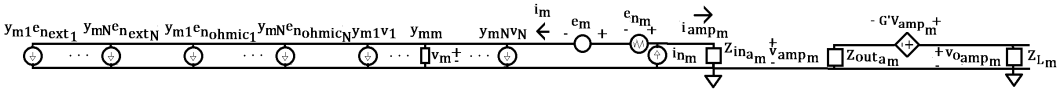

Figure 3.2: Channel m of receiver with noisy source and no matching network

No Matching Network: With reference to figure 3.2, in this simple case we define the auxiliary equations 3.1.

$$i_{s_m} = -Y_{in_{am}} v_{amp_m} \tag{3.1a}$$

$$= \sum_{k=1}^{N} y_{mk} v_{s_k} \tag{3.1b}$$

$$v_{s_m} = v_{amp_m} - e_m \tag{3.1c}$$

Through manipulation of matrices, the auxiliary equations can be rewritten to find the signal voltage at the source port in terms of the open circuit signal voltage in the form

$$\begin{aligned}[\tilde{\boldsymbol{v}}_{\boldsymbol{s}}] &= -\left[[Y] + [Y_{in_{a_d}}]\right]^{-1}[Y_{in_{a_d}}][\tilde{\boldsymbol{e}}_{\boldsymbol{s}}] \\ &= [T_x][\tilde{\boldsymbol{e}}_{\boldsymbol{s}}]\end{aligned} \tag{3.2}$$

At reference line A-A, as seen on figure 3.3, with $[Y]$ the array admittance parameters and $[Y_{in_{a_d}}]$ the $N \times N$ diagonal LNA input admittance matrix, the signal voltage is then given by

$$\begin{aligned}[\tilde{\boldsymbol{v}}_{\boldsymbol{s_{ampm}}}] &= \left[[Y] + [Y_{in_{a_d}}]\right]^{-1}[Y][\tilde{\boldsymbol{e}}_{\boldsymbol{s}}] \\ &= [T_x{}'][\tilde{\boldsymbol{e}}_{\boldsymbol{s}}]\end{aligned} \tag{3.3}$$

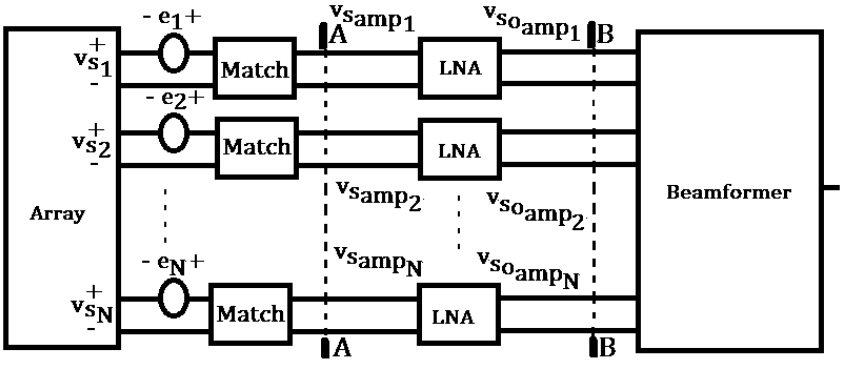

Figure 3.3: Reference line and node voltage names on circuit diagram

The matrix $[T_x]$ effectively transforms the open circuit signal voltage vector $[\tilde{\boldsymbol{e}}_{\boldsymbol{s}}]$ to a loaded signal port voltage at the array terminals and $[T_x{}']$ transforms $[\tilde{\boldsymbol{e}}_{\boldsymbol{s}}]$ to the voltages at the LNA input ports. The signal voltage correlation matrix at the LNA input ports is given by

$$\begin{aligned}[R_{s_{amp}}] &= \overline{[\tilde{\boldsymbol{v}}_{\boldsymbol{s_{ampm}}}][\tilde{\boldsymbol{v}}_{\boldsymbol{s_{ampm}}}]^{\dagger}} \\ &= \overline{\left([T_x{}'][\tilde{\boldsymbol{e}}_{\boldsymbol{s}}]\right)\left([T_x{}'][\tilde{\boldsymbol{e}}_{\boldsymbol{s}}]\right)^{\dagger}} \\ &= [T_x{}'][E_s][T_x{}']^{\dagger}\end{aligned} \tag{3.4}$$

At reference line B-B, the signal voltage response is given by

$$[\tilde{\boldsymbol{v}}_{\boldsymbol{s_{o_{amp}}}}] = [G_{v_d}][T_x{}'][\tilde{\boldsymbol{e}}_{\boldsymbol{s}}] \tag{3.5}$$

where $[G_{v_d}]$ is the diagonal LNA voltage gain matrix. The signal voltage correlation matrix at the beamformer input ports is then given by

$$\begin{aligned}[R_{s_{beam}}] &= \begin{bmatrix} |G_{v_1}|^2\,\overline{|v_{s_{amp_1}}|^2} & \cdots & G_{v_1}{G_{v_N}}^*\,\overline{v_{s_{amp_1}}{v_{s_{amp_N}}}^*} \\ \vdots & \ddots & \vdots \\ G_{v_N}{G_{v_1}}^*\,\overline{v_{s_{amp_N}}{v_{s_{amp_1}}}^*} & \cdots & |G_{v_N}|^2\,\overline{|v_{s_{amp_N}}|^2} \end{bmatrix} \\ &= [G_{v_d}][R_{s_{amp}}][G_{v_d}]^\dagger \end{aligned} \tag{3.6}$$

The derivations for the Series-Shunt, Shunt-Series and Single-Series topology signal transformation matrices at the antenna ports, $[T_x]$, as well as after the matching section, $[T_x']$, follow similarly and are shown in appendix B. For each topology, $[T_x]$ and $[T_x']$ are given as

Series-Shunt Matching Network:

$$[T'_{x_{sesh}}] = \Big[[I] + \big[[I] + j[X_{1_d}][Y]\big][T_x]\Big] \tag{3.7}$$

$$[T_{x_{sesh}}] = -\Big[\big[[Y_{in_{a_d}}] + j[B_{2_d}]\big]\big[[I] + j[X_{1_d}][Y]\big] + [Y]\Big]^{-1}\Big[[Y_{in_{a_d}}] + j[B_{2_d}]\Big] \tag{3.8}$$

Shunt-Series Matching Network:

$$[T'_{x_{shse}}] = [Z_{in_{a_d}}]\big[j[X_{2_d}] + [Z_{in_{a_d}}]\big]^{-1}\big[[T_x] + [I]\big] \tag{3.9}$$

$$\begin{aligned}[T_{x_{shse}}] = &-\Big[[Y] + j[B_{1_d}] + \big[j[X_{2_d}] + [Z_{in_{a_d}}]\big]^{-1}\Big]^{-1} \\ &\Big[\big[j[X_{2_d}] + [Z_{in_{a_d}}]\big]^{-1} + j[B_{1_d}]\Big]\end{aligned} \tag{3.10}$$

Single-Series Matching Network:

$$[T'_{x_{sse}}] = \Big[[I] + \big[[I] + j[X_{1_d}][Y]\big][T_x]\Big] \tag{3.11}$$

$$[T_{x_{sse}}] = -\Big[[Y_{in_{a_d}}]\big[[I] + j[X_{1_d}][Y]\big] + [Y]\Big]^{-1}[Y_{in_{a_d}}] \tag{3.12}$$

3.1.2 Noise Response Transformation Matrices for Array with or without Matching Network

For the noise-no-signal case, with the receiver model as shown in figure 3.2, for each channel the signal voltage source is shorted. This corresponds to

$$e_m = 0 \quad \forall \quad m \in [1, \cdots, N]$$

To determine the noise generated by a single noisy antenna element, an antenna model as shown in figure 3.4 is used.

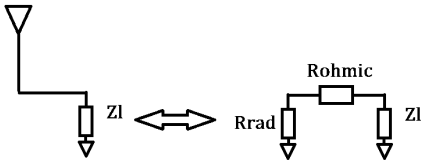

Figure 3.4: Radiating antenna model

The antenna resistance is made up of a radiation resistance, R_{rad}, and an Ohmic loss resistance, R_{ohmic}. The loss resistance can be determined for any given antenna and in the case of a dipole antenna, [34], is given by

$$R_{ohmic} = \frac{l\rho_{dipole}}{A} \tag{3.13}$$

where ρ_{dipole} is the resistivity of the dipole antenna material, l the dipole length and A the cross section area of the circumference of the dipole. The expected value of the equivalent noise voltage source is then given by

$$\overline{|e_{n_{ohmic}}|^2} = 4k_B T B R_{ohmic} \tag{3.14}$$

In a coupled array, the correlation between the ohmic noise voltage sources of each channel is such that the correlation matrix of the noise voltage sources is given by Twiss's Theorem. It can be assumed that the receiver will operate in the presence of an external noise source which is spatially variant over ϕ and θ. It can be shown [34] that the voltage correlation matrix of this external noise at the antenna ports can be written in terms of the radiation resistance matrix of the antenna, with $[R_{rad}] = \Re\{[Z_A]\} - [R_{A,loss}]$.

$$[E_{ext}] = 4k_B T_{ext}(\phi, \theta) B [R_{rad}] \tag{3.15}$$

Many models exist for T_{ext}. In this work it will be assumed constant over θ, ϕ. Similarly than in section 3.1.1, one of three topologies for the matching network, or no matching network, is then used. The noise voltage models, with the antenna array noise souce included are then determined as shown in sections 3.1.2 and B.2.

No Matching Network: The noisy array and environment are represented by a quiet array with N ohmic loss and N external noise current sources added to the N source ports of the array channels. The total noise current added to the m-th channel is given by

$$i_{n_{s_m}} = \sum_{k=1}^{N} y_{mk}(e_{n_{ohmic_k}} + e_{n_{ext_k}}) \tag{3.16}$$

The circuit model for the m-th channel of the receiver is shown in figure 3.2. The source port noise voltages can be determined using auxiliary equations for each of the N channels. The auxiliary equations for the m-th channel of the receiver model are given by equations 3.17. ${v_{n_m}}'$ is defined at the negative terminal of e_{n_m} and because there is no matching network, ${v_{n_m}}' = v_{n_m}$

$$i_{n_{s_m}} = i_{n_m} - Y_{in_{a_m}} e_{n_m} - Y_{in_{a_m}} {v_{n_m}}' \tag{3.17a}$$

$$= \sum_{k=1}^{N} y_{mk}(v_{n_k} + e_{n_{ohmic_k}} + e_{n_{ext_k}}) \tag{3.17b}$$

$$v_{n_m} = v_{amp_m} - e_{n_m} \tag{3.17c}$$

Equations 3.17 can then be combined and manipulated for all N channels in matrix form to solve simultaneously for the source port noise voltages.

$$\begin{aligned}[\tilde{\boldsymbol{v}}_{\boldsymbol{n}}] &= \Big[[Y]+[Y_{in_{a_d}}]\Big]^{-1}[\boldsymbol{i_n} - \tilde{\boldsymbol{y}}_{\boldsymbol{in_a}} \boldsymbol{e_n}] - \Big[[Y] + [Y_{in_{a_d}}]\Big]^{-1}[Y]\big[[\tilde{\boldsymbol{e}}_{\boldsymbol{n_{ohmic}}}]+[\tilde{\boldsymbol{e}}_{\boldsymbol{n_{ext}}}]\big] \\ &= [T_z][\tilde{\boldsymbol{i}}_{\boldsymbol{x}}] + [T_s]\big[[\tilde{\boldsymbol{e}}_{\boldsymbol{n_{ohmic}}}] + [\tilde{\boldsymbol{e}}_{\boldsymbol{n_{ext}}}]\big]\end{aligned} \tag{3.18}$$

In equation 3.18, the matrix $[Y_{in_{a_d}}]$ represents the $N \times N$ diagonal matrix which has each entry on its diagonal equal to the m-th input LNA admittance, $Y_{in_{a_m}}$. The matrices $[T_z]$ and $[T_s]$ respectively transform the equivalent LNA input port noise current, $[\tilde{\boldsymbol{i}}_{\boldsymbol{x}}]$ and antenna ohmic losses, $[\tilde{\boldsymbol{e}}_{\boldsymbol{n_{ohmic}}}]$, to source port noise voltages. The noise voltages and currents are zero-mean random processes however, and therefore it is more convenient to do noise calculations through use of the corresponding correlation matrices and the expected values of the square of the voltage and current sources. The noise voltage correlation matrix at the source port is then calculated as shown in equation 3.19 with the source noise voltage source uncorrelated with the LNA noise voltage and current sources.

$$
\begin{aligned}
[R_n] &= \begin{bmatrix} \overline{|v_{n_1}|^2} & \overline{v_{n_1} {v_{n_2}}^*} & \cdots & \overline{v_{n_1} {v_{n_N}}^*} \\ \overline{v_{n_2} {v_{n_1}}^*} & \overline{|v_{n_2}|^2} & \cdots & \overline{v_{n_2} {v_{n_N}}^*} \\ \vdots & \vdots & \ddots & \vdots \\ \overline{v_{n_N} {v_{n_1}}^*} & \overline{v_{n_N} {v_{n_2}}^*} & \cdots & \overline{|v_{n_N}|^2} \end{bmatrix} \\
&= \overline{[\tilde{\boldsymbol{v}}_{\boldsymbol{n}}][\tilde{\boldsymbol{v}}_{\boldsymbol{n}}]^\dagger} \\
&= \overline{\left([T_z][\tilde{\boldsymbol{i}}_{\boldsymbol{x}}] + [T_s]\left[[\tilde{\boldsymbol{e}}_{\boldsymbol{n_{ohmic}}}] + [\tilde{\boldsymbol{e}}_{\boldsymbol{n_{ext}}}]\right]\right)\left([T_z][\tilde{\boldsymbol{i}}_{\boldsymbol{x}}] + [T_s]\left[[\tilde{\boldsymbol{e}}_{\boldsymbol{n_{ohmic}}}] + [\tilde{\boldsymbol{e}}_{\boldsymbol{n_{ext}}}]\right]\right)^\dagger} \\
&= \overline{[T_z][\tilde{\boldsymbol{i}}_{\boldsymbol{x}}][\tilde{\boldsymbol{i}}_{\boldsymbol{x}}]^\dagger [T_z]^\dagger + [T_z][\tilde{\boldsymbol{i}}_{\boldsymbol{x}}]\left[[\tilde{\boldsymbol{e}}_{\boldsymbol{n_{ohmic}}}] + [\tilde{\boldsymbol{e}}_{\boldsymbol{n_{ext}}}]\right]^\dagger [T_s]^\dagger} \\
&+ [T_s]\left[[\tilde{\boldsymbol{e}}_{\boldsymbol{n_{ohmic}}}] + [\tilde{\boldsymbol{e}}_{\boldsymbol{n_{ext}}}]\right][\tilde{\boldsymbol{i}}_{\boldsymbol{x}}]^\dagger [T_z]^\dagger + [T_s]\left[[\tilde{\boldsymbol{e}}_{\boldsymbol{n_{ohmic}}}] + [\tilde{\boldsymbol{e}}_{\boldsymbol{n_{ext}}}]\right][\tilde{\boldsymbol{e}}_{\boldsymbol{n_{ohmic}}}]^\dagger [T_s]^\dagger \\
&= [T_z][I_x][T_z]^\dagger + [T_s]\left[[E_x] + [E_{ext}]\right][T_s]^\dagger
\end{aligned}
\tag{3.19}
$$

The expected value of the noise voltage at each source port is given by the square root of the diagonal of the noise voltage correlation matrix as shown in 3.19, with $[I_x]$ being the diagonal LNA input port noise current correlation matrix given in terms of the m-th channel correlation admittance Y_{c_m} and uncorrelated noise current i_{u_m} from equations 2.9 and 2.10, by

$$
[I_x] = \begin{bmatrix} |Y_{c_1} - Y_{in_{a_1}}|^2 \overline{|e_{n_1}|^2} + \overline{|i_{u_1}|^2} & \cdots & 0 \\ \vdots & \ddots & \vdots \\ 0 & \cdots & |Y_{c_N} - Y_{in_{a_N}}|^2 \overline{|e_{n_N}|^2} + \overline{|i_{u_N}|^2} \end{bmatrix} \tag{3.20}
$$

$[E_x]$ represents the noise voltage source correlation matrix and is determined through Twiss's Theorem as shown in equation 3.21, [35], with $[Z]$ representing the impedance parameters of the antenna array. For each port, the expected value of the port noise voltage collapses to equation 3.14, while for reciprocal arrays, the correlation matrix $[E_x]$ will be purely real.

$$
[E_x] = 2k_B T B\left[[Z] + [Z]^\dagger\right] \tag{3.21}
$$

At the input ports of the LNA for the m-th channel, the noise voltage is given by $v_{n_{amp_m}} = v_{n_m} + e_{n_m}$. The noise correlation matrix at the input ports of the LNA sections is given by equation 3.28, with the entries of $[R_{n_{amp}}{}']$ the same as in the case of a noiseless source, given by

$$[R_{n_{amp}}{}'] = \begin{bmatrix} \overline{|v_{n_{amp_1}}|^2} & \overline{v_{n_{amp_1}} v_{n_{amp_2}}{}^*} & \cdots & \overline{v_{n_{amp_1}} v_{n_{amp_N}}{}^*} \\ \overline{v_{n_{amp_2}} v_{n_{amp_1}}{}^*} & \overline{|v_{n_{amp_2}}|^2} & \cdots & \overline{v_{n_{amp_2}} v_{n_{amp_N}}{}^*} \\ \vdots & \vdots & \ddots & \vdots \\ \overline{v_{n_{amp_N}} v_{n_{amp_1}}{}^*} & \overline{v_{n_{amp_N}} v_{n_{amp_2}}{}^*} & \cdots & \overline{|v_{n_{amp_N}}|^2} \end{bmatrix} \tag{3.22}$$

For the entries of equation 3.22,

$$\overline{v_{n_{amp_m}} v_{n_{amp_k}}{}^*} = \overline{v_{n_m} v_{n_k}{}^*} + 2\Re\{\overline{v_{n_m} e_{n_k}{}^*}\} + \overline{e_{n_m} e_{n_k}{}^*} \tag{3.23}$$

$$\overline{v_{n_m} v_{n_k}{}^*} = T_{z_{m1}} T_{z_{k1}}{}^* I_{x_{11}} + \cdots + T_{z_{mN}} T_{z_{kN}}{}^* I_{x_{NN}} \tag{3.24}$$

$$\overline{v_{n_m} e_{n_k}{}^*} = T_{z_{mk}} (Y_{c_k} - Y_{in_{a_k}}) \overline{|e_{n_k}|^2} \tag{3.25}$$

$$\overline{e_{n_m} e_{n_k}{}^*} = 0, \qquad (m \neq k) \tag{3.26}$$

So that with $[E_n] = \overline{[\tilde{\boldsymbol{e}}_{\boldsymbol{n}}][\tilde{\boldsymbol{e}}_{\boldsymbol{n}}]^\dagger}$ for a lossless, reciprocal antenna in a noiseless environment,

$$[R_{n_{amp}}{}'] = [T_z][I_x][T_z]^\dagger + \Big[[I] + 2\Re\Big\{[T_z]\big[[Y_{c_d}] - [Y_{in_{a_d}}]\big]\Big\}\Big][E_n] \tag{3.27}$$

With ohmic losses in the antenna and external noise considered, the LNA input noise correlation matrix is given by

$$\begin{aligned} [R_{n_{amp}}] &= \overline{[\tilde{\boldsymbol{v}}_{\boldsymbol{n_{amp_m}}}][\tilde{\boldsymbol{v}}_{\boldsymbol{n_{amp_m}}}]^\dagger} \\ &= \overline{\Big([T_z][\tilde{\boldsymbol{i}}_{\boldsymbol{x}}] + [T_s]\big[[\tilde{\boldsymbol{e}}_{\boldsymbol{n_{ohmic}}}] + [\tilde{\boldsymbol{e}}_{\boldsymbol{n_{ext}}}]\big] + [\tilde{\boldsymbol{e}}_{\boldsymbol{n}}]\Big)} \\ &\quad \overline{\Big([T_z][\tilde{\boldsymbol{i}}_{\boldsymbol{x}}] + [T_s]\big[[\tilde{\boldsymbol{e}}_{\boldsymbol{n_{ohmic}}}] + [\tilde{\boldsymbol{e}}_{\boldsymbol{n_{ext}}}]\big] + [\tilde{\boldsymbol{e}}_{\boldsymbol{n}}]\Big)^\dagger} \\ &= [R_{n_{amp}}{}'] + [T_s]\big[[E_x] + [E_{ext}]\big][T_s]^\dagger \\ &= [R_{n_{amp}}{}'] + [R_{n_{ohmic}}] + [R_{n_{ext}}] \end{aligned} \tag{3.28}$$

The beamformer input noise voltage correlation matrix is then determined similarly as in equations 3.22 to 3.26 and shown in equation 3.29, with $[G_{v_d}]$ the diagonal LNA voltage gain matrix.

$$\begin{aligned} [R_{n_{beam}}] &= \begin{bmatrix} |G_{v_1}|^2 \overline{|v_{n_{amp_1}}|^2} & \cdots & G_{v_1} G_{v_N}{}^* \overline{v_{n_{amp_1}} v_{n_{amp_N}}{}^*} \\ \vdots & \ddots & \vdots \\ G_{v_N} G_{v_1}{}^* \overline{v_{n_{amp_N}} v_{n_{amp_1}}{}^*} & \cdots & |G_{v_N}|^2 \overline{|v_{n_{amp_N}}|^2} \end{bmatrix} \\ &= [G_{v_d}][R_{n_{amp}}][G_{v_d}]^\dagger \end{aligned} \tag{3.29}$$

The derivations for the Series-Shunt, Shunt-Series and Single-Series topology noise transformation matrices at the antenna ports, $[T_z]$ and $[T_s]$, as well as after the matching section, $[T_z']$ and $[T_s']$, follow similarly and are shown in appendix B. For each topology, $[T_z]$, $[T_s]$, $[T_z']$ and $[T_s']$ are given as

Series-Shunt Matching Network:

$$[T_{z_{sesh}}] = [Z]\Big[[I]-\big[[Y_{in_{a_d}}]+j[B_{2_d}]\big]\big[T'_{z_{sesh}}\big]\Big] \tag{3.30}$$

$$[T'_{z_{sesh}}] = \Big[j[Y][X_{1_d}]\big[[Y_{in_{a_d}}]+j[B_{2_d}]+j[B_{1_d}]\big]+j[B_{2_d}]+[Y_{in_{a_d}}]\Big]^{-1} \Big[[I]+j[Y][X_{1_d}]\Big] \tag{3.31}$$

$$[T_{s_{sesh}}] = -\Big[[I]+[Z]\big[[Y_{in_{a_d}}]+j[B_{2_d}]\big]\big[T'_{s_{sesh}}\big]\Big] \tag{3.32}$$

$$[T'_{s_{sesh}}] = -\Big[j[Y][X_{1_d}]\big[[Y_{in_{a_d}}]+j[B_{2_d}]+j[B_{1_d}]\big]+j[B_{2_d}]+[Y_{in_{a_d}}]\Big]^{-1}[Y] \tag{3.33}$$

Shunt-Series Matching Network:

$$[T_{z_{shse}}] = \big[[Y]+j[B_{1_d}]\big]^{-1}\big[[I]-[Y_{in_{a_d}}][T'_{z_{shse}}]\big] \tag{3.34}$$

$$[T'_{z_{shse}}] = \Big[j\big[[Y]+j[B_{1_d}]\big][X_{2_d}]\big[[Y_{in_{a_d}}]+j[B_{2_d}]\big]+[Y_{in_{a_d}}]\Big]^{-1} \Big[[I]+j\big[[Y]+j[B_{1_d}]\big][X_{2_d}]\Big] \tag{3.35}$$

$$[T_{s_{shse}}] = -\big[[Y]+j[B_{1_d}]\big]^{-1}\big[[Y]+[Y_{in_{a_d}}][T'_{s_{shse}}]\big] \tag{3.36}$$

$$[T'_{s_{shse}}] = -\Big[j\big[[Y]+j[B_{1_d}]\big][X_{2_d}]\big[[Y_{in_{a_d}}]+j[B_{2_d}]\big]+[Y_{in_{a_d}}]\Big]^{-1}[Y] \tag{3.37}$$

Single-Series Matching Network:

$$[T_{z_{sse}}] = [Z]\big[[I]-[Y_{in_{a_d}}][T'_{z_{sse}}]\big] \tag{3.38}$$

$$[T'_{z_{sse}}] = \Big[j[Y][X_{1_d}]\big[[Y_{in_{a_d}}]+j[B_{1_d}]\big]+[Y_{in_{a_d}}]\Big]^{-1}\big[[I]+j[Y][X_{1_d}]\big] \tag{3.39}$$

$$[T_{s_{sse}}] = -[Z]\big[[Y]+[Y_{in_{a_d}}][T'_{s_{sse}}]\big] \tag{3.40}$$

$$[T'_{s_{sse}}] = -\Big[j[Y][X_{1_d}]\big[[Y_{in_{a_d}}]+j[B_{1_d}]\big]+[Y_{in_{a_d}}]\Big]^{-1}[Y] \tag{3.41}$$

3.2 ADS Simulation Model

All theoretical models were confirmed using the Keysight Technologies Advanced Design System 2016.01 (ADS). Modeling in ADS allowed for the use of non-ideal elements and elements that are unique between receiver channels. ADS also allows for a node signal and noise voltage analysis. ADS was therefore a suitable software to test the accuracy of the transformation matrix based model that incorporates unique and non-ideal elements. Figure 3.5 shows a full view of the circuit model in ADS for the Series-Shunt topology. Section 3.2.1 describes the implementation in detail.

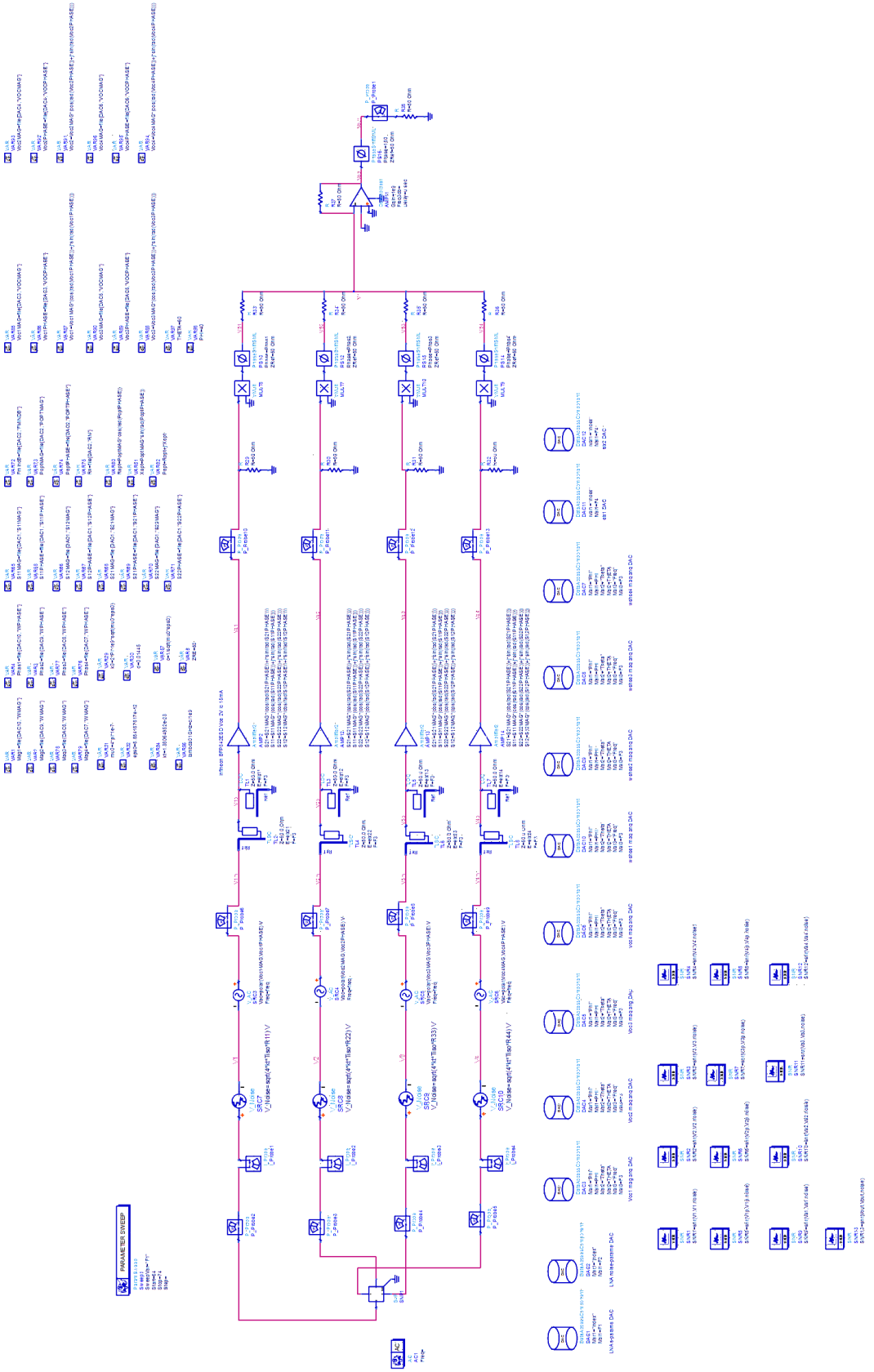

Figure 3.5: ADS model for Series-Shunt topology

3.2.1 ADS Model Implementation

An AC simulation is performed between $f = 5$ GHz and $f = 6$ GHz to simulate the receiver network behavior for a four antenna array. The network can be broken down into four distinct sections, namely

- Antenna array source
- Matching section
- Amplifier stage
- Beamformer

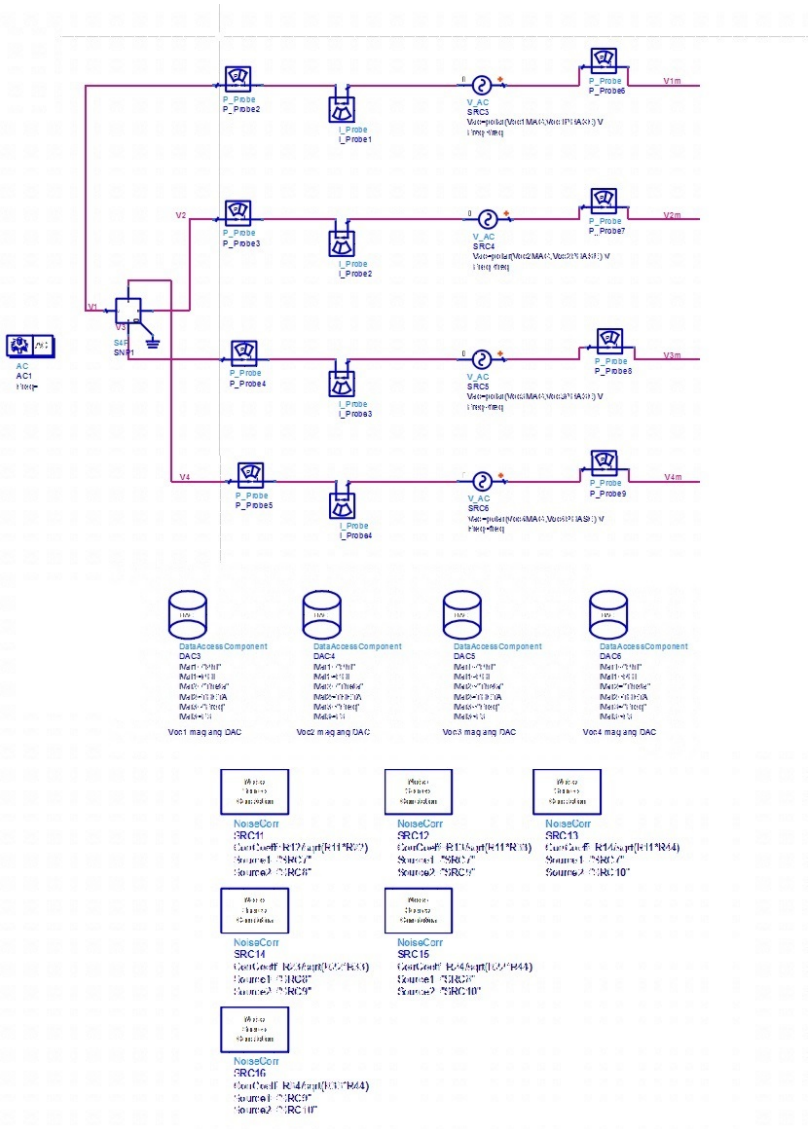

Figure 3.6: Coupled four-port source array

Coupled Noisy Source Array A four port S-parameter touchstone file is read through a Data Access Component (DAC) and interpolated linearly over the simulation frequency range as shown in figure 3.6. The S-parameter block is simulated at a temperature of $T_0 = 290$ K. The external noise is simulated by adding correlated noise voltage sources in series to each port. The open circuit signal voltage is read per channel from MDIF files through DACs. Voltage nodes, power probes and current probes are defined for each node. At each node the node noise voltage is also requested.

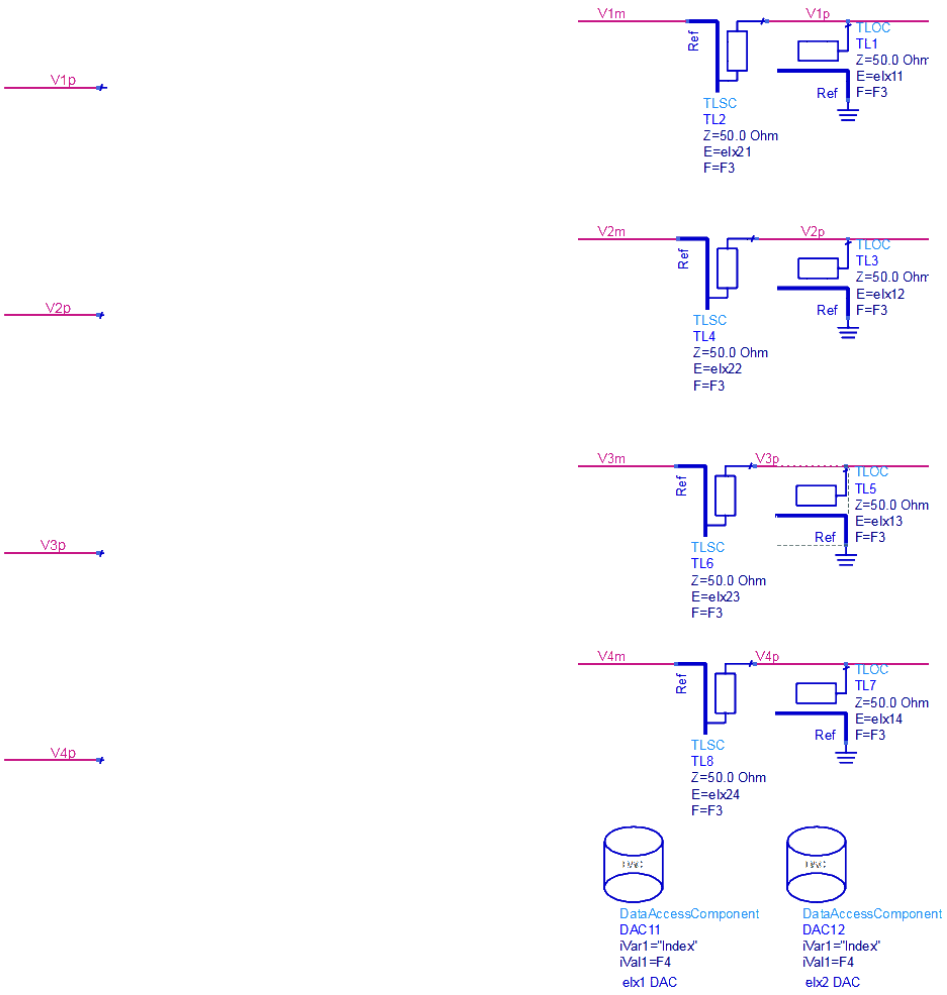

(a) No match (b) Series-Shunt

Figure 3.7: Four topologies for matching networks in ADS model

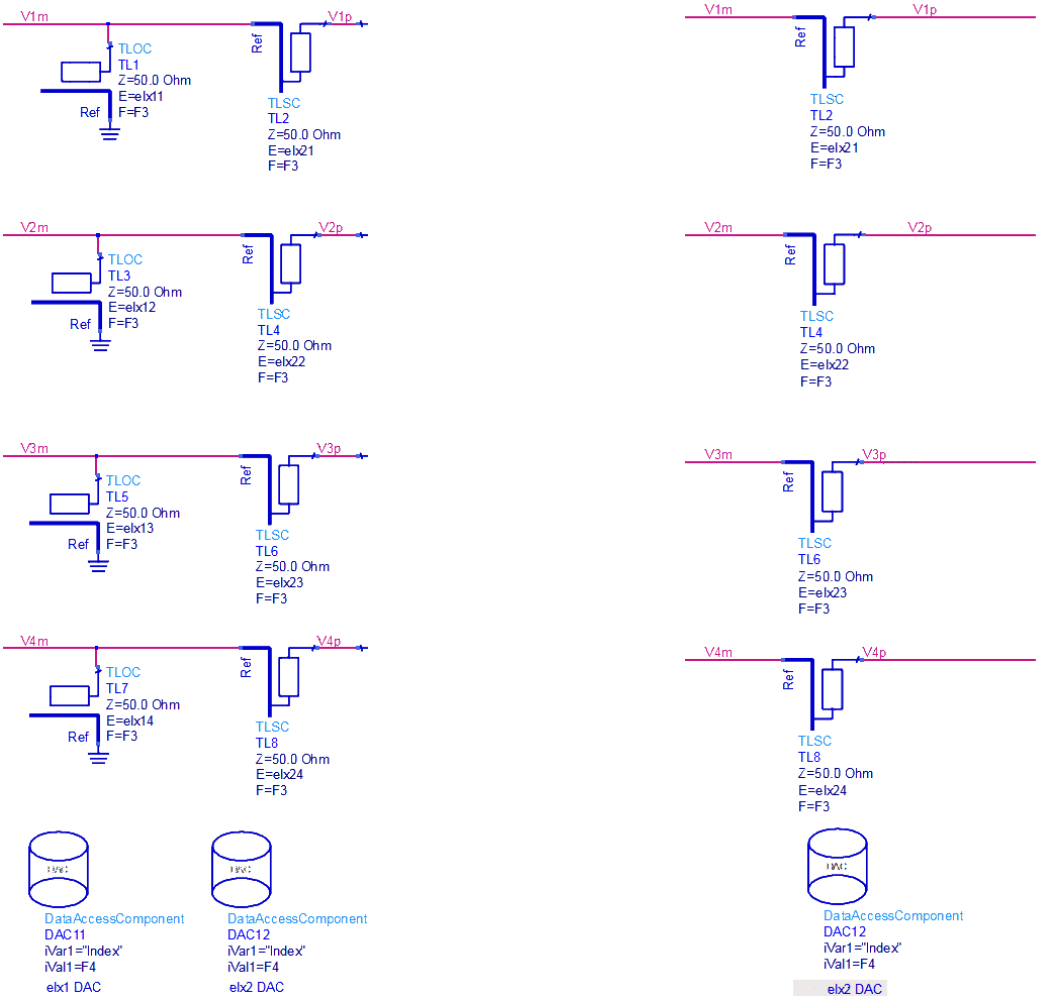

(c) Shunt-Series (d) Single Series

Figure 3.7: Four topologies for matching networks in ADS model

Matching Section Figure 3.7 shows the matching network implementation for each topology in ADS. In each topology, the series stub is implemented with a short circuited series stub and the shunt stub is implemented with an open circuited shunt stub. This is so that no short circuited path between the LNA and ground is created at DC and that no open circuit is created in series. The reactance of each stub is read through a Discrete format text file into a DAC.

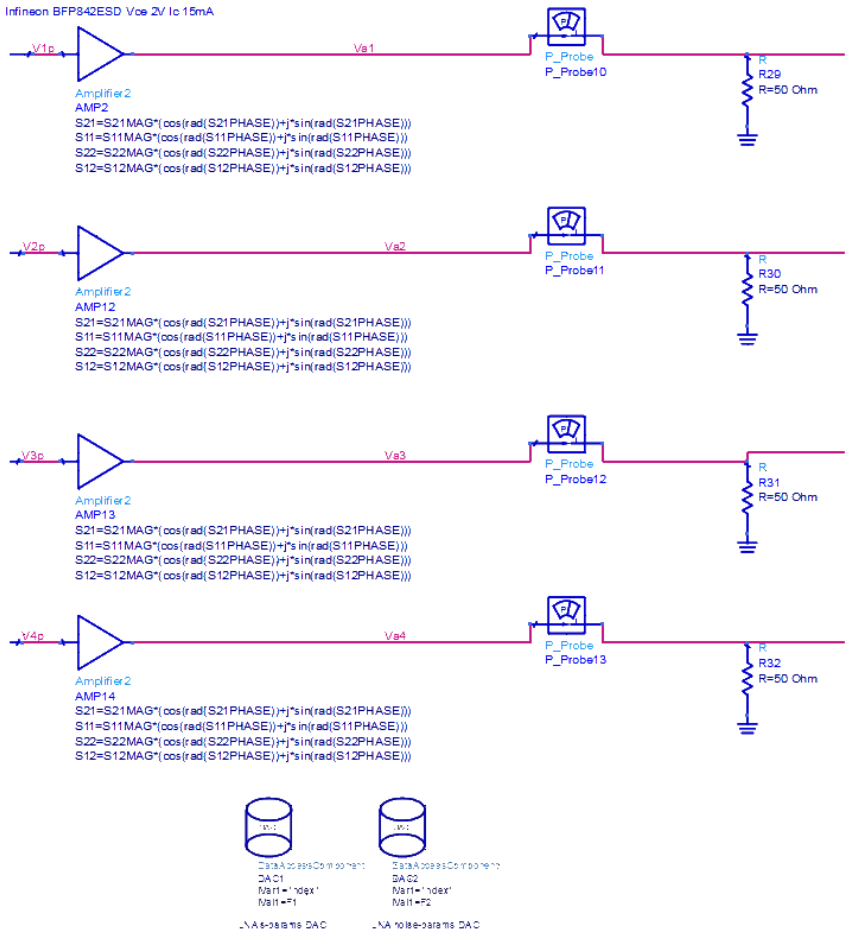

Figure 3.8: LNA section in ADS for each channel

LNA Stage Figure 3.8 shows the LNA section implementation in ADS. For each channel an identical amplifier, the Infineon BFP842ESD, is used. The LNA S-parameters and noise parameters are taken from supplier model files at a bias point of $V_{CE} = 2$ V, $I_C = 15$ mA. The parameters are read from Discrete format text files into DACs. The noise voltages are requested at the nodes before and after each LNA. A load impedance of $Z_L = 50\ \Omega$ is used to terminate each LNA. While identical amplifiers and loads are used in the simulation, this is not required for the simulation to run.

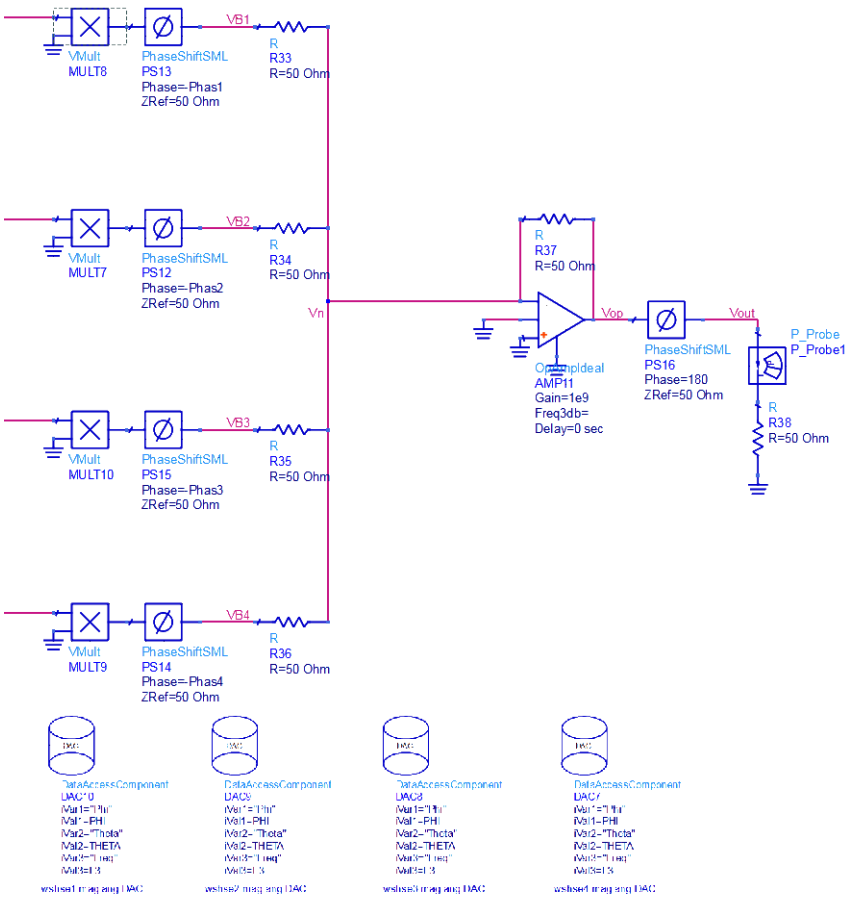

Figure 3.9: LNA beamformer implementation

Beamformer Figure 3.9 shows the implementation of the beamformer in ADS. The beamformer consists of a voltage multiplier, a 180° phase shifter and an ideal summing op-amp. The voltage multiplier has an input impedance of $Z_{in} = 50$ TΩ in parallel with the load impedance of $Z_L = 50$ Ω in order to sample the amplifier output voltage without effectively changing the load impedance. The beamformer weight coefficients are read in through DACs from MDIF format text files and converted to match the block input format. The 180° phase shifter is used to compensate for the negative sign in the output voltage of the ideal summing op-amp. The ideal summing op-amp implements the equation, [36],

$$V_{out} = -\left(\frac{R_f}{R_1}V_1 + \frac{R_f}{R_2}V_2 + \cdots + \frac{R_f}{R_N}V_N\right)$$

Where R_f is the feedback resistor, R_m is the resistor of the m-th branch connected to the op-amp inverting input and V_m is the voltage over R_m. At the inverting input, $V^- = V^+ = 0$ V. With $R_1 = R_2 = \cdots = R_N = R_f$, the

output voltage is thus given by the negative of the sum of the negative channel LNA output voltages scaled by the beamforming coefficients. The beamformer load impedance is given by $Z_{L_{beam}} = 50\ \Omega$.

3.2.2 Comparison Between ADS Model and Theoretical Model Using Transformation Matrices

To evaluate the equivalence of the ADS circuit model to the theoretical model, the antenna port, beamformer input port and beamformer output port signal and noise voltages must be equal. Finally, the models must also produce the same SNR at the output of the beamformer. A comparison between the theoretical model and ADS simulation signal and noise node voltages is performed for a signal source at $\phi = 52°$, $\theta = 42°$. The ratios between the calculated and simulated values are shown in tables 3.1 and 3.2.

Calculated vs Simulated Noise Voltages [V] at $f = 5.5$ GHz

	Cal Ch. 1	Sim Ch.1
Array Port (V_{m_q})	6.341e-6	6.341e-6
Post Amplifier (V_{a_m})	2.199e-5	2.199e-5
	Cal Ch. 2	Sim Ch.2
Array Port (V_{m_q})	6.340e-6	6.340e-6
Post Amplifier (V_{a_m})	2.199e-5	2.199e-5
	Cal Ch. 3	Sim Ch.3
Array Port (V_{m_q})	6.339e-6	6.339e-6
Post Amplifier (V_{a_m})	2.197e-5	2.197e-5
	Cal Ch. 4	Sim Ch.4
Array Port (V_{m_q})	6.339e-6	6.339e-6
Post Amplifier (V_{a_m})	2.198e-5	2.198e-5

Table 3.1: Comparison between node noise voltages for ADS simulation and model calculations

The beamformer output noise voltage for both the calculated and simulated cases is given by $v_{out} = 2.015\text{e}6$ V. The ADS model implements the external noise source as a series voltage source while the mathematical model implements it as a parallel current source. In order to verify the simulation model at the correct node, the noise voltage must therefore be simulated after the series noise voltage source (node V_{m_q}) as opposed to before (node V_m).

Calculated vs Simulated Signal Voltages [V] at $f = 5.5$ GHz

	Cal Ch. 1	Sim Ch.1
Array Port (V_m)	$1.623\angle 125.13°$	$1.623\angle 125.13°$
Pre Amplifier (V_{m_p})	$1.753\angle -126.51°$	$1.753\angle -126.51°$
Post Amplifier (V_{a_m})	$6.550\angle -113.77°$	$6.550\angle -113.77°$
	Cal Ch. 2	Sim Ch.2
Array Port (V_m)	$8.513\angle 164.12°$	$8.513\angle 164.12°$
Pre Amplifier (V_{m_p})	$4.675\angle -70.19°$	$4.675\angle -70.19°$
Post Amplifier (V_{a_m})	$17.462\angle -57.46°$	$17.462\angle -57.46°$
	Cal Ch. 3	Sim Ch.3
Array Port (V_m)	$7.520\angle -33.05°$	$7.520\angle -33.05°$
Pre Amplifier (V_{m_p})	$3.533\angle 105.65°$	$3.533\angle 105.65°$
Post Amplifier (V_{a_m})	$13.196\angle 118.39°$	$13.196\angle 118.39°$
	Cal Ch. 4	Sim Ch.4
Array Port (V_m)	$7.965\angle -11.26°$	$7.965\angle -11.26°$
Pre Amplifier (V_{m_p})	$4.100\angle 114.89°$	$4.100\angle 114.89°$
Post Amplifier (V_{a_m})	$15.316\angle 127.62°$	$15.316\angle 127.62°$

Table 3.2: Comparison between node signal voltages for ADS simulation and model calculations

For both the calculated and simulated case, the beamformer output signal voltage is given by $v_{out} = 2.396\text{e}12\angle 0°$ V. The magnitude of both the output signal and noise voltages are very large due to the large magnitude of the beamformer coefficients. In order to achieve output voltages and powers in orders of magnitude that processors such as Field Programmable Gate Arrays (FPGAs) can handle, the beamformer coefficients can be scaled by orders of magnitude, eg $[\tilde{\boldsymbol{w}}'] = A[\tilde{\boldsymbol{w}}]$, $A = 1 \times 10^{-12}$. As this scaling factor is applied to both the signal and noise voltages, it would not change the ratio and thus the output SNR will stay the same. Figures 3.10 to 3.13 show a comparison of the calculated and simulated noise voltages at each node and figures 3.14 to 3.17 show a comparison of the calculated and simulated signal voltages at each node. The black line is the calculated model response while the coloured lines are the ADS simulated response. The red line shows the design done at $f = 5$ GHz, the blue line at $f = 5.5$ GHz and the purple line at $f = 6$ GHz.

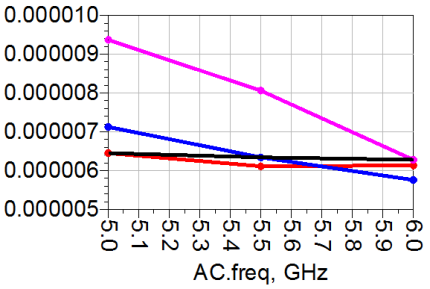

(a) Channel 1

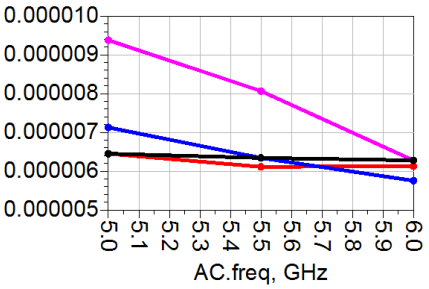

(b) Channel 2

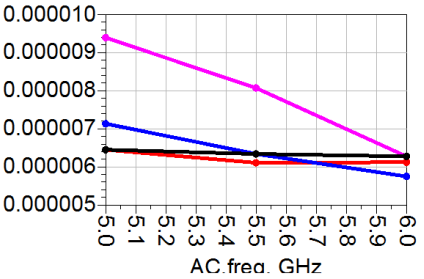

(c) Channel 3

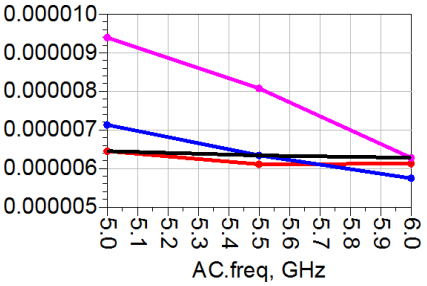

(d) Channel 4

Figure 3.10: Calculated (black) and simulated (coloured) noise voltages for each channel at array ports

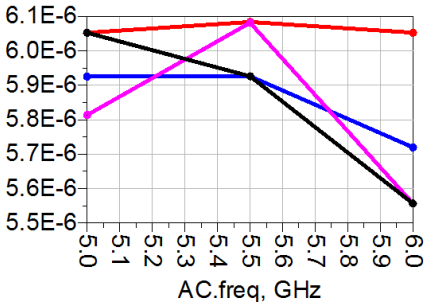

(a) Channel 1

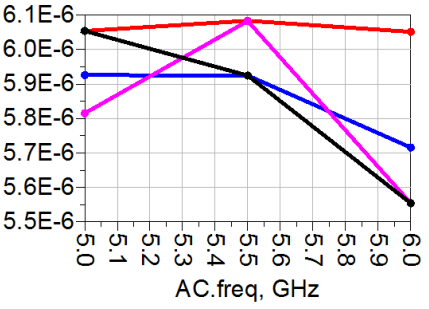

(b) Channel 2

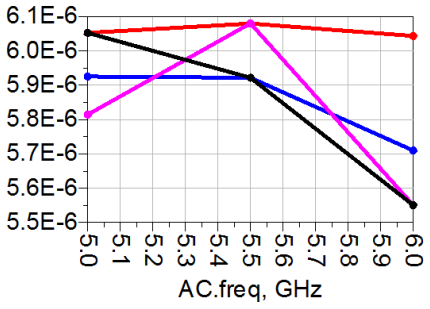

(c) Channel 3

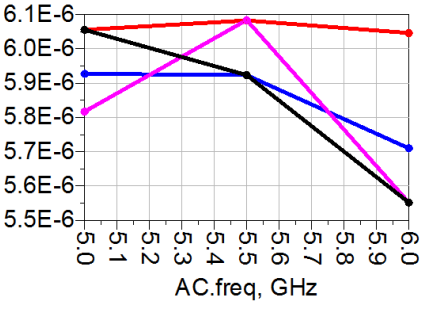

(d) Channel 4

Figure 3.11: Calculated (black) and simulated (coloured) noise voltages [V] for each channel after matching sections

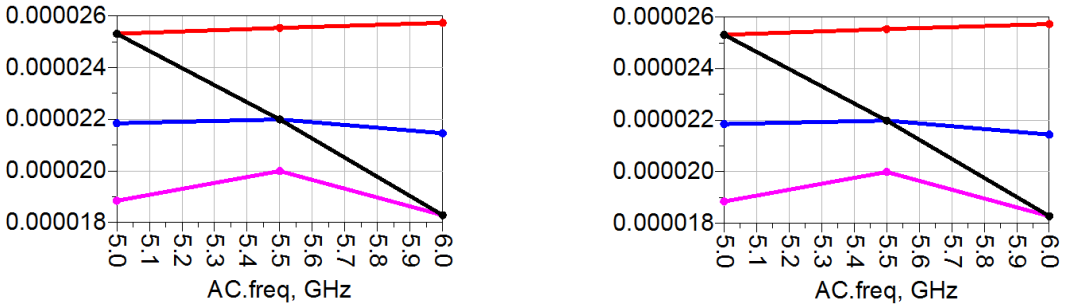

(a) Channel 1

(b) Channel 2

(c) Channel 3

(d) Channel 4

Figure 3.12: Calculated (black) and simulated (coloured) noise voltages [V] for each channel at the LNA outputs

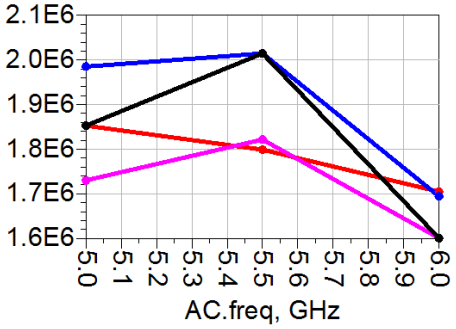

Figure 3.13: Calculated (black) and simulated (coloured) noise voltages [V] at beamformer output

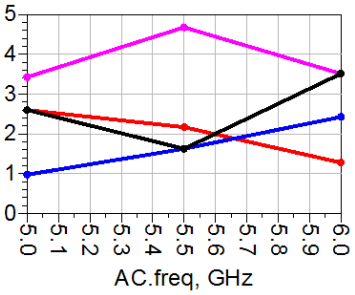

(a) Channel 1

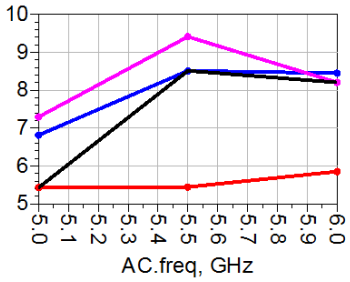

(b) Channel 2

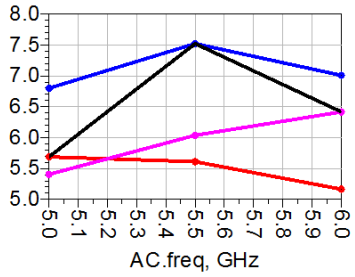

(c) Channel 3

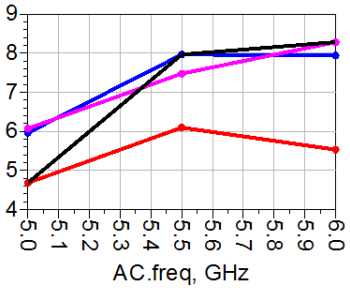

(d) Channel 4

Figure 3.14: Calculated (black) and simulated (coloured) signal voltages [V] for each channel at array ports

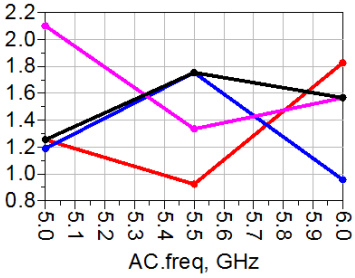

(a) Channel 1

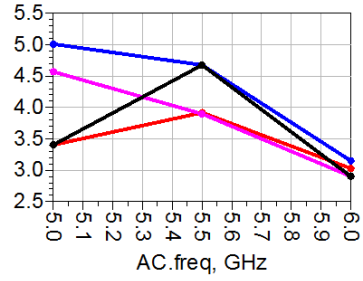

(b) Channel 2

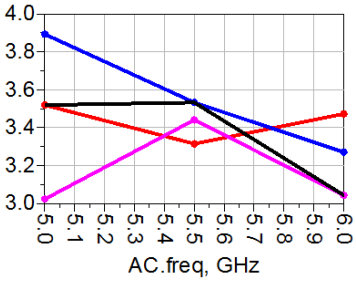

(c) Channel 3

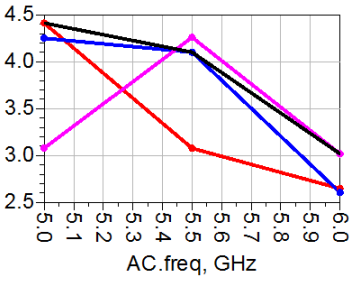

(d) Channel 4

Figure 3.15: Calculated (black) and simulated (coloured) signal voltages [V] for each channel after matching sections

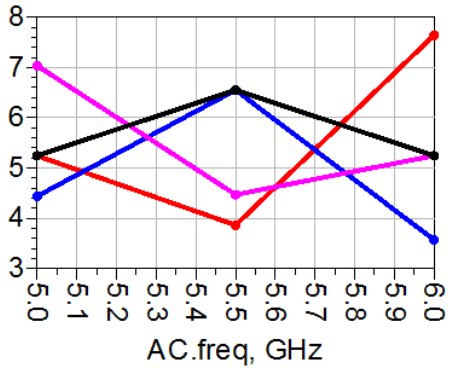

(a) Channel 1

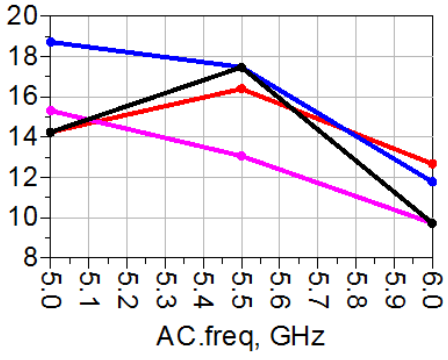

(b) Channel 2

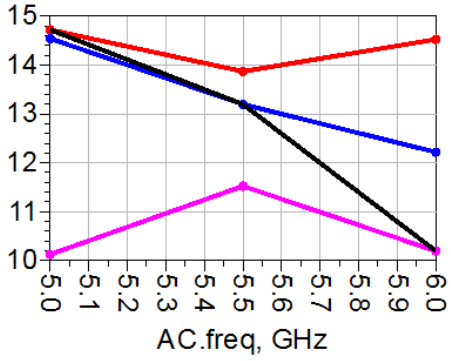

(c) Channel 3

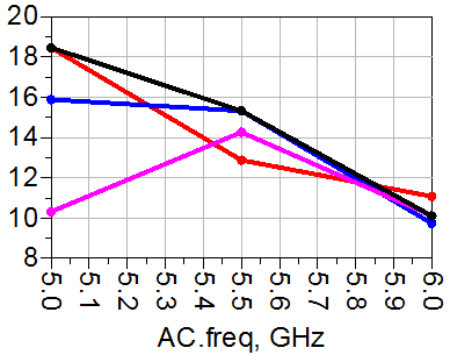

(d) Channel 4

Figure 3.16: Calculated (black) and simulated (coloured) signal voltages [V] for each channel at the LNA outputs

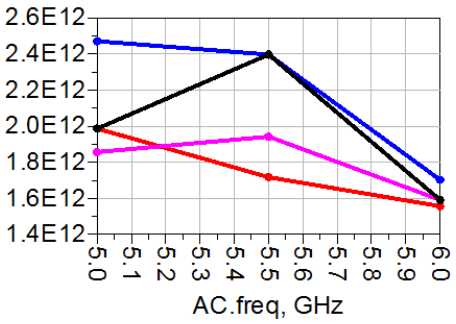

Figure 3.17: Calculated (black) and simulated (coloured) signal voltages [V] at beamformer output

The coloured lines correspond to values simulated in ADS while the black lines correspond to the values predicted by the theoretical model. The x-axis represents a sweep in the simulation frequency. The matrix indexing in ADS

for parameter swept variables lead to differences between the models at off-diagonal indices.

$$\begin{bmatrix} f_{sim_1} f_{design_1} & f_{sim_1} f_{design_2} & f_{sim_1} f_{design_3} \\ f_{sim_2} f_{design_1} & f_{sim_2} f_{design_2} & f_{sim_2} f_{design_3} \\ f_{sim_3} f_{design_1} & f_{sim_3} f_{design_2} & f_{sim_3} f_{design_3} \end{bmatrix}$$

On the main diagonal, the design frequency equals the simulation frequency and the results must be equal, as seen in figures 3.10 to 3.17. The coloured lines show how the circuit would respond over a frequency bandwidth while the black lines show the circuit response for a single frequency design. To have the theoretical model predict the same values as the ADS simulation model over a frequency band, instead of recalculating the impedances for the model at each frequency, the frequency dependence of the matching section must be modeled with the physical length of each stub held fixed. The frequency dependent reactance of each series stub is then given by

$$jX_{series} = \begin{cases} -jZ_0 \cot(\beta l), & \text{for open-circuit stubs} \\ jZ_0 \tan(\beta l), & \text{for short-circuit stubs} \end{cases}$$

The reactance of each shunt stub is given by

$$jB_{shunt} = \begin{cases} jY_0 \tan(\beta l), & \text{for open-circuit stubs} \\ -jY_0 \cot(\beta l), & \text{for short-circuit stubs} \end{cases}$$

The signal-no-noise and noise-no-signal active impedances at $f = 5.5$ GHz are shown as calculated and simulated in table 3.3.

Calculated vs Simulated Signal Active Impedances [Ω] at $f = 5.5$ GHz

	Calculated Z_{act_s}	Simulated Z_{act_s}	Calculated Z_{act_n}	Simulated Z_{act_n}
Ch. 1	$33.348\angle 39.94°$	$33.348\angle 39.94°$	$76.545\angle -22.32°$	$76.545\angle -22.32°$
Ch. 2	$65.591\angle 22.61°$	$65.591\angle 22.61°$	$76.510\angle -22.38°$	$76.510\angle -22.38°$
Ch. 3	$76.554\angle 9.58°$	$76.554\angle 9.58°$	$76.708\angle -22.16°$	$76.708\angle -22.16°$
Ch. 4	$69.869\angle 22.10°$	$69.869\angle 22.10°$	$76.622\angle -22.12°$	$76.622\angle -22.12°$

Table 3.3: Comparison between signal and noise active impedances for ADS simulation and model calculations

The signal power and noise power simulated in ADS compared to the calculated value at each node is shown in tables 3.4 and 3.5 and the comparison between the simulated and calculated SNR at each node is shown in table 3.6.

Calculated vs Simulated Noise Powers [W] at $f = 5.5$ GHz

	Cal Ch. 1	Sim Ch.1
Array Port	$-3.900e-13$	$-3.900e-13$
Pre Amplifier	$6.995e-13$	$6.995e-13$
Post Amplifier	$1.280e-11$	$1.280e-11$
	Cal Ch. 2	Sim Ch.2
Array Port	$-3.898e-13$	$-3.898e-13$
Pre Amplifier	$6.998e-13$	$6.998e-13$
Post Amplifier	$1.281e-11$	$1.281e-11$
	Cal Ch. 3	Sim Ch.3
Array Port	$-3.900e-13$	$-3.900e-13$
Pre Amplifier	$6.996e-13$	$6.996e-13$
Post Amplifier	$1.280e-11$	$1.280e-11$
	Cal Ch. 4	Sim Ch.4
Array Port	$-3.913e-13$	$-3.913e-13$
Pre Amplifier	$7.002e-13$	$7.002e-13$
Post Amplifier	$1.282e-11$	$1.282e-11$

Table 3.4: Comparison between node noise powers for ADS simulation and model calculations

Calculated vs Simulated Signal Powers [W] at $f = 5.5$ GHz

	Cal Ch. 1	Sim Ch.1
Array Port	-0.034	-0.034
Pre Amplifier	0.015	0.015
Post Amplifier	0.275	0.275
	Cal Ch. 2	Sim Ch.2
Array Port	-0.237	-0.237
Pre Amplifier	0.111	0.111
Post Amplifier	2.027	2.027
	Cal Ch. 3	Sim Ch.3
Array Port	-0.255	-0.255
Pre Amplifier	0.118	0.118
Post Amplifier	2.168	2.168
	Cal Ch. 4	Sim Ch.4
Array Port	-0.257	-0.257
Pre Amplifier	0.186	0.186
Post Amplifier	3.405	3.405

Table 3.5: Comparison between node signal powers for ADS simulation and model calculations

Calculated vs Simulated SNR at $f = 5.5$ GHz

	Cal Ch. 1	Sim Ch.1
Array Port	8.783e10	8.783e10
Pre Amplifier	2.145e10	2.145e10
Post Amplifier	2.148e10	2.148e10
	Cal Ch. 2	Sim Ch.2
Array Port	6.086e11	6.086e11
Pre Amplifier	1.580e11	1.580e11
Post Amplifier	1.582e11	1.582e11
	Cal Ch. 3	Sim Ch.3
Array Port	6.533e11	6.533e11
Pre Amplifier	1.690e11	1.690e11
Post Amplifier	1.693e11	1.693e11
	Cal Ch. 4	Sim Ch.4
Array Port	6.564e11	6.564e11
Pre Amplifier	2.663e11	2.663e11
Post Amplifier	2.656e11	2.656e11

Table 3.6: Comparison between node SNR for ADS simulation and model calculations

At the beamformer output port, the noise power is given for both the simulated and calculated cases by $P_{n_o} = 8.118\text{e}10$ W, while the signal power is given for both the simulated and calculated cases by $P_{s_o} = 5.739\text{e}22$ W. This corresponds to an SNR for both the simulated and calculated cases of $SNR = 7.070\text{e}11 = 118.494$ dB.

In this section, signal and noise response models were derived in matrix form without assuming any components, analogous across receiver channels, to be identical. This allows freedom for components with differing parameters to be used to fulfill the criteria for impedance matching where the active impedance of different receiver channels vary greatly. The response models were formulated in terms of transformation matrices which transform a source voltage to a voltage referenced at other receiver nodes. The transformation matrices were derived directly in terms of physical circuit impedances and admittances. The transformation matrices can be used to determine the signal or noise correlation matrices at reference points of interest. The noise transformation matrices are seen to elegantly relate the LNA two-port noise parameters to the noise correlation matrices referenced at points throughout the receiver. The theoretically predicted values from the mathematical model were confirmed using a premium circuit simulation software package. A tool like MATLAB which posesses powerful optimization and solver functions and the ability to script functions can then be used to optimize the receiver performance directly

in terms of physical impedances and admittances thanks to the transformation matrices, with more control than the proprietary optimizer tools available in a software package such as ADS.

Chapter 4

Noise Matching Criteria and Active Impedance Approximation

4.1 Active Impedance

It was shown in section 2.5.1 that the noise performance of a system is determined by the matching to the active impedances of the array. This process is called noise matching. When an antenna array is excited, the coupling between array elements causes currents to be induced on the ports of each other element. These induced currents change the effective impedance seen into the array. As discussed before, the ratio of the voltage across any given port to the current flowing into the port is then defined as the active impedance at that port. The active impedance varies as the array is driven to scan into different directions and differs for the signal-no-noise and noise-no-signal cases. For each case the port voltage excitation must be determined so that the active impedance can be calculated as a weighted ratio of the antenna impedance parameters.

4.1.1 Analytical Form Signal-no-Noise case

For each matching network topology, the signal active impedance can be determined for the open circuit excitation voltage vector $[\tilde{\boldsymbol{e}}_{\boldsymbol{s}}]$ and the source port signal transformation matrix $[T_x]$ by solving the equation

$$[\tilde{\boldsymbol{Y}}_{\boldsymbol{act_s}}] = [\tilde{\boldsymbol{Z}}_{\boldsymbol{act_s}}]^{-1} = [v_{s_d}]^{-1}[Y][\tilde{\boldsymbol{v}}_{\boldsymbol{s}}]$$
$$[\tilde{\boldsymbol{v}}_{\boldsymbol{s}}] = [T_x][\tilde{\boldsymbol{e}}_{\boldsymbol{s}}]$$

The entries of the $N \times N$ diagonal matrix $[v_{s_d}]$ are that of the port signal voltage vector $[\tilde{\boldsymbol{v}}_{\boldsymbol{s}}]$. $[T_x]$ is given for each topology by equations 3.3 and 3.7 to 3.11. The signal active impedance is dependent on the spatially varying signal voltage response and thus also varies as a function of ϕ and θ.

4.1.2 Analytical Form Noise-no-Signal case

In the case of the noise active impedance, the impedance is determined by solving the equation

$$[\tilde{\boldsymbol{Y}}_{\boldsymbol{act_n}}] = [\tilde{\boldsymbol{Z}}_{\boldsymbol{act_n}}]^{-1} = [v_{n_d}]^{-1}[Y][\tilde{\boldsymbol{v}}_{\boldsymbol{n}}]$$
$$[\tilde{\boldsymbol{v}}_{\boldsymbol{n}}] = diag\Big(\big[[T_z][I_x][T_z]^{\dagger} + [T_s]\big[[E_x] + [E_{ext}(\phi,\theta)]\big][T_s]^{\dagger}\big]^{1/2}\Big)$$

In equation 4.1.2, † denotes the complex conjugate transpose, $[I_x]$ the LNA port input noise current correlation matrix, $[E_x]$ the antenna source port noise voltage correlation matrix from Twiss's Theorem and $[E_{ext}]$ the external noise source voltage correlation matrix as shown in figure 4.1.

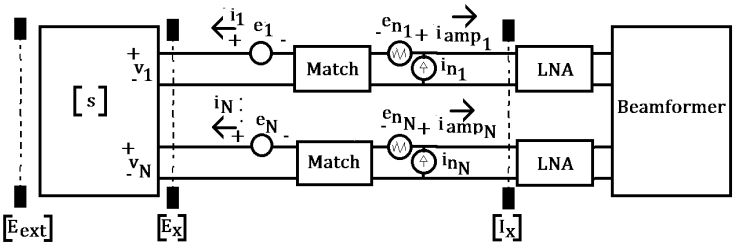

Figure 4.1: Reference planes for noise correlation matrices in receiver

In the case of an isotropic external noise source, the noise active impedance does not vary as a function of ϕ and θ as the internally generated antenna and amplifier noise sources are spatially invariant. The entries of the $N \times N$ diagonal matrix $[v_{n_d}]$ are given by the port noise voltage vector $[\tilde{\boldsymbol{v}}_{\boldsymbol{n}}]$. The source port noise transformation matrices $[T_z]$ and $[T_s]$ their respective post-matching section noise transformation matrices $[T'_z]$ and $[T'_s]$ are given for each topology by equations 3.18 and 3.30 to 3.41.

4.1.3 Magnitude of Active Reflection Coefficient

As the active impedance is a mathematical ratio and not a physical impedance, it is possible for the ratio to be such that the magnitude of the associated source reflection coefficient will go above unity.

$$|\Gamma_s| > 1$$

This corresponds to a negative real part of the source active impedance. Because Ohm's Law requires the ratio of the voltage across and the current through a resistor to be related by $R = V/I$, at first glance this can seem counter-intuitive as for a passive device, the resistance must be positive. Considering the active reflection coefficient in terms of signals applied to and received from a coupled antenna element, [37], for a phased array the active

reflection coefficient of the m-th channel of an N channel array is given by

$$\Gamma_{m_{act}} = \sum_{n=-\infty}^{\infty} s_{mn} e^{-jn\alpha} \tag{4.1}$$

Where α is the angle of the voltage phasor excitation for the channel. It is seen that an α can possibly be chosen such that the s-parameters add constructively so that the magnitude of the resulting active reflection coefficient becomes larger than unity. In addition, for a general array, it will be shown that the ratio of the magnitudes of the excitations voltages are not necessarily equal. In the case of the QMA, as the array is scanned over ϕ and θ, the open circuit voltages excited at the ports of the antenna have spatially varying magnitudes due to the non-isotropic gain pattern of each antenna element as well as the excitation source. The corresponding active impedance is given, with i_m and i_k the currents flowing into the m-th and and k-th array port respectively, by

$$z_{act_{s_m}} = \frac{1}{i_m} \sum_{k=1}^{N} z_{mk} i_k$$

In such an event, the ratio of the port currents can be such that the real part of the active impedance is negative, even if the angle of the excitations α is not chosen to create constructive interference. If the active reflection coefficient is defined as the ratio of the voltage wave received by the channel to the voltage wave applied as in 4.1, the ratio of the corresponding powers received from and applied to a channel is given by $|\Gamma_{act}|^2$. In order to satisfy the conservation of energy, it is required that

$$|\Gamma_{act_{tot}}|^2 \leq N$$

where $\Gamma_{act_{tot}}$ is the total active reflection coefficient for the N-port array, as shown in Appendix D. A real receiver system thus would allow a given channel to have an active reflection coefficient with magnitude greater than unity at an angle, but the other channels will compensate by having active reflection coefficients with smaller magnitudes at the same angle. The magnitude of the reflection coefficient of a channel can be lowered by increasing the spacing between elements of an antenna array, [32]. Negative source resistance must be kept in mind during receiver design as at these points, such as the noise figure in equation 4.2, break down.

$$F = F_{min} + \frac{R_n}{G_s} |Y_s - Y_{s_{opt}}|^2 \tag{4.2}$$

Equation 4.2 assumes a positive source resistance or corresponding conductance, $G_s > 0$. If the conductance is smaller than 0, equation 4.2 implies that the amplifier would operate at a noise figure smaller than its minimum noise figure F_{min} and possibly at a negative noise figure F. The negative resistance

observed in actively scanned antenna arrays is different than the negative differential resistances observed in active, non-linear devices such as S-shape and N-shape resistors [38], resonant tunneling diodes [39], barrier diodes [40] and field effect transistors [41]-[42].

4.2 Approximation Method for Active Impedance

The signal active impedance for a single channel of a network consisting of an N-port array with no matching section introduced, scanned over ϕ and θ, is shown in figure 4.2. Although the signal active impedances, seen looking into the antenna ports, vary over ϕ, θ and frequency, only one physical matching network can be introduced between the terminals of the antenna array and the LNA input ports.

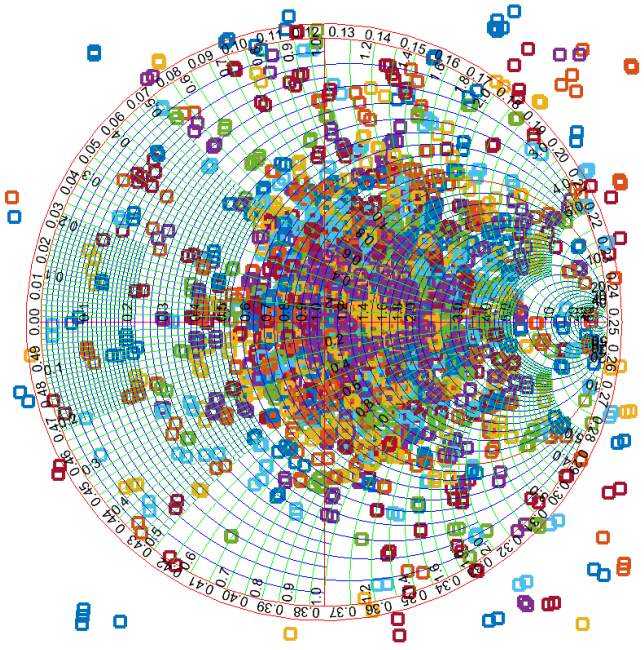

Figure 4.2: Z_{act_s} for a Quad Mode Antenna channel at a single frequency scanned in range $\phi \in [0°, 358°], \theta \in [0°, 90°]$

A matching network will effectively transform the LNA optimal noise source impedance $Z_{s_{opt}}$ to a new optimal impedance value $Z_{s'_{opt}}$ as shown in figure 4.3.

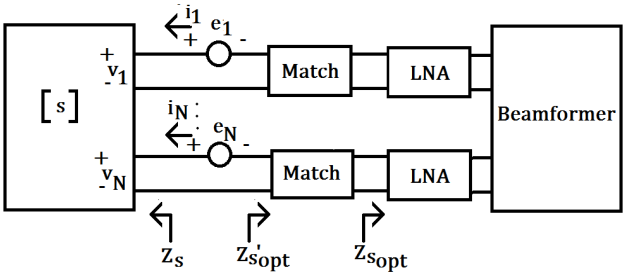

Figure 4.3: Transformation of $Z_{s_{opt}}$ to $Z'_{s_{opt}}$ in receiver

As the network is fixed, the choice of $Z'_{s_{opt}}$ becomes an exceedingly difficult design choice. Various strategies have been proposed for this. Some of the most important of these techniques are the Stochastic Field Matching, Unknown Field Matching, [43], Multibeam Average Noise Optimization techniques [18] and Decoupling Networks [44].

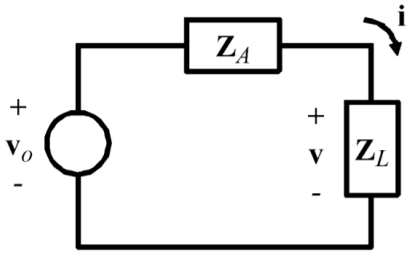

Figure 4.4: Receiver model for Stochastic and Unknown Field Matched Arrays

The two field matching techniques operate on the similar principal of specifying a load impedance in a receiver network, as shown in figure 4.4 , that will achieve some output goal. Each load is specified in terms of a set of active impedances $[\tilde{\boldsymbol{Z}}_{\boldsymbol{act}}^{(p)}]$ which is observed under P sets of excitations, $[\tilde{\boldsymbol{v}}_{\boldsymbol{o}}^{(p)}]$ and $[\tilde{\boldsymbol{i}}^{(p)}]$. The Stochastic Field Match technique achieves maximum power transfer to the load Z_{L_m}. Finding the load impedance that on average matches the active impedances is done by minimizing the objective function

$$\gamma_z = \frac{1}{P}\sum_{p=1}^{P}\sum_{m=1}^{M}\left|Z_{L_m} i_m^{(P)} - Z_{act_m}^{(P)*} i_m^{(P)}\right|^2 \tag{4.3}$$

where M is the number of array elements. Setting the derivative to zero with respect to $Z_{L_m}^*$ and solving leads to a load impedance given, for the Stochastic Field Matching technique, by

$$Z_{L_m} = \frac{\left[[Z_A]^\dagger [U]\right]_{mm}}{U_{mm}} \tag{4.4}$$

In equation 4.4, $[Z_A]$ refers to the antenna array Z-parameters, while

$$[U] = [Y]\frac{1}{P}\sum_{p=1}^{P}[\tilde{\boldsymbol{v}}_{\boldsymbol{o}}^{(p)}][\tilde{\boldsymbol{v}}_{\boldsymbol{o}}^{(p)}]^{\dagger}[Y]^{\dagger}$$

$$[Y] = \left[[Z_L] + [Z_A]\right]^{-1}$$

$[Z_L]$ appears in $[U]$, thus equation 4.4 must be solved by first initializing $Z_{L_m} = Z^*_{A_{mm}}$, then constructing $[U]$ and $[Y]$ and then iteratively solving equation 4.4 and updating $[U]$ and $[Y]$ until the solution converges. The matching network for the m-th channel is determined as the network which transforms the LNA input impedance to Z_{L_m}.

If the incident field is completely unknown, a solution is to consider the array as a transmitter, with $[\tilde{\boldsymbol{i}}] = [Y][\tilde{\boldsymbol{v}}_{\boldsymbol{s}}]$ and $[\tilde{\boldsymbol{v}}] = [Z_A][\tilde{\boldsymbol{i}}]$. The array is excited with voltage v_s at the m-th port and zero voltage elsewhere. The input impedance looking into the m-th port is calculated and the load impedance is chosen as the conjugate of the input impedance

$$Z_{L_m} = \left\{\frac{\left[[Z_A][Y]\right]_{mm}}{Y_{mm}}\right\}^* \tag{4.5}$$

The load impedance is again solved iteratively as for the Stochastic Field Matching technique and the matching network determined in terms of the LNA input impedance.

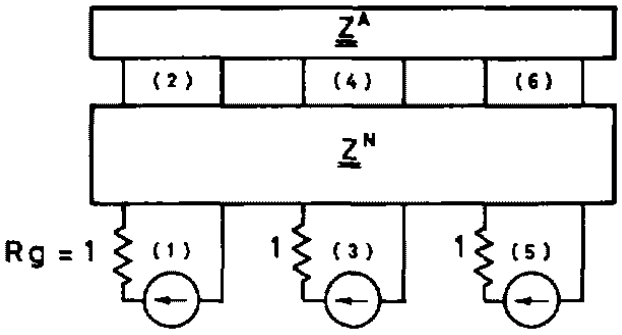

Figure 4.5: Receiver array network model with decoupling network N

The antenna array will be decoupled, [44] if the combination of the decoupling network and multiport array has an impedance matrix of the form

$$[Z'_N] = \begin{bmatrix} z_{11} & z_{12} & 0 & 0 & \cdots & 0 \\ z_{12} & z_{22} & 0 & 0 & \cdots & 0 \\ 0 & 0 & z_{33} & z_{43} & \cdots & 0 \\ 0 & 0 & z_{34} & z_{44} & \cdots & 0 \\ \vdots & \vdots & \vdots & \vdots & \ddots & \vdots \end{bmatrix} \tag{4.6}$$

Any antenna mutual impedances must be purely reactive to achieve lossless decoupling. The impedance matrix of only the decoupling network can then be calculated from the combined network impedance matrix as

$$[Z'_N] = \begin{bmatrix} z_{11} & z_{12} & 0 & 0 & 0 & 0 & \cdots & 0 \\ z_{12} & z_{22} & 0 & -z^A_{24} & 0 & -z^A_{26} & \cdots & 0 \\ 0 & 0 & z_{33} & z_{43} & 0 & 0 & \cdots & 0 \\ 0 & -z^A_{24} & z_{34} & z_{44} & 0 & -z^A_{46} & \cdots & 0 \\ \vdots & \vdots & \vdots & \vdots & \vdots & \vdots & \ddots & \vdots \end{bmatrix} \tag{4.7}$$

Once the array has been decoupled, an LNA load can be matched to the port impedances.

Each of the discussed strategies to deal with the varying active impedance has its drawbacks. The Stochastic and Unknown Field Matching techniques rely on iterative solving of equations and calculation is thus slow and resource intensive. They also focus on maximum power transfer, which corresponds to non optimal noise matching. The decoupling network technique relies on complex decoupling networks that have strict constraints such as the requirement that mutual impedance between array elements must be reactive. This puts a constraint on the physical dimensions of the array and matching network. The multibeam average cannot be beamformed for maximum SNR as the beamformer coefficients are required to be known to calculate the optimum impedance.

A very simple and quick approach would be to simply calculate an average. The averaging method considered is the geometric mean of a recursive calculated set of complex impedances. The goal of the algorithm is to pair entries in the set with small and large magnitudes together so that the average of each pair is close to the geometric mean of the set in order to diminish the effect that an outlying value in the set has on the average of the set. The recursion can be done a varying number of times before the geometric mean of the produced set is taken. Based on the position of the entry in the set, the relative weight of the entry in the final average can be shown to differ. The calculation of the recursive average is as follows. Suppose that a set of N complex impedances a_i exist, where N can be an even or odd integer.

$$A = [a_1, a_2, \ldots, a_N]$$

The set of impedances is sorted in ascending order before the calculation of the average. Complex numbers of the same magnitude are sorted with ascending phase.

$$B = sort(A)$$

The entries of the set are then paired from the outside inward by adding two entries and dividing by two to find the average of the entries as an entry in

the next set. If N is an odd number, the median of the set is taken as its own average.

$$b'_n = \frac{b_n + b_{N+1-n}}{2}, \quad \forall \quad n \in \mathbb{N}, \quad n \leq \frac{N}{2}$$

This produces a new set of complex impedances, A', of length $\lceil \frac{N}{2} \rceil$. At this point, this operation can be performed recursively until only one entry remains and is taken as the recursive impedance of the set. The amount of times that this operation has been performed will hereafter be referred to as the level of the recursive average. The level of the recursive average is an integer in the range

$$0 \leq L_{rec} \leq \lceil \log_2 N \rceil$$

$L_{rec} = 0$ corresponds to the geometric mean of the set, while $L_{rec} = \lceil \log_2 N \rceil$ corresponds to the fully recursively averaged mean of the set. In the case that $L_{rec} < \lceil \log_2 N \rceil$, the recursive average of the set is determined by taking the geometric mean of the set after the recursive pairing has been performed L_{rec} times.

$$A_{avg_{recursive}} = \frac{1}{M} \sum_{n=1}^{M} b''^{\ldots(L_{rec})}_n, \quad M = \left\lceil \frac{N}{2^{L_{rec}}} \right\rceil$$

Whether or not entries are re-sorted after each recursion level affects the weighting in the final average. If the set is re-sorted at each level, the median entry possibly changes for each level. In sets with odd numbers the median is weighted differently to the other entries. Therefore changing the median changes the average. The recursive averages for $L_{rec} = \lceil \log_2 N \rceil$ and $L_{rec} = \lceil \log_2 N \rceil - 1$ will always be identical. The level of the recursive average determines the speed of the operation where each of the L_{rec} levels have $\lceil \frac{N}{2^k} \rceil$ summation and multiplication operations for the k-th level. In the event that $N = 2^k$, where k is an integer in the range $0 \leq L_{rec} \leq \lceil \log_2 N \rceil$, the recursive average of the set will be equal to the geometric mean of the set, regardless of the level of recursion. This implies that for sets where, after a number of iterations of recursion the number of entries in the set satisfy $N = 2^k$, further recursive calculations are unnecessary. Each data dimension must be averaged over to yield a single output average value.

In order to illustrate the working and properties of the averaging method, an example will be shown for $N = 7$ in Appendix C.

4.3 Iterative Point Noise Figure Search

The noise figure search is an extension of the concept of noise matching using the active impedance at a given angle. As a differing active impedance can be calculated for either the signal or noise only response, either the signal active impedance or the noise active impedance can be matched to the optimal

impedance of the LNA at one time. In the event that the noise active impedance is spatially invariant due to an isotropic external noise distribution, the noise active impedance will be a singular value. Firstly the LNA noise figure equation, [45], is considered as shown in equation 4.8.

$$F(f,\phi,\theta) = F_{min}(f) + 4\frac{R_n(f)}{Z_0}\frac{|\Gamma_{s_{act}}(f,\phi,\theta) - \Gamma_{s_{opt}}(f)|^2}{(1-|\Gamma_{s_{act}}(f,\phi,\theta)|^2)|1+\Gamma_{s_{opt}}(f)|^2} \tag{4.8}$$

A matching network can be chosen to match the LNA optimal source reflection coefficient, $\Gamma_{s_{opt}}$ to each value in the set of the active reflection coefficient $\Gamma_{s_{act}}$. Then, looking into the matching network, $\Gamma'_{s_{opt}}(f_0) = \Gamma_s(f_0,\phi_0,\theta_0)$. It must be noted that introducing a matching network will change the set of active source reflection coefficients. When the optimum reflection coefficient has been matched, the noise figure can then be determined for each active source reflection coefficient value of the original set. This produces a noise curve for each matched optimal reflection coefficient, as shown in figure 4.6 for a two-dipole array averaged over azimuthal scan angle along the horizon and scan frequency.

The iterative point noise figure optimal impedance is determined by iteratively finding the maximum noise figure that the LNA will produce over the set of active reflection coefficients for every given transformed optimum source reflection coefficient, and then selecting the optimum source impedance that minimizes the maximum noise figure. This can therefore be viewed as a minimax optimization and will produce the smallest maximum noise figure.

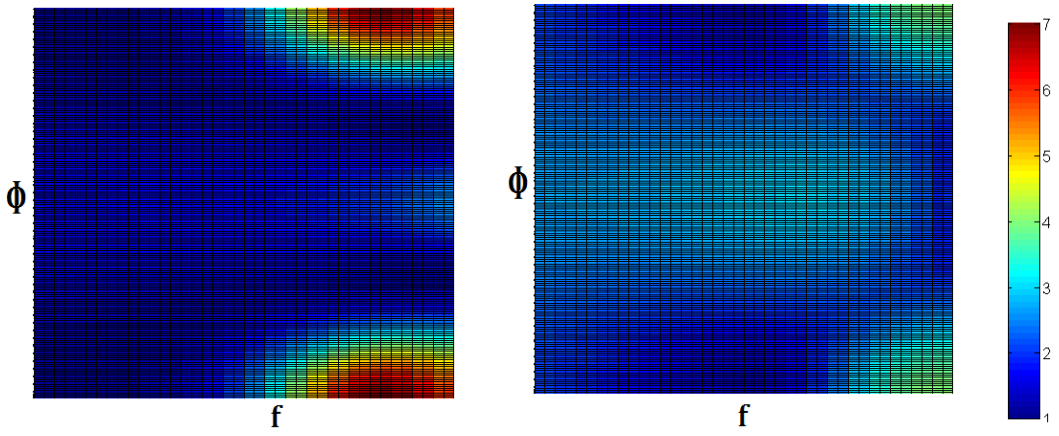

(a) $L_{rec_1} = 0, L_{rec_2} = 0$ Average (b) $L_{rec_1} = \lceil \log_2 M_1 \rceil, L_{rec_2} = \lceil \log_2 M_2 \rceil$

Figure 4.6: Noise figure curves for a two-dipole array scanned over frequency and azimuth along $\theta = 90°$

The optimum source impedance selection is subject to two restrictions. Firstly, the real part of the optimum impedance, $R'_{s_{opt}}$ must be larger than 0 to ensure real behaviour of the LNA device. Secondly, each channel of the receiver must have its optimum impedance selected so that the real parts $R'_{s_{opt}}$ for all channels are simultaneously either smaller, equal to, or larger than $R_{s_{opt}}$. In other words,

$$\begin{aligned} \text{either } R'_{s_{opt_m}} &> R_{s_{opt_m}}, \ \forall\ m = [1, 2, \cdots, N] \\ \text{or } R'_{s_{opt_m}} &= R_{s_{opt_m}}, \ \forall\ m = [1, 2, \cdots, N] \\ \text{or } R'_{s_{opt_m}} &< R_{s_{opt_m}}, \ \forall\ m = [1, 2, \cdots, N] \end{aligned}$$

This is that each channel can have the same matching network topology to yield purely imaginary, diagonal $[jX_{1_d}]$ and $[jX_{2_d}]$ matrices. Attempting to solve the closed form expressions for matching section reactances will lead to complex reactance values for X_{1_d} and X_{2_d} if the second $R'_{s_{opt}}$ condition is not obeyed. The criteria is thus as shown by equations 4.9.

$$\text{Series-Shunt:} \quad 0 < R'_{s_{opt}} < R_{s_{opt}} \tag{4.9a}$$

$$\text{Shunt-Series:} \quad R'_{s_{opt}} > R_{s_{opt}} \tag{4.9b}$$

$$\text{Single-Series:} \quad R'_{s_{opt}} = R_{s_{opt}} \tag{4.9c}$$

As noted previously, inserting a matching network section between the antenna and LNA terminals of each channel changes the active impedance seen looking into the antenna terminals from the active impedance in the absence of the matching network. It is therefore possible that even though the design algorithm attempts to match to the active impedance at a given angle, the optimum noise match, resulting in a noise figure of $F = F_{min}$ can either occur at another angle, or not occur at all. In the event that an optimum noise match is not obtained, it can still however be possible to achieve a match close to the optimum if the change in active impedance is small. A method to quantify the similarity between the array active impedance with and without the matching section is therefore required. With some pre-processing, the Structural Similarity Index can be used as a quantitative measure.

4.4 Source Impedance Match Parameter Sweep

The previously discussed methods and criteria for impedance noise matching all consider points that are included in the set of values generated as signal or noise active impedances through the operation of the antenna, or mathematical averages thereof. It is important to note that unless a large set of approximated data points is considered, these approaches can lead to the case where large areas on the Smith chart are not considered as options for source impedance matching, as shown in figure 4.7. It is therefore of interest to do a parameter

sweep on $|\Gamma'_{s_{opt}}|$ and $\angle\Gamma'_{s_{opt}}$ in fine enough steps to sample the unconsidered areas of the Smith chart. This can be viewed as a brute-force search of all available matching conditions.

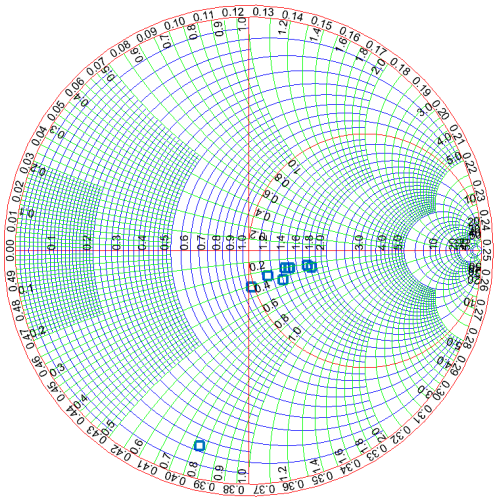

Figure 4.7: Approximated Z_{act_s} for a Quad Mode Antenna channel without parameter sweep considered

The techniques discussed above must be repeated for each channel of the receiver and will be used in the following section to design an optimum noise matching network for the QMA.

Chapter 5

Application to Quad-Mode Antenna

5.1 Introduction

In this section, the previously discussed methods will be used to design a receiver for a Quad Mode Antenna that uses four antenna elements in an array to achieve hemispherical gain patterns. Design considerations and methodology will be put forth and confirmed using professional simulation software. This will be the first instance of an optimal noise matching design for the QMA.

5.2 Design of MIMO Antenna Array

5.2.1 Four Channel Quad Mode Antenna at f=5.5 GHz

A four element quad-mode antenna (QMA), fed with quadraxial transmission lines, is considered as the source array for the antenna receiver [19]. The antenna array achieves near hemispherical coverage and can be described using its multi-mode S-,Y- or Z-parameters. The single-ended (SE) parameters can be obtained through simulation in CST Microwave Studio Suite 2018, and to determine the multi-mode (MM) parameters, the transforms [46]

$$[S^{MM}] = \left[[M_c] + [M_s][S^{SE}]\right]\left[[M_s] + [M_c][S^{SE}]\right]^{-1} \tag{5.1}$$

$$[M_s] = \frac{1}{2}[Z^{MM}]^{-\frac{1}{2}}[K^v][Z^{SE}]^{\frac{1}{2}} + \frac{1}{2}[Z^{MM}]^{\frac{1}{2}}[K^i][Z^{SE}]^{-\frac{1}{2}} \tag{5.2}$$

$$[M_c] = \frac{1}{2}[Z^{MM}]^{-\frac{1}{2}}[K^v][Z^{SE}]^{\frac{1}{2}} - \frac{1}{2}[Z^{MM}]^{\frac{1}{2}}[K^i][Z^{SE}]^{-\frac{1}{2}} \tag{5.3}$$

can be used, where $[Z^{MM}]$ and $[Z^{SE}]$ are diagonal matrices containing the

characteristic impedances of the ports, and

$$[K^v] = \begin{bmatrix} \frac{1}{2} & \frac{1}{2} & -\frac{1}{2} & -\frac{1}{2} \\ \frac{1}{2} & -\frac{1}{2} & -\frac{1}{2} & \frac{1}{2} \\ \frac{1}{4} & \frac{1}{4} & \frac{1}{4} & \frac{1}{4} \\ \frac{1}{2} & -\frac{1}{2} & \frac{1}{2} & -\frac{1}{2} \end{bmatrix} \tag{5.4}$$

$$[K^i] = \begin{bmatrix} \frac{1}{2} & \frac{1}{2} & -\frac{1}{2} & -\frac{1}{2} \\ \frac{1}{2} & -\frac{1}{2} & -\frac{1}{2} & \frac{1}{2} \\ 1 & 1 & 1 & 1 \\ \frac{1}{2} & -\frac{1}{2} & \frac{1}{2} & -\frac{1}{2} \end{bmatrix} \tag{5.5}$$

For the purposes of this design, the QMA is simulated in the wifi band between $f = 5$ GHz and $f = 6$ GHz, with the single frequency stub reactance calculations done at the center frequency of $f = 5.5$ GHz. The port numbering sequence for the QMA as simulated in CST, is shown in figure 5.1.

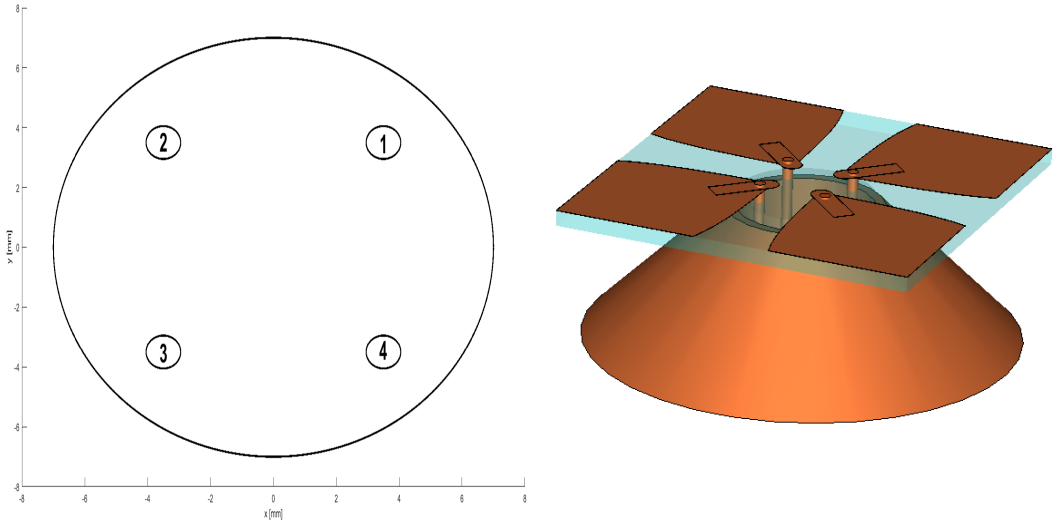

(a) Numbering of ports in QMA (b) QMA in CST software

Figure 5.1: QMA in simulation software

For the ports as shown in figure 5.1, the single-ended S-parameters over frequency for the QMA is then as in figure 5.2.

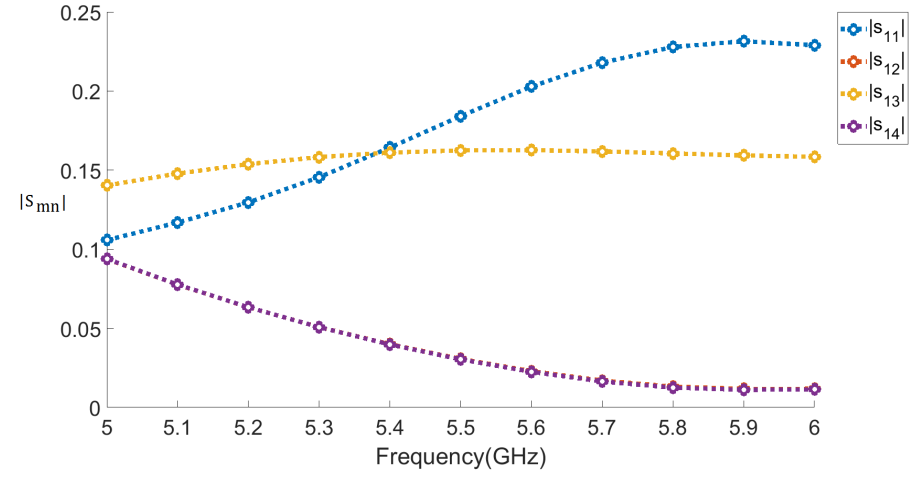

(a) $|s_{1m}(f)|$

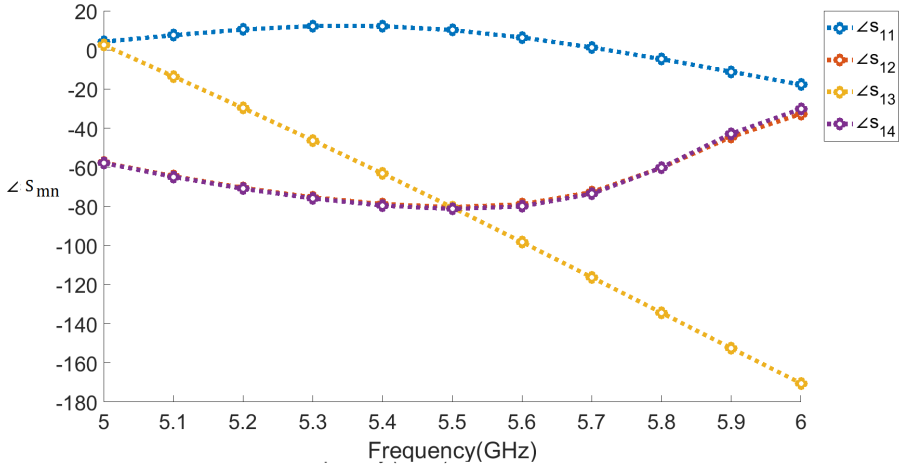

(b) $\angle s_{1m}(f)$

Figure 5.2: Array S-parameters s_{1m} for channel 1 over frequency

For channels $k \in [2, 4]$, the forms of s_{km} are the same as shown in figure 5.2, with the indices changing to have the ports adjacent to k be represented by the red and purple curves and the opposite port represented by the yellow curve while the blue curve represents the kth port. This is due to the geometrical symmetry and proves the reciprocity of the antenna array. The electric far-field patterns for each channel as well as the array far-field pattern are shown over ϕ and θ in figure 5.3.

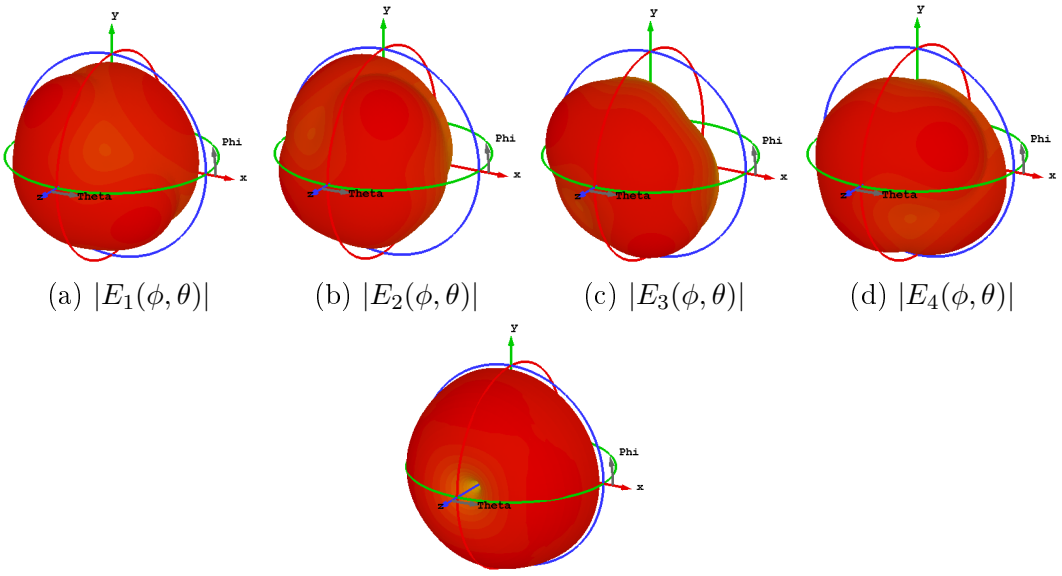

(a) $|E_1(\phi, \theta)|$ (b) $|E_2(\phi, \theta)|$ (c) $|E_3(\phi, \theta)|$ (d) $|E_4(\phi, \theta)|$

(e) $|E_{total}(\phi, \theta)|$ for unity excitation at all ports

Figure 5.3: Model farfields per channel and full array at frequency $f = 5.5$ GHz

5.2.2 Infineon BFP842ESD Low Noise Amplifier

The Infineon BFP842ESD LNA was selected as the LNAs for the receiver. Infineon was selected as it provides complete SPICE models and S-parameter touchstone files containing noise parameter information for simulation purposes over wide frequency ranges (300 MHz to 10 GHz), containing all the information necessary to do a software or theoretical model based design. Furthermore, the BFP842ESD LNA input reflection coefficient magnitude exhibits a minimum between $f = 5$ GHz and $f = 6$ GHz which translates to low reflections in the frequency band of interest. While the C-band ($f = 4$ GHz to $f = 8$ GHz) s_{21} is much lower than the UHF band ($f = 0.3$ GHz to $f = 3$ GHz s_{21}, the forward voltage gain magnitude decreases at a slow rate in the C band, which ensures a more constant voltage gain over frequency. Between $f = 5$ GHz and $f = 6$ GHz, the noise parameters also exhibit good stability, which means that achieving an optimal match at $f = 5.5$ GHz can translate to good noise matching performance over the entire frequency range of interest. This is offset by the frequency dependency of the active impedance and the matching network however. At a bias of $V_{CE} = 2$ V, $I_C = 15$ mA, the S-parameters and two-port noise parameters over frequency are as shown in figure 5.4 and table 5.1.

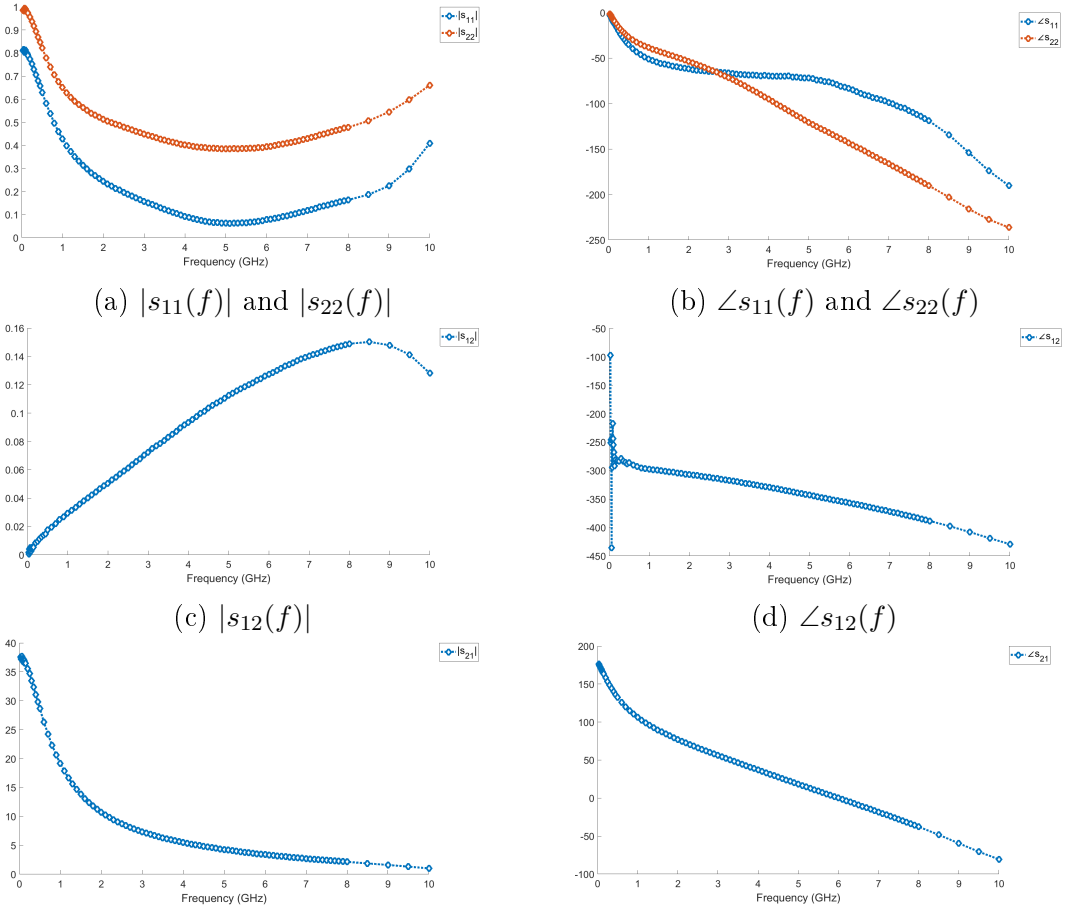

(a) $|s_{11}(f)|$ and $|s_{22}(f)|$

(b) $\angle s_{11}(f)$ and $\angle s_{22}(f)$

(c) $|s_{12}(f)|$

(d) $\angle s_{12}(f)$

(e) $|s_{21}(f)|$

(f) $\angle s_{21}(f)$

Figure 5.4: LNA S-parameters over frequency

Infineon BFP842ESD

f(GHz)	$\lvert s_{11}\rvert$	$\lvert s_{22}\rvert$	F_{min}(dB)	Γ_{opt}	$R_n(\Omega)$
5	0.0630	0.3856	0.90	0.13$\angle$-112°	4.5
5.5	0.0647	0.3867	1.01	0.15$\angle$-109°	5
6	0.0787	0.3945	1.11	0.15$\angle$-106°	5.5

Table 5.1: Infineon BFP842ESD parameters between $f = 5$ GHz and $f = 6$ GHz

Using the $K - \Delta$ test for unconditional amplifier stability [45], at $f = 5.5$ GHz, it can be shown that for the LNA parameters as given in table 5.1.

$$K = \frac{1 - |s_{11}|^2 - |s_{22}|^2 + |\Delta|^2}{2|s_{12}s_{21}|} = 1.1723 > 1 \tag{5.6}$$

$$|\Delta| = |s_{11}s_{22} - s_{12}s_{21}| = 0.4743 < 1 \tag{5.7}$$

The BFP842ESD amplifier provides its best gain characteristics at low frequencies, but still exhibits strong low noise performance, unconditional stability at the bias conditions for the operating frequency and low input and output reflections at high frequencies, while being cost efficient and was thus selected.

5.2.3 Determining of Active Impedance

For the LNA parameters as given in table 5.1, a noise bandwidth of $B = 100$ MHz and a LNA termination load $Z_L = 50\ \Omega$, from the noise theory fundamentals, the correlation admittance, Y_c, LNA input admittance, y_{in_a} and the amplifier noise sources e_n and i_u can be determined over frequency as shown in table 5.2.

Noise Theory Fundamental Values

f(GHz)	Y_c(S)	y_{in_a}(S)	$\overline{\lvert e_n\rvert^2}(\mathrm{V}^2)$	$\overline{\lvert i_u\rvert^2}(\mathrm{A}^2)$
5	0.0067∠-51.29°	0.0192∠6.86°	7.456×10^{-12}	3.277×10^{-15}
5.5	0.0079∠-50.57°	0.0194∠7.19°	8.284×10^{-12}	3.491×10^{-15}
6	0.0084∠-47.25°	0.0196∠8.94°	9.112×10^{-12}	3.650×10^{-15}

Table 5.2: Values for admittances and sources from noise theory fundamentals

5.2.3.1 Signal-no-Noise case Excitation and Active Impedance

From antenna theory, [47] the open circuit port voltages at the terminals of an antenna that is illuminated by an incident electric field can be determined in terms of the effective antenna length vector $\bar{\boldsymbol{l}}_{\boldsymbol{eff}}$.

$$v_{oc}(r, \phi, \theta) = \bar{\boldsymbol{l}}_{\boldsymbol{eff}} \cdot \overline{\boldsymbol{E}}_{\boldsymbol{inc}}(r, \phi, \theta) \tag{5.8}$$

The antenna effective length can be related to the known radiated farfield of the antenna, [31], by the equation

$$\overline{\boldsymbol{E}}_{\boldsymbol{far}}(r, \phi, \theta) = \frac{-j\eta k I_{in}}{4\pi r} e^{-jkr} \bar{\boldsymbol{l}}_{\boldsymbol{eff}}(\phi, \theta) \tag{5.9}$$

Taking the source as a Hertzian dipole in free space, the incident electric farfield is approximately equal to only its θ component, given by the equation

$$E_\theta = \frac{j\eta I_o \Delta l k}{4\pi r} e^{-jkr} \sin\theta \tag{5.10}$$

$I_0\Delta l$ can be chosen and the dipole orientated so that the Hertzian dipole z-axis is always perpendicular to the $\overline{\boldsymbol{r}}$ vector between the source and observation points. This causes the $\sin\theta$ factor in equation 5.10 to vanish. The single ended open circuit port voltages for each channel can be determined and the magnitudes are as shown in figure 5.5.

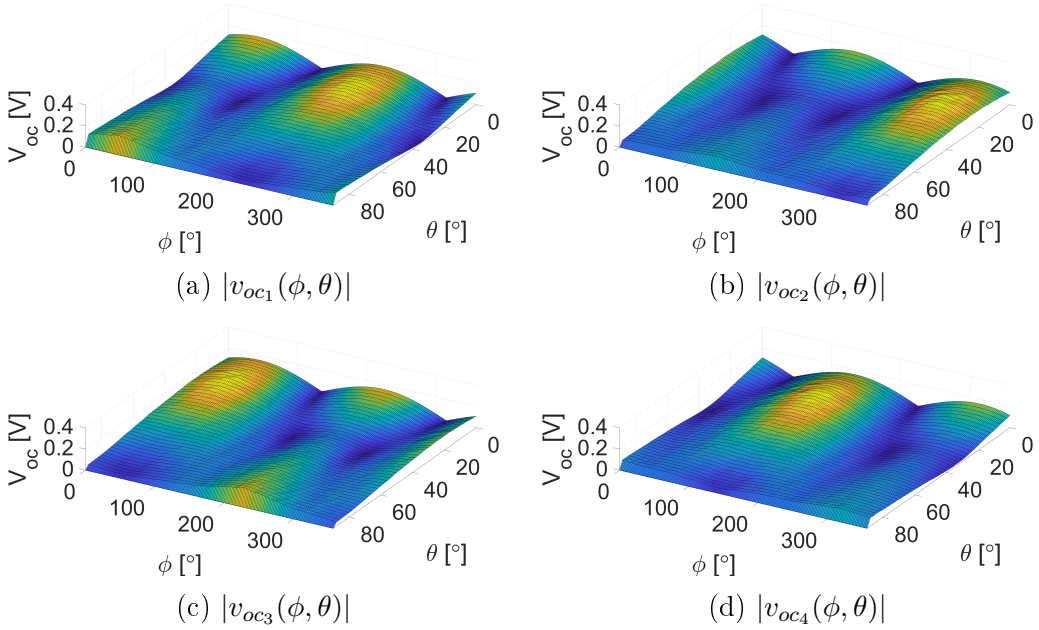

(a) $|v_{oc_1}(\phi,\theta)|$ (b) $|v_{oc_2}(\phi,\theta)|$

(c) $|v_{oc_3}(\phi,\theta)|$ (d) $|v_{oc_4}(\phi,\theta)|$

Figure 5.5: Array $|v_{oc_m}(\phi,\theta)|$ at $f = 5.5$ GHz

For the receiver model without a matching network selected and the circuit parameters as described, at $f = 5.5$ GHz, the signal source port transformation matrix $[T_{x_{nm}}]$ is then given by equation 3.2 as seen in equation 5.11.

$$[T_{x_{nm}}] = \begin{bmatrix} 0.5852\angle 4.681^\circ & 0.0152\angle -81.94^\circ & 0.0823\angle -81.67^\circ & 0.0151\angle -82.92^\circ \\ 0.0152\angle -81.94^\circ & 0.5854\angle 4.679^\circ & 0.0152\angle -83.23^\circ & 0.0825\angle -81.80^\circ \\ 0.0823\angle -81.67^\circ & 0.0152\angle -83.23^\circ & 0.5858\angle 4.712^\circ & 0.0150\angle -82.65^\circ \\ 0.0151\angle -82.92^\circ & 0.0825\angle -81.80^\circ & 0.0150\angle -82.65^\circ & 0.5856\angle 4.739^\circ \end{bmatrix} \tag{5.11}$$

It can be seen from $[T_{x_{nm}}]$ that the off-diagonal elements of the transformation network are identical, as expected for a symmetric antenna array. The port loaded circuit voltage can then be found by using

$$[\tilde{\boldsymbol{v}}_{\boldsymbol{s}}] = [T_{x_{nm}}][\tilde{\boldsymbol{e}}_{\boldsymbol{s}}]$$

where $[\tilde{\boldsymbol{e}}_{\boldsymbol{s}}] = [\tilde{\boldsymbol{v}}_{\boldsymbol{oc}}]$. The port impressed voltages for the unmatched receiver case at $f = 5.5$ GHz can then be seen in figure 5.6.

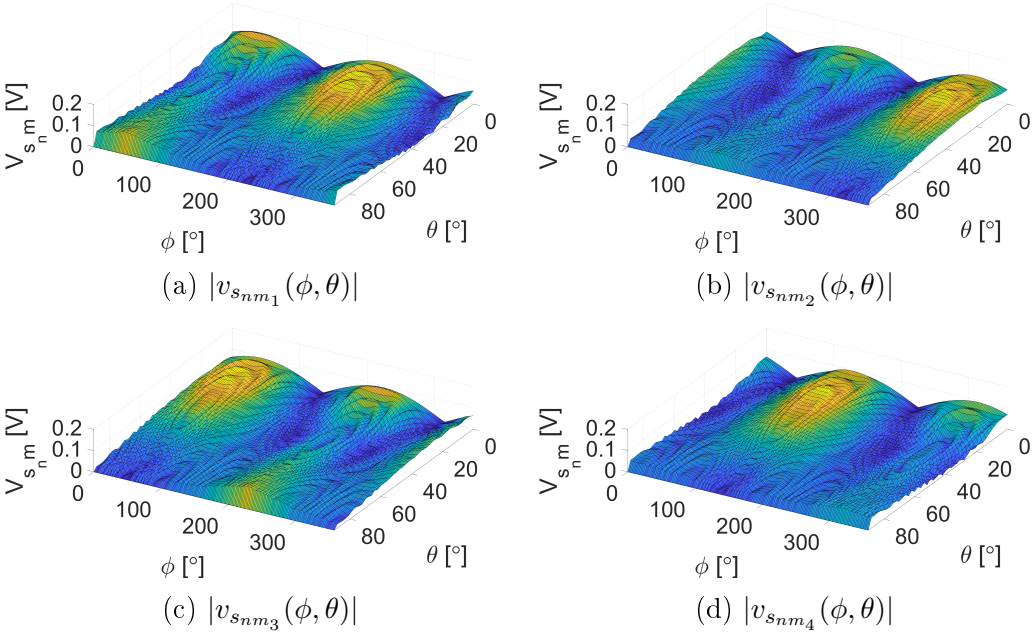

(a) $|v_{s_{nm_1}}(\phi,\theta)|$ (b) $|v_{s_{nm_2}}(\phi,\theta)|$

(c) $|v_{s_{nm_3}}(\phi,\theta)|$ (d) $|v_{s_{nm_4}}(\phi,\theta)|$

Figure 5.6: Array $|v_{s_{nm_k}}(\phi,\theta)|$ at $f = 5.5$ GHz

It can be seen that the port voltages are similar to the open-circuit voltages but the curves are less smooth. The peaks in the voltage curves also lead to exaggerated peaks in the active impedance. The active impedance is determined through the equation

$$[\tilde{\boldsymbol{Z}}_{\boldsymbol{act_s}}] = [\tilde{\boldsymbol{Y}}_{\boldsymbol{act_s}}]^{-1} = \left[[v_{s_d}]^{-1}[Y][\tilde{\boldsymbol{v}}_{\boldsymbol{s}}]\right]^{-1}$$

The active impedance for each channel as calculated for an unmatched receiver at $f = 5.5$ GHz over the space $\phi \in [0°, 358°]$, and $\theta \in [0°, 90°]$ is shown in figure 5.7.

5.2.3.2 Noise-no-Signal case Excitation and Active Impedance

The temperature of the receiver network includes all external noise sources, the environment and the lossy receiver. In the absence of interfering external noise sources, the excited port noise voltage is a function only of the antenna array and receiver. For a reciprocal array, $z_{mk} = z_{km}$, so that Twiss's theorem as seen in equation 3.21 simplifies to

$$[E_x] = 4k_B T B[R] \tag{5.12}$$

where $[R]$ is the real part of the antenna impedance parameter matrix. For the array as given, at $f = 5.5$ GHz, the noise voltage transformation matrix $[T_s]$ then becomes

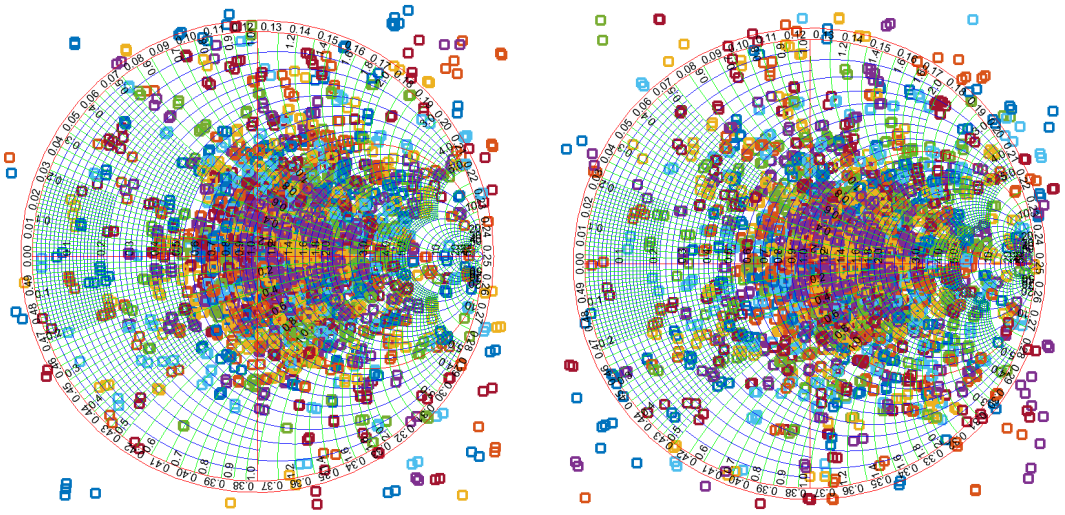

(a) $Z_{act_{s_1}}(\phi,\theta)$ (b) $Z_{act_{s_2}}(\phi,\theta)$

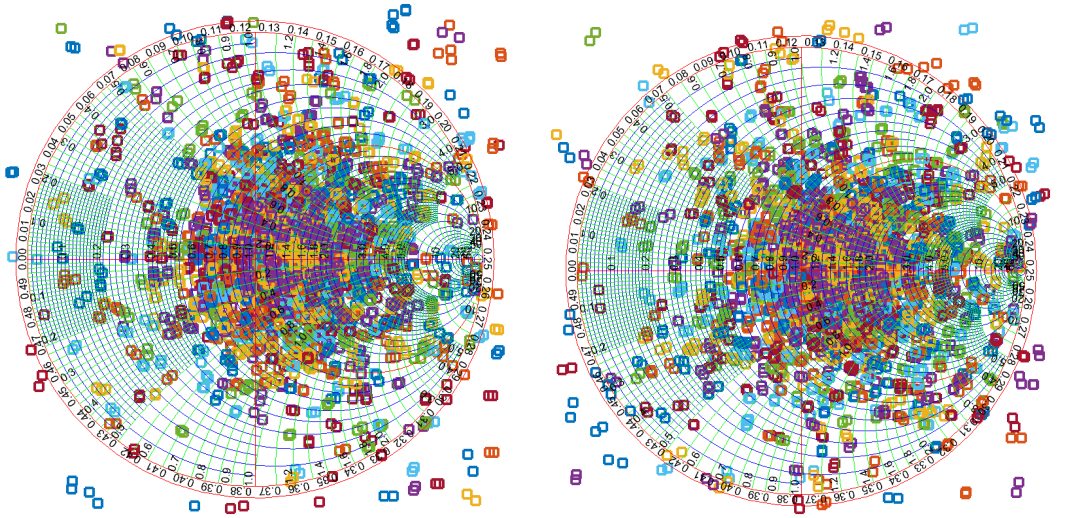

(c) $Z_{act_{s_3}}(\phi,\theta)$ (d) $Z_{act_{s_4}}(\phi,\theta)$

Figure 5.7: Unmatched array $Z_{act_{s_k}}(\phi,\theta)$ at $f = 5.5$ GHz

$$[T_{s_{nm}}] = \begin{bmatrix} 0.4195\angle{-6.54}^\circ & 0.0152\angle{98.065}^\circ & 0.0823\angle{98.331}^\circ & 0.0151\angle{97.085}^\circ \\ 0.0152\angle{98.065}^\circ & 0.4193\angle{-6.54}^\circ & 0.0152\angle{96.772}^\circ & 0.0825\angle{98.196}^\circ \\ 0.0823\angle{98.331}^\circ & 0.0152\angle{96.772}^\circ & 0.4190\angle{-6.60}^\circ & 0.0150\angle{97.347}^\circ \\ 0.0151\angle{97.085}^\circ & 0.0825\angle{98.196}^\circ & 0.0150\angle{97.347}^\circ & 0.4192\angle{-6.63}^\circ \end{bmatrix} \tag{5.13}$$

The noise current transformation matrix $[T_z]$ is also given by

$$[T_{z_{nm}}] = \begin{bmatrix} 30.186\angle{-2.51}^\circ & 0.785\angle{-89.122}^\circ & 4.245\angle{-88.855}^\circ & 0.778\angle{-90.101}^\circ \\ 0.785\angle{-89.122}^\circ & 30.198\angle{-2.51}^\circ & 0.784\angle{-90.414}^\circ & 4.254\angle{-88.991}^\circ \\ 4.245\angle{-88.855}^\circ & 0.784\angle{-90.414}^\circ & 30.217\angle{-2.47}^\circ & 0.774\angle{-89.840}^\circ \\ 0.778\angle{-90.101}^\circ & 4.254\angle{-88.991}^\circ & 0.774\angle{-89.840}^\circ & 30.205\angle{-2.45}^\circ \end{bmatrix} \tag{5.14}$$

The source port noise correlation matrix $[R_n]$ can then be calculated and by taking the element-wise square root of the main diagonal, the expected source port noise voltage. The expected noise active impedance can then be determined as

$$\begin{aligned} [\tilde{\boldsymbol{Z}}_{\boldsymbol{act_n}}] &= [\tilde{\boldsymbol{Y}}_{\boldsymbol{act_n}}]^{-1} \\ &= \left[[v_{n_d}]^{-1}[Y][\tilde{\boldsymbol{v}}_{\boldsymbol{n}}]\right]^{-1} \\ &= \begin{bmatrix} 76.56\angle{-22.28}^\circ \\ 76.52\angle{-22.36}^\circ \\ 76.69\angle{-22.21}^\circ \\ 76.61\angle{-22.14}^\circ \end{bmatrix} \end{aligned} \tag{5.15}$$

5.2.3.3 Active Reflection Coefficient Magnitude

As can be seen in figure 5.7, as the antenna is scanned over ϕ and θ the active impedance periodically falls outside the boundaries of the Smith chart. For the case of the unmatched QMA, the regions over space, where the differential resistance of each channel becomes negative are shown for each channel in figure 5.8 with the red markers indicating points with $|\Gamma_{s_{act_k}}| > 1$.

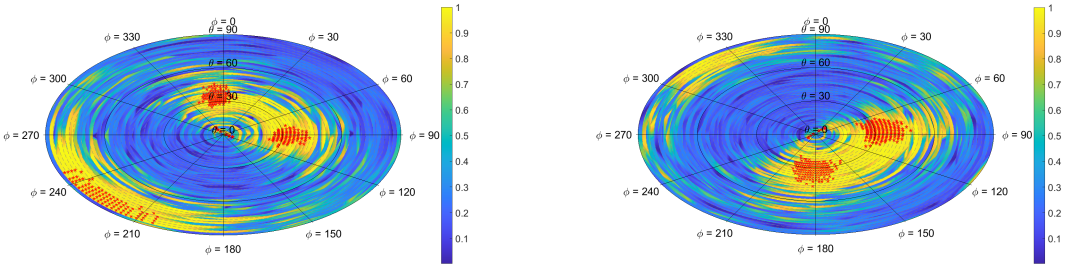

(a) $|\Gamma_{act_{s_1}}(\phi,\theta)|$ (b) $|\Gamma_{act_{s_2}}(\phi,\theta)|$

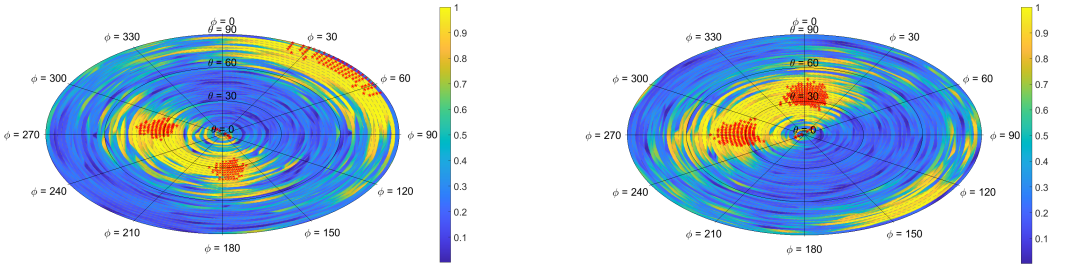

(c) $|\Gamma_{act_{s_3}}(\phi,\theta)|$ (d) $|\Gamma_{act_{s_4}}(\phi,\theta)|$

Figure 5.8: $|\Gamma_{act_{s_k}}(\phi,\theta)|$ at $f = 5.5$ GHz for each channel, red indicates $|\Gamma_{act_s}| > 1$

It can be observed from figure 5.8 that at an angle where a given channel active reflection coefficient magnitude is larger than unity, for each such channel at least one of the other channels exhibit an active reflection coefficient with a small magnitude to compensate.

5.2.3.4 Interpreting of Signal- and Noise Active Impedances

Due to the separation of the signal-no-noise and noise-no-signal cases and mathematical calculations, two distinct active impedances have arisen. The signal active impedance is a spatially variable active impedance dependent on the external signal of interest, while the noise active impedance is assumed spatially invariable and is dependent only on the internal receiver and antenna behaviour. In real operation, only one matching network can be implemented however, so it becomes of interest to consider what the practical meaning of each active impedance is and what matching to the specific impedance implicitly attempts to do.

Considering the noise figure of an amplifier, it is known that

$$F_{LNA} = \frac{SNR_i}{SNR_o} = \frac{P_{s_i}}{P_{n_i}} \frac{P_{n_o}}{P_{s_o}}$$

It is thus clear that in order to manipulate the noise figure, the signal power P_s can be optimized with the noise power P_n taken as is, or vice versa. During the construction of the signal-no-noise case, the noise sources in the

receiver were explicitly made zero. This, in effect, creates a solution where the noise figure is optimized in terms of the signals of interest by implementing an ideal match by focusing on the signal power, P_s. The noise power, P_n, will then constrict itself to maximize the output SNR. Conversely in the noise-no-signal case, the noise figure is optimized by focusing on the noise power P_n to maximize the output SNR.

5.2.4 Matching Topology Selection and SNR Performance

The various approaches discussed in chapters 2 and 3 can be applied to the signal active impedance to determine a single impedance value for each channel to which the LNA $Z_{s_{opt}}$ can be matched. Once the impedance has been determined, a matching network topology can be selected based on the criteria as set forth in equations 4.9. The unmatched max SNR beamformer output SNR as the array is scanned is plotted in figure 5.9 for a receiver at temperature $T = 290$ K. The elevation angle θ is plotted along the radial distance and the azimuth angle ϕ is plotted around the circumference of the circle. Only values in the space $\phi \in [0°, 358°]$, $\theta \in [0°, 90°]$ are plotted, as below the horizontal ground plane, the antenna gain is zero. Selected plots over ϕ and θ for other matching criteria can be seen in Figure 5.13. All plots have an input signal power level of $P_s = 0.1328$ W.

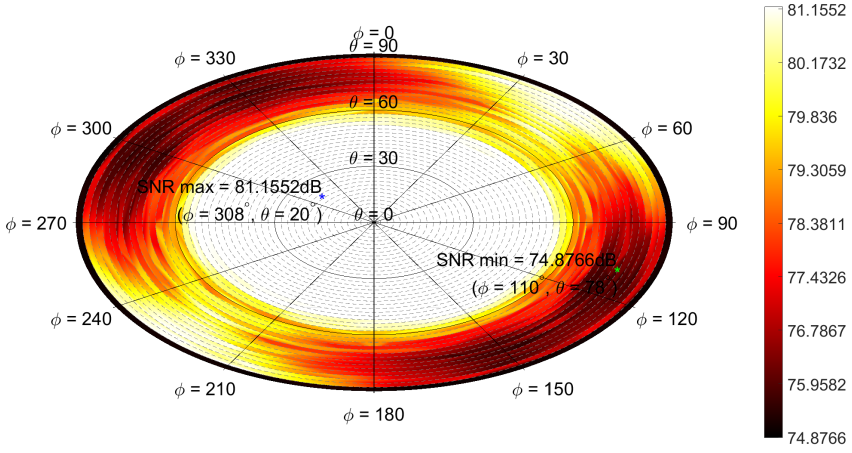

Figure 5.9: $QMA\ SNR_{o_{unmatched}}(\phi, \theta)$ [dB] at $f = 5.5$ GHz

5.2.4.1 Noise Active Impedance Direct Match

Due to the isotropic external noise distribution nature, the noise active impedance is a singular value and therefore can directly be matched to using the appropriate topology. The noise active impedances and optimal noise source impedance are given at $f = 5.5$ GHz for the unmatched case by

$$[\tilde{\boldsymbol{Z}}_{\boldsymbol{act_n}}] = \begin{bmatrix} 76.56\angle{-22.28}^\circ \\ 76.52\angle{-22.36}^\circ \\ 76.69\angle{-22.21}^\circ \\ 76.61\angle{-22.14}^\circ \end{bmatrix}$$

$$[\tilde{\boldsymbol{Z}}_{\boldsymbol{s_{opt}}}] = \begin{bmatrix} 45.43\angle{-16.18}^\circ \\ 45.43\angle{-16.18}^\circ \\ 45.43\angle{-16.18}^\circ \\ 45.43\angle{-16.18}^\circ \end{bmatrix}$$

Note that $R_{act_{nm}} > R_{s_{opt}}$ for each channel, so a Shunt-Series matching network topology must be implemented. Attempting to match $[\tilde{\boldsymbol{Z}}_{\boldsymbol{s_{opt}}}]$ to $[\tilde{\boldsymbol{Z}}_{\boldsymbol{act_n}}]$ using a Series-Shunt topology will result in complex reactance matrices for $j[X_{1_d}]$ and $j[X_{2_d}]$. It is known [45] that for open circuited shunt stubs and short circuited series stubs respectively, the corresponding susceptance and reactance values in terms of the line characteristic impedance Z_0 and the electric length βl is given by

$$jB_{shunt_{open}} = jY_0 \tan \beta l \tag{5.16a}$$

$$jX_{series_{short}} = jZ_0 \tan \beta l \tag{5.16b}$$

It can be seen from equations 5.16 that complex reactances cannot physically be realized using stub lines for real valued characteristic impedances Z_0, hence the Shunt-Series topology must be selected. The reactance matrices can then be calculated at $f = 5.5$ GHz as

$$j[X_{1_d}] = \begin{bmatrix} 154.06\angle{-90}^\circ & 0 & 0 & 0 \\ 0 & 154.55\angle{-90}^\circ & 0 & 0 \\ 0 & 0 & 153.49\angle{-90}^\circ & 0 \\ 0 & 0 & 0 & 153.32\angle{-90}^\circ \end{bmatrix} \tag{5.17}$$

$$j[X_{2_d}] = \begin{bmatrix} 28.644\angle{-90}^\circ & 0 & 0 & 0 \\ 0 & 28.646\angle{-90}^\circ & 0 & 0 \\ 0 & 0 & 28.698\angle{-90}^\circ & 0 \\ 0 & 0 & 0 & 28.634\angle{-90}^\circ \end{bmatrix} \tag{5.18}$$

The corresponding transformation matrices $[T_x]$, $[T_s]$ and $[T_z]$ are then given by

$$[T_x] = \begin{bmatrix} 0.378\angle{-5.85}^\circ & 0.014\angle{116.32}^\circ & 0.084\angle{116.36}^\circ & 0.014\angle{115.06}^\circ \\ 0.014\angle{116.36}^\circ & 0.378\angle{-5.83}^\circ & 0.014\angle{114.75}^\circ & 0.084\angle{116.24}^\circ \\ 0.084\angle{116.32}^\circ & 0.014\angle{114.67}^\circ & 0.377\angle{-5.95}^\circ & 0.013\angle{115.44}^\circ \\ 0.014\angle{115.01}^\circ & 0.084\angle{116.15}^\circ & 0.013\angle{115.42}^\circ & 0.377\angle{-6.02}^\circ \end{bmatrix} \tag{5.19}$$

$$[T_s] = \begin{bmatrix} 0.454\angle{146.89}^\circ & 0.016\angle{-90.93}^\circ & 0.101\angle{-90.89}^\circ & 0.016\angle{-92.19}^\circ \\ 0.016\angle{-90.90}^\circ & 0.454\angle{146.91}^\circ & 0.016\angle{-92.51}^\circ & 0.101\angle{-91.02}^\circ \\ 0.101\angle{-90.97}^\circ & 0.016\angle{-92.63}^\circ & 0.454\angle{146.75}^\circ & 0.016\angle{-91.86}^\circ \\ 0.016\angle{-92.24}^\circ & 0.101\angle{-91.10}^\circ & 0.016\angle{-91.83}^\circ & 0.454\angle{146.74}^\circ \end{bmatrix} \tag{5.20}$$

$$[T_z] = \begin{bmatrix} 27.06\angle{-0.501}^\circ & 0.664\angle{-113.22}^\circ & 4.073\angle{-113.26}^\circ & 0.657\angle{-114.57}^\circ \\ 0.664\angle{-113.22}^\circ & 27.08\angle{-0.478}^\circ & 0.662\angle{-114.88}^\circ & 4.084\angle{-113.40}^\circ \\ 4.075\angle{-113.30}^\circ & 0.663\angle{-114.91}^\circ & 27.08\angle{-0.518}^\circ & 0.653\angle{-114.24}^\circ \\ 0.657\angle{-114.57}^\circ & 4.084\angle{-113.39}^\circ & 0.653\angle{-114.20}^\circ & 27.08\angle{-0.518}^\circ \end{bmatrix} \tag{5.21}$$

As seen in figure 5.13, after matching, the shunt-series matching to noise impedance criteria yields a maximum SNR at $\phi_{max} = 308^\circ, \theta_{max} = 20^\circ$, of

$$SNR_{max_{shse}} = 81.149 \text{ dB} \tag{5.22}$$

5.2.4.2 Signal Active Impedance Averaging

The external noise source distribution is isotropic and therefore a singular value for the noise impedance was determined, as in section 5.2.4.1. It is thus only necessary to average the signal active impedance over ϕ and θ at the operating frequency. As $\phi \in [0^\circ, 358^\circ]$ and $\theta \in [0^\circ, 90^\circ]$ and both are sampled at every two degrees, this corresponds to $M_\phi = 180$ values and $M_\theta = 46$ values respectively. The maximum level of recursion over each variable is thus

$$L_{rec_\phi} = \lceil \log_2 M_\phi \rceil = 8$$
$$L_{rec_\theta} = \lceil \log_2 M_\theta \rceil = 6$$

As the average is taken over $M_{tot} = M_\phi \times M_\theta = 8190$ samples, it is reasonable to expect that for such a large sample set, the average will not vary by much if the majority of the values are closely spaced to each other, as seen in figure 5.7. The set of impedances is re-sorted between every level of recursion. Table 5.3 shows the averaged signal active impedance for each L_{rec_ϕ} and L_{rec_θ} for $k = 1$.

Recursively Averaged Active Impedance Values [Ω]

	$L_{rec_\phi} = 0$	$L_{rec_\phi} = 1$	$L_{rec_\phi} = 2$
$L_{rec_\theta} = 0$	$68.280\angle 6.33°$	$68.280\angle 6.33°$	$68.280\angle 6.33°$
$L_{rec_\theta} = 1$	$68.311\angle 6.33°$	$68.311\angle 6.33°$	$68.311\angle 6.33°$
$L_{rec_\theta} = 2$	$68.311\angle 6.33°$	$68.311\angle 6.33°$	$68.311\angle 6.33°$
$L_{rec_\theta} = 3$	$68.416\angle 6.26°$	$68.416\angle 6.26°$	$68.416\angle 6.26°$
$L_{rec_\theta} = 4$	$68.416\angle 6.26°$	$68.416\angle 6.26°$	$68.416\angle 6.26°$
$L_{rec_\theta} = 5$	$68.287\angle 6.24°$	$68.287\angle 6.24°$	$68.287\angle 6.24°$
$L_{rec_\theta} = 6$	$68.287\angle 6.24°$	$68.287\angle 6.24°$	$68.287\angle 6.24°$
	$L_{rec_\phi} = 3$	$L_{rec_\phi} = 4$	$L_{rec_\phi} = 5$
$L_{rec_\theta} = 0$	$68.269\angle 6.34°$	$68.261\angle 6.42°$	$68.261\angle 6.42°$
$L_{rec_\theta} = 1$	$68.300\angle 6.34°$	$68.294\angle 6.42°$	$68.294\angle 6.42°$
$L_{rec_\theta} = 2$	$68.300\angle 6.34°$	$68.294\angle 6.42°$	$68.294\angle 6.42°$
$L_{rec_\theta} = 3$	$68.402\angle 6.27°$	$68.400\angle 6.18°$	$68.400\angle 6.18°$
$L_{rec_\theta} = 4$	$68.402\angle 6.27°$	$68.400\angle 6.18°$	$68.400\angle 6.18°$
$L_{rec_\theta} = 5$	$68.272\angle 6.24°$	$68.255\angle 6.11°$	$68.255\angle 6.11°$
$L_{rec_\theta} = 6$	$68.272\angle 6.24°$	$68.255\angle 6.11°$	$68.255\angle 6.11°$
	$L_{rec_\phi} = 6$	$L_{rec_\phi} = 7$	$L_{rec_\phi} = 8$
$L_{rec_\theta} = 0$	$68.261\angle 6.42°$	$68.259\angle 6.39°$	$68.259\angle 6.39°$
$L_{rec_\theta} = 1$	$68.294\angle 6.42°$	$68.290\angle 6.37°$	$68.290\angle 6.37°$
$L_{rec_\theta} = 2$	$68.294\angle 6.42°$	$68.290\angle 6.37°$	$68.290\angle 6.37°$
$L_{rec_\theta} = 3$	$68.400\angle 6.18°$	$68.389\angle 6.20°$	$68.389\angle 6.20°$
$L_{rec_\theta} = 4$	$68.400\angle 6.18°$	$68.389\angle 6.20°$	$68.389\angle 6.20°$
$L_{rec_\theta} = 5$	$68.255\angle 6.11°$	$68.257\angle 6.17°$	$68.257\angle 6.17°$
$L_{rec_\theta} = 6$	$68.255\angle 6.11°$	$68.257\angle 6.17°$	$68.257\angle 6.17°$

Table 5.3: Signal Active Impedance Values Recursively Averaged over ϕ and θ by L_{rec}

The optimum recursively averaged active impedance match occurs at multiple values of L_{rec_ϕ} and L_{rec_θ} as shown in table 5.4, which corresponds to identical averages as seen in table 5.3. All matches were implemented with a Shunt-Series matching section.

L_{rec_ϕ} and L_{rec_θ} and SNR_{max}

L_{rec_ϕ}	L_{rec_θ}	$SNR_{max_{avg}}$ (dB)
7	1	81.1007
7	2	81.1007
8	1	81.1007
8	2	81.1007

Table 5.4: L_{rec_ϕ} and L_{rec_θ} Values for Best maximum SNR Using Averaging

For each of the combinations of L_{rec_ϕ} and L_{rec_θ}, the maximum SNR is achieved at $\phi = 308°, \theta = 20°$. It should be clear that the different averaging levels produce almost identical results.

5.2.4.3 Self Impedance Matching

The LNA $\Gamma_{s_{opt}}$ was matched to the QMA self impedance at $f = 5.5$ GHz using a Shunt-Series matching section. The vector $[\tilde{\boldsymbol{Z}}_{\boldsymbol{self}}]$ is given by

$$[\tilde{\boldsymbol{Z}}_{\boldsymbol{self}}] = \begin{bmatrix} Z_{11} \\ Z_{22} \\ Z_{33} \\ Z_{44} \end{bmatrix} = \begin{bmatrix} 67.4533\angle 2.498° \\ 67.4884\angle 2.508° \\ 67.6067\angle 2.597° \\ 67.5147\angle 2.662° \end{bmatrix}$$

The maximum output SNR was achieved at $\phi = 308°, \theta = 20°$ with a value of

$$SNR_{max_{self}} = 81.1198 \text{ dB}$$

5.2.4.4 Noise Figure Iterative Point Search

The optimal noise impedance of the LNA was varied through each value in the set of active impedances for the unmatched case for each channel. The maximum noise figure over ϕ and θ was then calculated with the LNA noise figure equation. The minimum maximum noise figure was identified and the corresponding optimal source impedance determined as $Z'_{s_{opt}} = Z_{act_{snm}}(\phi_0, \theta_0)$. $Z'_{s_{opt}}$ was then evaluated for each channel and frequency to determine whether the majority of the real parts of the optimal noise impedances $R'_{s_{opt}}$ satisfy the criteria for Shunt-Series, Series-Shunt or Single-Series impedance matching. This was done as the equations for the transformation matrices require each channel to have the same topology for the matching network. The majority of impedances required Series-Shunt matching, therefore if an optimal impedance was found where $R'_{s_{opt}} > R_{s_{opt}}$, the next smallest maximum noise figure would be found and the new $Z'_{s_{opt}}$ determined iteratively until each channel conformed to the requirement. If the optimal noise impedance had a negative real part, a new $Z'_{s_{opt}}$ was also determined iteratively. This was necessary because any

stub based match can only transform an impedance inside the Smith Chart to another impedance inside the Smith Chart. The LNA $Z_{s_{opt}}$ had a positive real part and would thus correspond to a point inside the Smith Chart when plotted. At $f = 5.5$ GHz, the set of optimal impedances produced by this method is given by

$$[\tilde{\boldsymbol{Z}}_{\boldsymbol{minmax}}] = \begin{bmatrix} 23.5439\angle \quad 19.356° \\ 33.6605\angle -58.327° \\ 35.6916\angle -13.512° \\ 26.4608\angle -64.116° \end{bmatrix}$$

The introduction of the Series-Shunt matching network caused a difference in the active impedance calculated for each scan angle. As seen for channel 1 from figure 5.10, $Z'_{s_{opt}}$ (red) does not match any point in the new set of active impedances, $Z_{act_{s_{minmax}}}$ (blue), produced after the impedance matching. Similar results are observed for each other channel. This implies that the LNAs will not achieve a noise figure of $F = F_{min}$ at any scan angle.

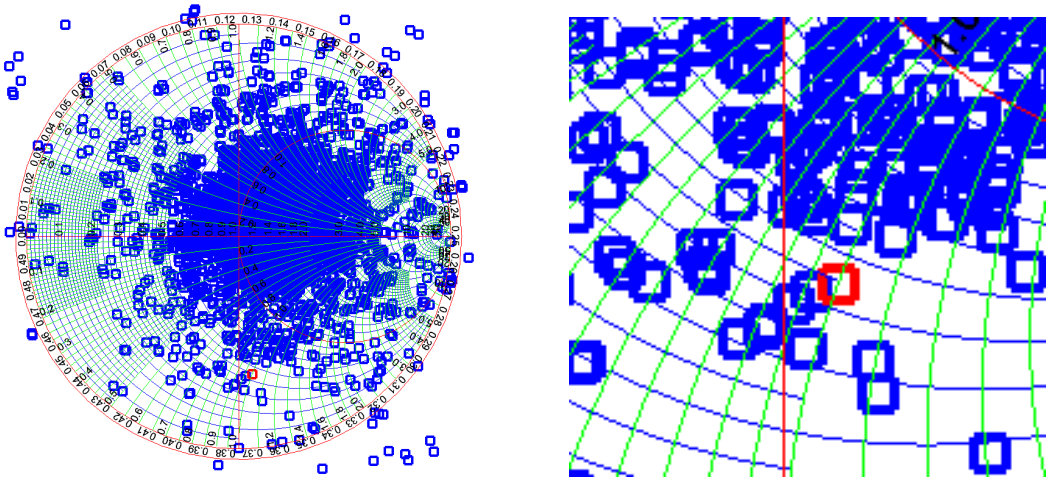

(a) Full view (b) Zoomed in

Figure 5.10: $Z_{act_{s_{minmax}}}(\phi, \theta)$ and $Z'_{s_{opt}}$ at $f = 5.5$ GHz for channel 1

To achieve a noise figure of $F = F_{min}$ at a desired scan angle, ϕ_0, θ_0, it is necessary to simultaneously numerically solve the equations

$$\begin{aligned} [\tilde{\boldsymbol{Z}}_{\boldsymbol{act_s}}] &= \left[[v_{s_d}]^{-1}[Y][\tilde{\boldsymbol{v}}_{\boldsymbol{s}}]\right]^{-1} \\ [\tilde{\boldsymbol{v}}_{\boldsymbol{s}}] &= [T_{x_{sesh}}][\tilde{\boldsymbol{e}}_{\boldsymbol{s}}(\boldsymbol{\phi_0}, \boldsymbol{\theta_0})] \\ [Z'_{s_{opt_d}}] &= j[X_{1_d}] + j[X_{2_d}][Z_{s_{opt_d}}]\left[j[X_{2_d}] + [Z_{s_{opt_d}}]\right]^{-1} \\ [Z_{act_{s_d}}] &= [Z'_{s_{opt_d}}] \end{aligned}$$

The maximum output SNR was achieved at $\phi = 308°, \theta = 20°$ with a value of

$$SNR_{max_{minmax}} = 81.0072 \text{ dB}$$

5.2.4.5 $\Gamma'_{s_{opt}}$ Parameter Sweep

The optimal noise source reflection coefficient was transformed to a new optimum coefficient $\Gamma'_{s_{opt}}$, where the value of $\Gamma'_{s_{opt}}$ was swept in the ranges

$$|\Gamma'_{s_{opt}}| = [0, 0.2, 0.4, 0.6, 0.8]$$
$$\angle\Gamma'_{s_{opt}} = [0°, 30°, 60°, 90°, 120°, 150°, 180°, 210°, 240°, 270°, 300°, 330°]$$

For each channel, $\Gamma_{s_{opt}}$ was transformed to the same value of $\Gamma'_{s_{opt}}$. As each channel had the same $\Gamma'_{s_{opt}}$, matching topology requirement differences between channels was not a problem. Both Series-Shunt and Shunt-Series topologies were implemented to perform the impedance matching. The transformed optimum source impedances are plotted on the Smith Chart in figure 5.11 to show the coverage of the Smith Chart.

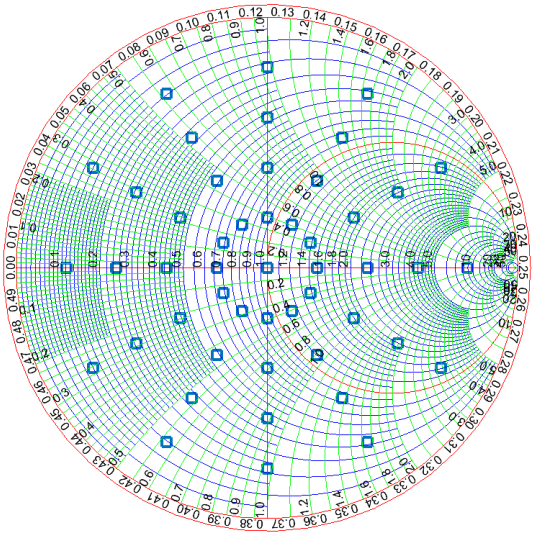

Figure 5.11: $Z'_{s_{opt_{sweep}}}$ impedances

The maximum SNR for each value of $\Gamma'_{s_{opt}}$ is shown in table 5.5

Maximum SNR (dB) over ϕ and θ

$\angle\Gamma'_{s_{opt}}$	$\lvert\Gamma'_{s_{opt}}\rvert = 0$	$\lvert\Gamma'_{s_{opt}}\rvert = 0.2$	$\lvert\Gamma'_{s_{opt}}\rvert = 0.4$	$\lvert\Gamma'_{s_{opt}}\rvert = 0.6$	$\lvert\Gamma'_{s_{opt}}\rvert = 0.8$
0°	81.2117	81.093	80.935	80.7292	80.2801
30°	81.2117	81.0527	80.8058	80.4772	79.8522
60°	81.2117	81.0554	80.739	81.0127	80.3123
90°	81.2117	81.1244	81.1446	80.8616	80.1139
120°	81.2117	81.2211	81.0981	80.8017	80.0272
150°	81.2117	81.2196	81.0957	80.8099	80.0086
180°	81.2117	81.2251	81.1276	80.8717	80.066
210°	81.2117	81.2293	81.1776	80.9767	80.2237
240°	81.2117	81.2072	81.2155	81.0999	80.4859
270°	81.2117	81.1944	81.1611	81.1671	80.799
300°	81.2117	81.1951	81.1878	80.8107	80.9334
330°	81.2117	81.1495	81.0768	80.9765	80.6575

Table 5.5: $SNR_{max_{sweep}}$ for each $\Gamma'_{s_{opt}}$

The scan angle at which each SNR_{max} is achieved is the same for all values of $\Gamma'_{s_{opt}}$. The maximum SNR for the parameter sweep was achieved for $\Gamma'_{s_{opt}} = 0.2\angle 210°$. For $\Gamma'_{s_{opt}} = 0.2\angle 210°$, the maximum SNR is achieved at $\phi = 308°, \theta = 20°$ and has a value of

$$SNR_{max_{sweep}} = 81.2293 \text{ dB}$$

5.2.4.6 Optimized Simplex Search Solution

An optimizer was implemented in MATLAB R2017a using the fminsearch function. fminsearch is a direct search method that utilizes a simplex search [48]. The function works by taking a starting point as argument and locally searching iteratively around the point to minimize an error function. The function can be set to terminate after the error function converges to a value or after a number of iterations. An iteration is defined as a function evaluation that yields a smaller error function value than the current optimized value.

The function was set up to optimize the SNR by maximizing the minimum SNR achived over the range $\phi \in [0°, 358°], \theta \in [0°, 90°]$ by implementing the error function

$$err = 1000 - SNR_{min}(dB)$$

To conserve memory, the optimizer was set to terminate after a number of iterations had been reached

$$MaxIter = 750$$

The optimizer was run for both a Series-Shunt and Shunt-Series topology. The matching criteria with the highest SNR_{min} for each topology was used as the

starting point for the optimizer by feeding the matching network stub reactances, $[\tilde{\boldsymbol{X}}_1]$ and $[\tilde{\boldsymbol{X}}_2]$, as input arguments. The optimizer then evaluated the entire system using the equations shown in chapter 3 and determines the output SNR over scan angle to reevaluate the error function. Figure 5.12 shows the graphic output of the optimizer after the maximum number of iterations have been reached for both topologies.

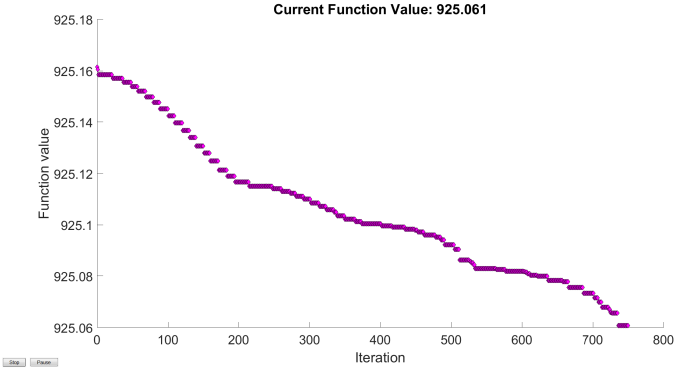

(a) Shunt-Series

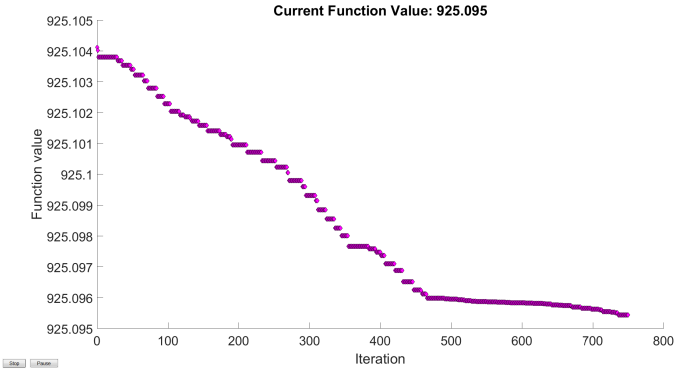

(b) Series-Shunt

Figure 5.12: MATLAB Optimizer error function output windows

For the Shunt-Series topology, an improvement of 0.1 dB was achieved through optimizing, while for the Series-Shunt topology, an improvement of 0.01 dB was achieved. It is thus clear that no significant improvement is achieved using the optimizer. The maximum SNR for the optimized Series-Shunt and Shunt-Series topologies were respectively achieved at $\phi_{sesh} = 308°, \theta_{sesh} = 20°$ and $\phi_{shse} = 308°, \theta_{shse} = 20°$. The corresponding maximum SNR values are given

by

$$SNR_{max_{optim_{sesh}}} = 81.2157 \text{ dB}$$
$$SNR_{max_{optim_{shse}}} = 81.2403 \text{ dB}$$

5.2.5 Comparison of Degree of Similarity of of Active Impedance for Matched and Unmatched Cases

5.2.5.1 Interpretation and Pre-Processing to Utilize the Structural Similarity Index

The Structural Similarity Index [49] is an image processing technique that quantifies the distortion or degradation of an image with regards to a reference image. The visibility of errors are quantified in terms of luminance, contrast and structure. The Structural Similarity Index requires that the reference image and distorted image be similar in order to be a sensible measurement of the noise or distortion added to the reference image in order to produce the distorted image. It is also required that the images have the same dimensions in pixels so that each pixel has another to be compared to. In MATLAB R2017a, the Structural Similarity Index Measurement (SSIM) function produces a rational number in the range $0 \leq SSIM \leq 1$, where $SSIM = 0$ corresponds to no similarity and $SSIM = 1$ corresponds to perfect similarity. The SSIM provides a novel way of comparing the different matching criteria.

In order to take full advantage of the SSIM, the physical structure of the active impedance plot must be considered so that the expected differences between plots for different criteria can be meaningfully quantified, in terms of the three parameters of the SSIM. The active impedance plots, as seen in figure 5.7, plot two-dimensional data, namely the active imedance as scanned over ϕ and θ. This data can be represented by an $L_\phi \times L_\theta$ matrix. Each row or column of the matrix represents a change in the value of one variable, while keeping the other constant. Each such a vector is plotted in a different colour so that the change in the value over the scanning range of one variable can be observed.

Luminance For two images produced in MATLAB, luminance will be the same for the two images and thus will not have effect the value of the SSIM. For any reference and distorted image, the luminance value in the SSIM will be the same.

Contrast Differences in colour between the two images will change the value of contrast in the SSIM. As stated, the color of the data points in the active impedance plot carries information on the scan data that produces any given

point. There are two implementations to consider when quantifying the contrast differences using the SSIM.

In the first implementation, the matrices can be plotted with each vector plotted in a different colour. Interpreted together with the structure data, this implementation can be used to determine how similar a vector is plotted in each image, given that the vector is plotted in the same colour in both images. The colour can be used to identify the vector in the distorted image and as such information on how much the plot of each vector of the active impedance shifts over the Smith Chart for each matching network implementation can be extracted.

There are drawbacks to this implementation. Firstly, as there is more information to quantify, this implementation will be more computationally expensive. Secondly, if sample points in space produce the same active impedance, points will overlap on the Smith Chart. Depending on the degree to which points overlap, the information for which the increased computational resources were sacrificed can be lost regardless. Thirdly, if there are a large number of vectors to plot, each with a unique colour, eventually the vectors will become hard to distinguish from each other visually. This translates to a low contrast between similarly coloured vectors, and therefore a lack of information. The SSIM would still produced an effected value that internally quantifies the differences in vectors, but the ability to interpret the changes by a designer would be diminished.

In the second implementation, the matrices can be plotted in a single colour. This method discards the angular data in the plot. In terms of meaning, a plot of the active impedance in a single colour can be used to determine the similarity of two matrices based on total structure alone. The changes in the position of each individual vector of the matrix can not be quantified.

The main drawback to this implementation is the loss of data. The implementation is less computationally expensive, but it must be noted that this implementation will inherently produce a higher SSIM than for the first implementation as the difference information has been discarded.

For the purposes of this work, the second implementation was selected as the drawbacks of the first implementation outweigh the benefits thereof.

Structure The main focus of the SSIM is to determine the similarity of the structure of the plot of active impedances. As the algorithm is meant to detect minor errors and not meaningful differences in structure, it is required that the two images be largely similar to each other. As seen in figure 5.7, the large

majority of points on the Smith Chart are lumped together. For the algorithm to function effectively this is also required to be the case for the matched cases. The further lying points such as those on the edge of the lumped group or outside the Smith Chart can have structural differences however, which is what the structure parameter of the SSIM will seek to quantify.

Following the calculation of the SSIM for any given matching topology, the similarity index can be compared to a threshold. Above this similarity threshold, the set of active impedances can be considered close enough and thus the receiver systems as similar enough, that the design considerations and assumptions would be reasonable for the matched receiver network. Differences in implementation outcomes and design criteria, such as the noise figure at a given angle, would then also be minimal enough that it would be suffficient to design for the unmatched case as opposed to solving simultaneous equations.

5.2.5.2 SSIM Results

A similarity threshold of $SSIM_{thresh} = 0.85$ was used for the interpretation of the similarity of active impedance sets. The procedure for determining the SSIM of a design implementation was as follows

- Plot $Z_{act_{snm}}$ for each channel in a single colour on the Smith Chart
- Plot $Z_{act_{s_{criteria}}}$ for each channel in a single colour on the Smith Chart
- Save active impedance plots to .PNG files
- Read active impedance plots into MATLAB as image data using imread function
- Compare images in MATLAB using the ssim function

The resulting SSIM data for each channel of the noise figure iterative point search is shown in table 5.6. It is clear that the SSIM for each channel has a high value. There is thus a large degree of structural similarity in the plot of the impedance before and after matching. The area on the Smith Chart occupied by the total set of active impedances is not changed much by matching. This implies that the change in value of the active impedance as swept over either ϕ while θ is held constant, or vice versa, will likely produce a value contained in the original set of active impedances. Because the SSIM was taken for a single colour plot of the active impedances, no conclusion can be made on how much a single impedance vector will change within the area covered on the Smith Chart. For sets of data that have smaller sampling intervals, and thus do not span large percentages of the Smith chart, the SSIM can provide better insight. The traces of each vector can be plotted in a different colour, enabling the SSIM to keep track of the similarity in colour inside the covered area of the

Smith chart. The SSIM threshold is chosen as 0.85. In other words, above an 85% similarity, the set of active impedances is considered similar enough pre and post matching, that designing for the pre match case leads to acceptable post matching performance. As the SSIM values for each channel is above the SSIM threshold, the deviation is within the acceptable range. The SSIM threshold can be chosen as a specification by the designer.

	$SSIM_{minmax}$			
$SSIM_{thresh}$	$SSIM(k=1)$	$SSIM(k=2)$	$SSIM(k=3)$	$SSIM(k=4)$
0.85	0.9019	0.8851	0.8947	0.8910

Table 5.6: SSIM data at $f = 5.5$ GHz for the noise figure iterative point search case

Figure E.1 of Appendix E shows the maximum output SNR over $\phi = [0°, 358°]$, $\theta = [0°, 90°]$ per criteria for the QMA. It can be seen that for a mostly flat radiation pattern, optimizing the minimum output SNR over the scan range will lead to the maximum output SNR occurring for the optimized case. It can also be seen that for the QMA, any improvements in maximum output SNR from the unmatched case are marginal, while it is possible to achieve a lower maximum output SNR if the output criteria is chosen poorly. Figure E.2 of Appendix E shows the minimum output SNR over $\phi = [0°, 358°]$, $\theta = [0°, 90°]$ per criteria for the QMA. It can be seen that the choice of matching network can greatly influence the flatness of the output SNR over the scan range. It is possible to observe a drop of over 3 dB for the minimum output SNR from the unmatched case, while improvement from the unmatched case is marginal.

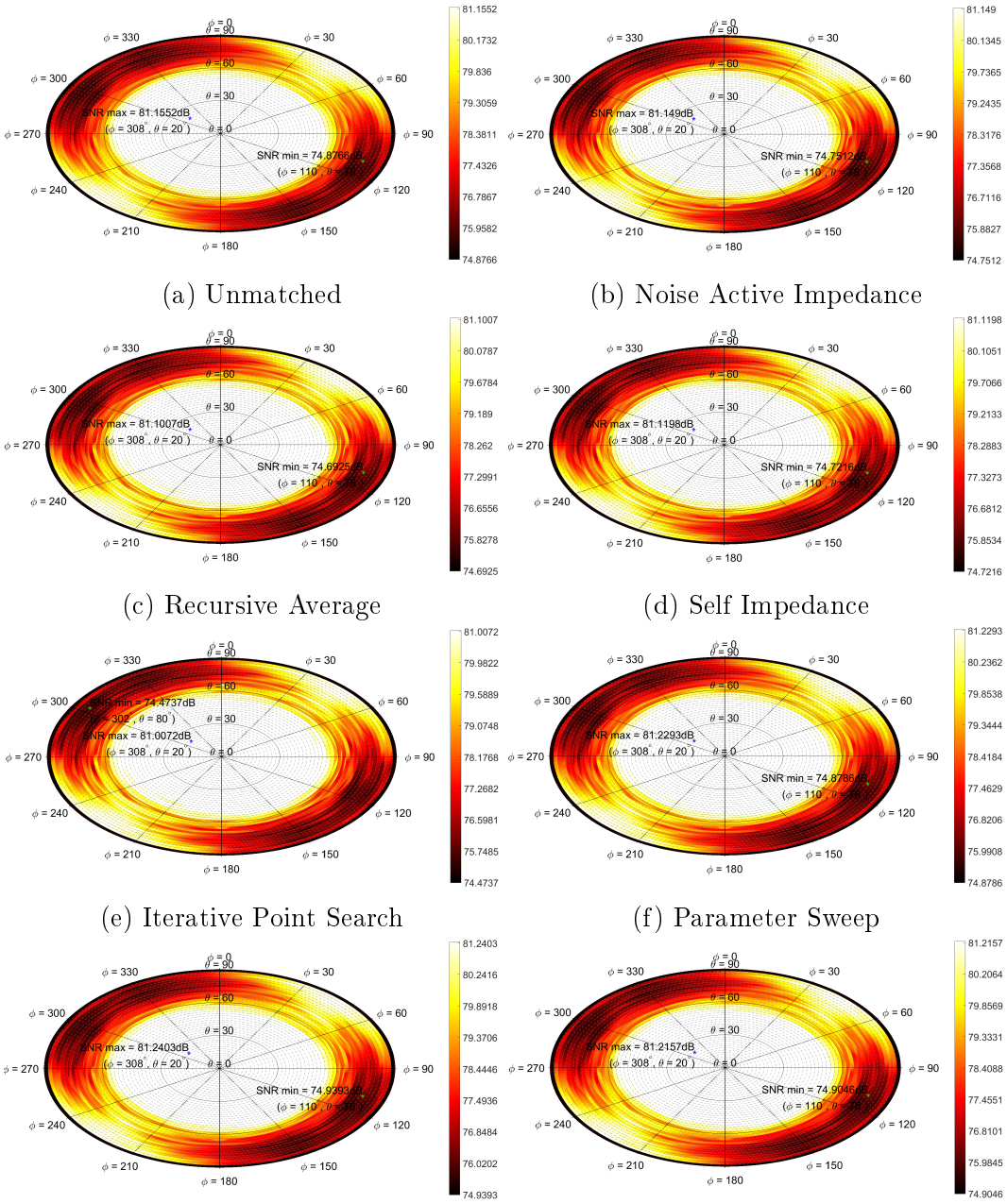

(a) Unmatched

(b) Noise Active Impedance

(c) Recursive Average

(d) Self Impedance

(e) Iterative Point Search

(f) Parameter Sweep

(g) Shunt-Series Optimized

(h) Series-Shunt Optimized

Figure 5.13: QMA SNR circles for best performing case of each matching criteria

Chapter 6

Comparison to Control Antenna Design Case

6.1 Design for Four Element Monopole Array

To draw conclusions on the SNR performance of the QMA and the degree to which it lends itself to optimization, as well as to further investigate the effectiveness of methods used on the QMA for SNR improvement, a secondary antenna array was investigated. The array consisted of four quarter wave monopoles placed above an finite conducting groundplane. The four monopole array (FMA) was simulated in Altair Hyperworks FEKO 14.0 as shown in figure 6.1. The FMA was chosen because quarter wave monopoles above ground planes are commonly used antennas.The monopoles were spaced identically to the spacing of the individual elements of the QMA at $\frac{\lambda_0}{2}$ at $f = 950$ MHz.

6.1.1 FMA at f=5.5 GHz

For the ports laid out as shown in figure 6.2, the FMA S-parameters were simulated in FEKO between $f = 5$ GHz and $f = 6$ GHz as shown in figure 6.3.

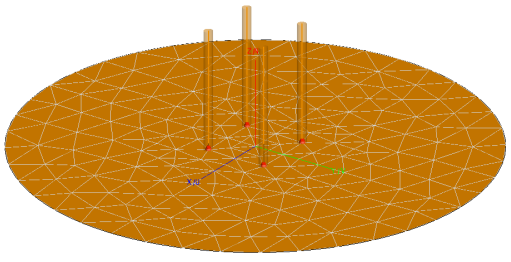

Figure 6.1: Four quarter wave monopoles above a conducting ground plane in FEKO

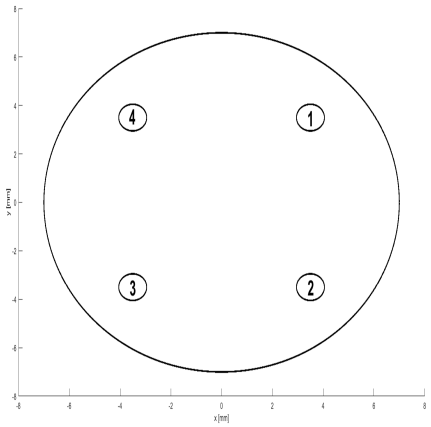

Figure 6.2: FMA port layout

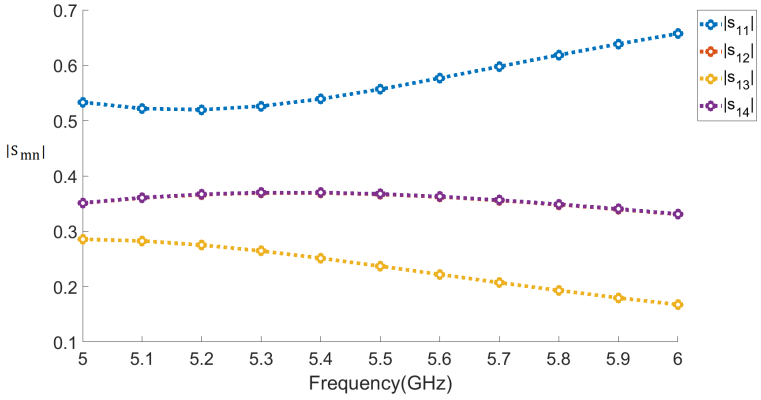

(a) $|s_{1m}(f)|$

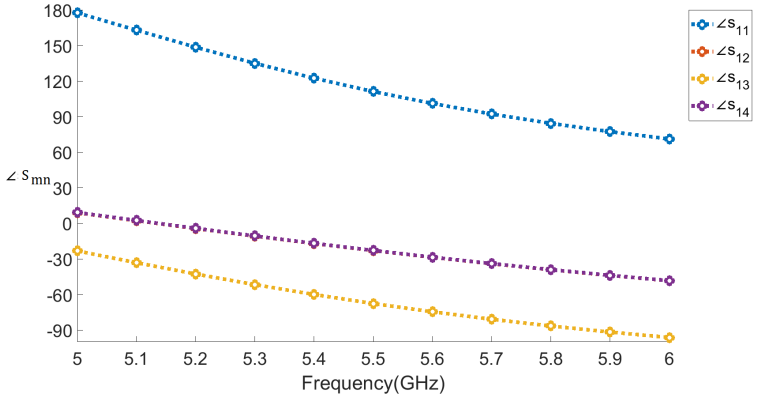

(b) $\angle s_{1m}(f)$

Figure 6.3: FMA S-parameters s_{1m} for channel 1 over frequency

The FMA E-field pattern over scan angle is as shown in figure 6.4.

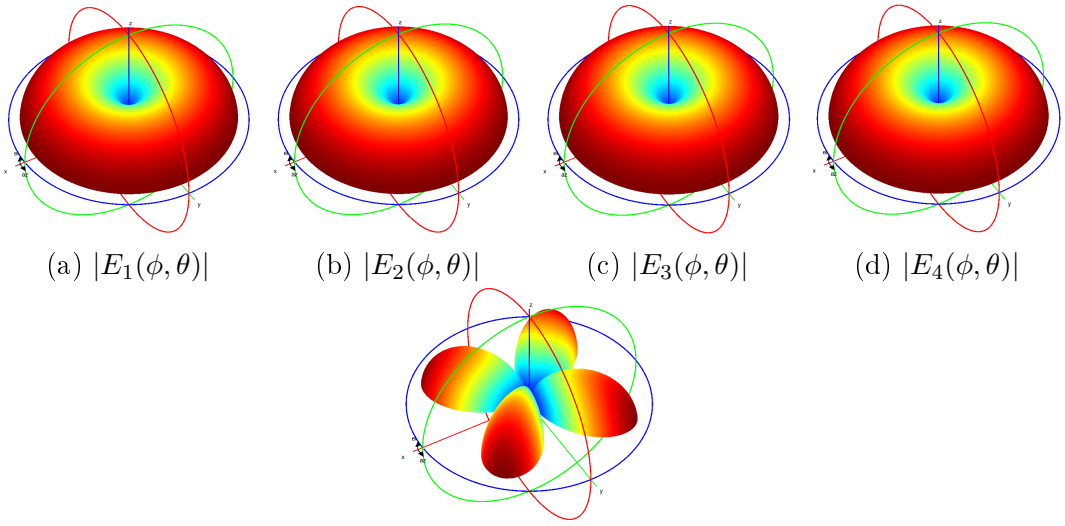

(a) $|E_1(\phi,\theta)|$ (b) $|E_2(\phi,\theta)|$ (c) $|E_3(\phi,\theta)|$ (d) $|E_4(\phi,\theta)|$

(e) $|E_{total}(\phi,\theta)|$ for unity excitation at all ports

Figure 6.4: FMA farfields per channel and full array at frequency $f = 5.5$ GHz

6.1.2 FMA Excitation and Active Impedance

For the incident E-field identical as for the QMA case, the open circuit voltage response, $[\tilde{\boldsymbol{v}}_{\boldsymbol{oc}}]$, is determined using the antenna effective length and the magnitude as shown in figure 6.5.

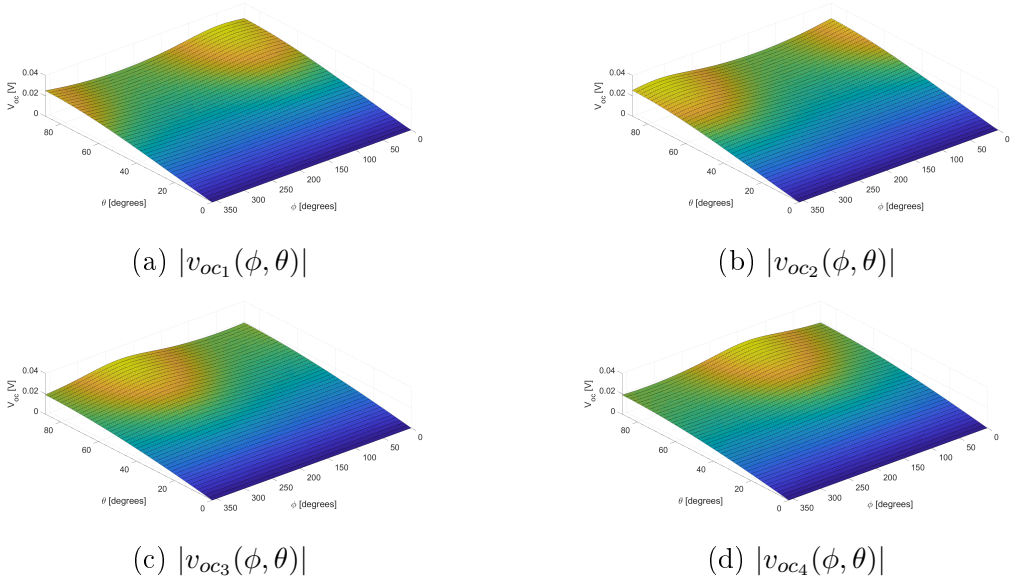

(a) $|v_{oc_1}(\phi,\theta)|$ (b) $|v_{oc_2}(\phi,\theta)|$

(c) $|v_{oc_3}(\phi,\theta)|$ (d) $|v_{oc_4}(\phi,\theta)|$

Figure 6.5: Array $|v_{oc_m}(\phi,\theta)|$ at $f = 5.5$ GHz

The signal active impedance is determined as for the QMA and is shown in figure 6.6. The ambient noise temperature distribution is taken as isotropic and the noise active impedance calculated as for the QMA.

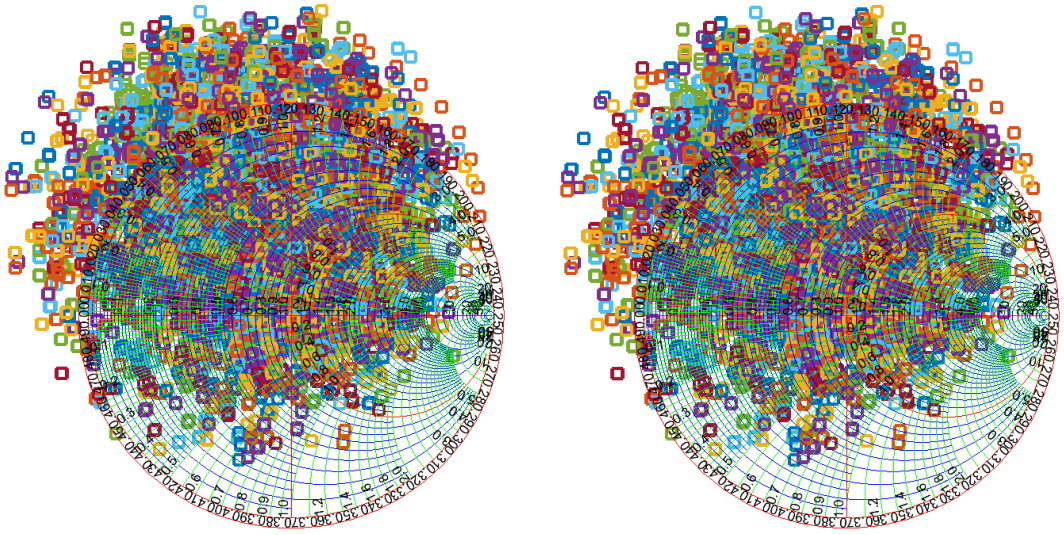

(a) $Z_{act_{snm_1}}(\phi, \theta)$ (b) $Z_{act_{snm_2}}(\phi, \theta)$

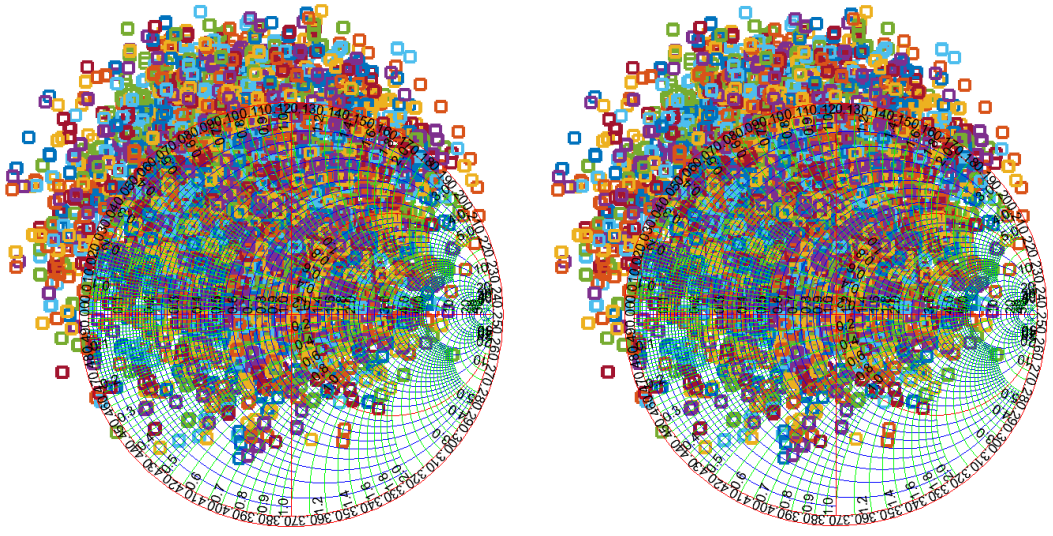

(c) $Z_{act_{snm_3}}(\phi, \theta)$ (d) $Z_{act_{snm_4}}(\phi, \theta)$

Figure 6.6: FMA $Z_{act_{snm_k}}(\phi, \theta)$ at $f = 5.5$ GHz

6.2 Comparison to Quad Mode Antenna Array

6.2.1 Output SNR Performance

For the unmatched case, the beamformer output SNR is plotted over the scan range $\phi \in [0°, 358°]$, $\theta \in [0°, 90°]$ in figure 6.7. Similar plots for the best performing case of each criteria is shown in Figure 6.9. The maximum output SNR is achieved at $\phi = 300°$, $\theta = 80°$ and has a value of

$$SNR_{max_{unmatched}} = 78.0367 \text{ dB}$$

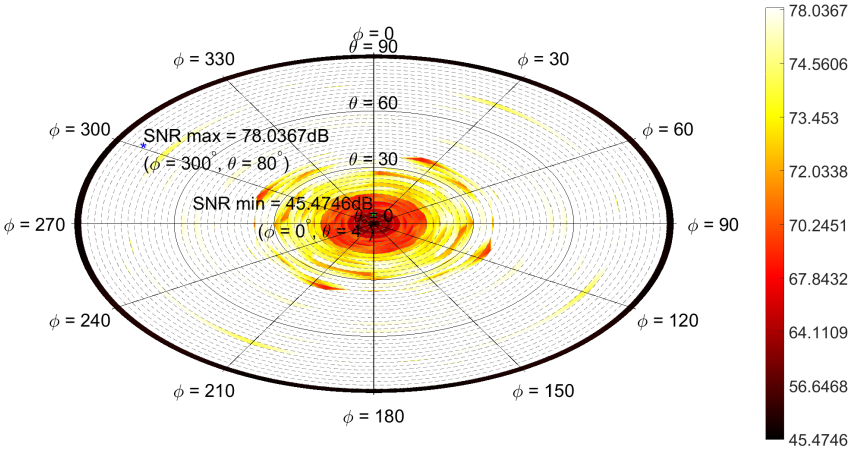

Figure 6.7: $FMA\ SNR_{o_{unmatched}}(\phi, \theta)$ at $f = 5.5$ GHz

It can be noted that the unmatched FMA has a lower maximum output SNR than the QMA and that a null occurs at $\theta = 0°$ as expected due to the z-axis directed current on the conductors. The minimum output SNR is defined to be taken at $\theta \geq 4°$ as the null in the antenna pattern is an inherent feature and thus does not give any information on the relative improvement using any of the techniques. Unlike the QMA, the total electric field pattern is not isotropic due to the destructive interference of out of phase individual radiator field patterns.

6.2.2 SNR Improvement Using Methods and Comparison to QMA

The matching topology is determined for each criteria and the maximum output SNR determined over the scan range, similarly than in section 5.2.4. The maximum output SNR and the angle at which it is achieved for each criteria is shown in table 6.1.

SNR_o by matching criteria for FMA

Criteria	$SNR_{o_{max}}$	ϕ_{max}	θ_{max}
z_{act_n}	79.1687 dB	120°	80°
$z_{act_{s_{avg}}}$	81.0782 dB	240°	80°
z_{self}	80.839 dB	60°	80°
$\Gamma'_{s_{opt}} = 0.8\angle 210°$	83.141 dB	60°	80°
$z_{optim_{sesh}}$	80.0385 dB	60°	80°
$z_{optim_{shse}}$	79.1687 dB	120°	80°

Table 6.1: FMA maximum output SNR and angle at which it is achieved per criteria

It can be seen from table 6.1 that the variation in maximum output SNR is much larger for the FMA than for the QMA. The values for L_{rec_ϕ} and L_{rec_θ} that yield the maximum SNR are shown in table 6.2.

L_{rec_ϕ} and L_{rec_θ}

L_{rec_ϕ}	L_{rec_θ}
7	6
8	6

Table 6.2: FMA L_{rec_ϕ} and L_{rec_θ} that produces maximum output SNR

For the optimizer, the minimum output SNR was optimized over $\phi \in [0°, 358°]$, $\theta \in [4°, 90°]$. A plot of the optimized minimum FMA output SNR is shown for both the Shunt-Series and Series-Shunt topologies in figure 6.8. The maximum number of optimizer iterations for each topology were set to 750. The starting reactances for the approximation were the values determined for $\Gamma'_{s_{opt}} = 0.4\angle 30°$ and $\Gamma'_{s_{opt}} = 0.6\angle 180°$ for the Shunt-Series and Series-Shunt topologies respectively. For the Shunt-Series topology, an improvement of 0.06 dB was achieved, while for the Series-Shunt topology, an improvement of about 0.6 dB was achieved.

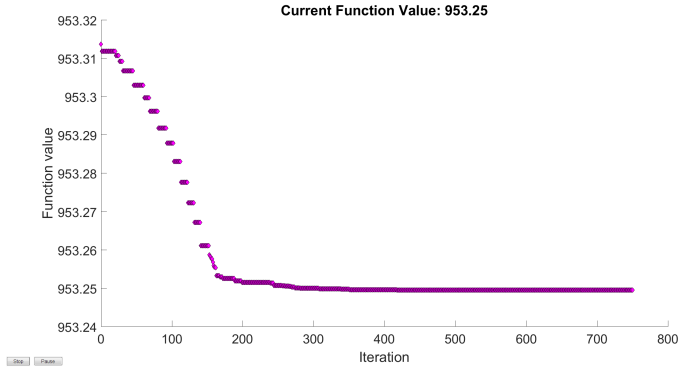

(a) Shunt-Series

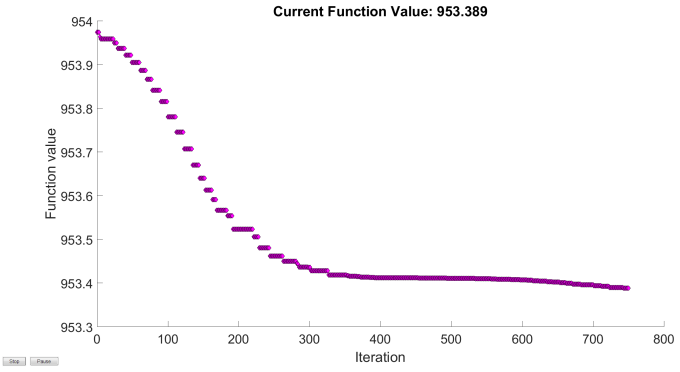

(b) Series-Shunt

Figure 6.8: MATLAB Optimizer error function output windows for FMA

Figure E.3 of Appendix E shows the maximum output SNR over $\phi = [0°, 358°]$, $\theta = [4°, 90°]$ per criteria for the FMA. It can be seen that unlike the QMA, optimizing the minimum output SNR over the scan range will not necessarily lead to the maximum output SNR occurring for the optimized case. This is due to the null in the pattern which removes the pattern flatness. It can also be seen that for the FMA, improvements in maximum output SNR from the unmatched case can be substantial, in the order of 5 dB, while it is still possible to achieve a lower maximum output SNR if the output criteria is chosen poorly. Figure E.4 of Appendix E shows the minimum output SNR over $\phi = [0°, 358°]$, $\theta = [4°, 90°]$ per criteria for the FMA. It can be seen that significant improvement of the minimum output SNR is possible. It is also however possible to have a large degradation of minimum output SNR. The FMA is more susceptible to SNR optimization techniques than the QMA.

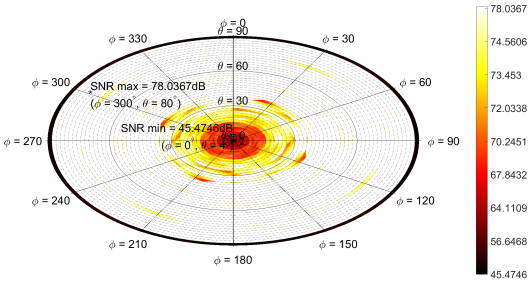

(a) Unmatched

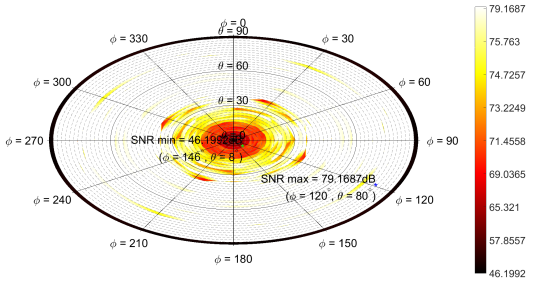

(b) Noise Active Impedance

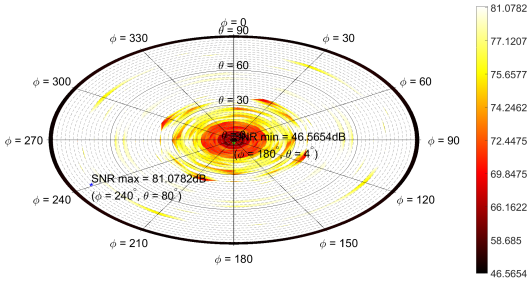

(c) Recursive Average

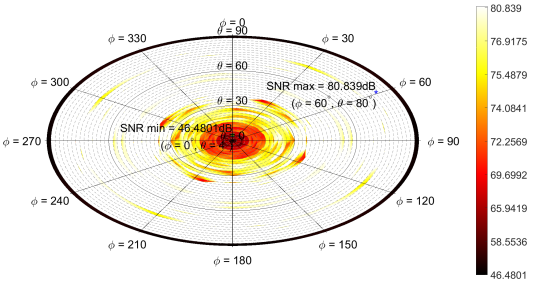

(d) Self Impedance

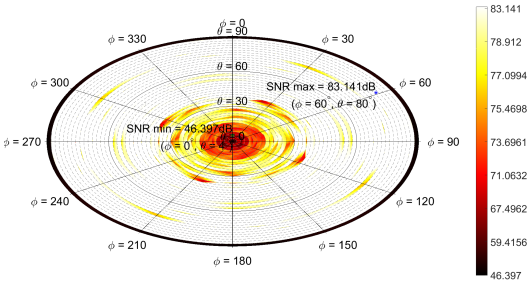

(e) Parameter Sweep

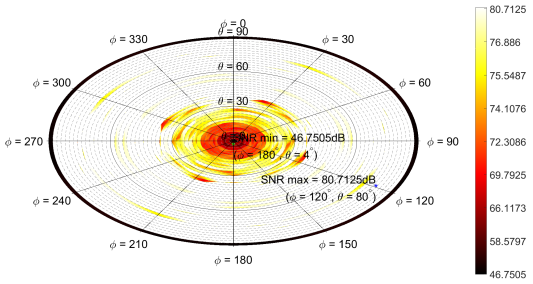

(f) Shunt-Series Optimized

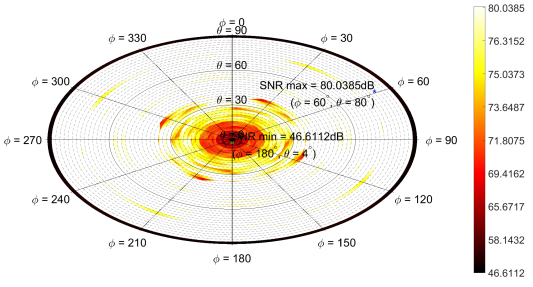

(g) Series-Shunt Optimized

Figure 6.9: FMA SNR circles for best performing case of each matching criteria

Chapter 7

Criteria Selection and Conclusions

7.1 Secondary Considerations for Selection of Matching Criteria

As seen in from figures E.1 and E.2, when the objective is to improve the maximum or minimum output SNR, it might be unclear which criteria to select, as the improvements may be incremental. In such cases it becomes necessary to look at secondary considerations for the selection of matching criteria. Possible secondary considerations can include, but are not limited to:

- Noise power at the output of the receiver
- Possible mitigation of scan blindness ($SNR = 0$) if present in array
- Complexity of calculation of matching section reactance values

The noise power at the output of the receiver was taken as the secondary criteria used for the selection of matching criteria. The SNR only tells part of the story when it comes to the noise performance of the system. When the absolute noise power is known together with the SNR, it also implies that the signal power is known. When the SNR of two criteria are equal, achieving a higher signal power is desirable. Selecting the criteria with a higher noise power then also selects the higher signal power. The noise power that is available at the output port of the receiver for each criteria can be compared to a benchmark noise power so that each criteria would not need to be directly compared to each other. The benchmark selected is the output noise power when each amplifier is fed by its optimal noise figure impedance. When this criteria is met, the amplifiers all operate at a noise figure of F_{min}. It must be noted that this condition implies the minimum ratio of LNA input SNR to output SNR, not minimum output noise power, and it is possible for a criteria to produce an output noise power lower than the benchmark. As shown by equation 7.1, when the criteria output noise power is lower than the

benchmark, the ratios of the other powers will guarantee that the noise figure of the amplifiers when fed by $Z_{s_{opt}}$ is lower.

$$\begin{aligned} F_{min} &< F_{crit} \\ \frac{SNR_{i_{min}}}{SNR_{o_{min}}} &< \frac{SNR_{i_{crit}}}{SNR_{o_{crit}}} \\ \frac{P_{s_{i_{min}}}}{P_{n_{i_{min}}}}\frac{P_{n_{o_{min}}}}{P_{s_{o_{min}}}} &< \frac{P_{s_{i_{crit}}}}{P_{n_{i_{crit}}}}\frac{P_{n_{o_{crit}}}}{P_{s_{o_{crit}}}} \\ \frac{P_{s_{i_{min}}}}{P_{s_{i_{crit}}}}\frac{P_{n_{i_{crit}}}}{P_{n_{i_{min}}}}\frac{P_{s_{o_{crit}}}}{P_{s_{o_{min}}}}P_{n_{o_{min}}} &< P_{n_{o_{crit}}} \end{aligned} \tag{7.1}$$

As ϕ and θ vary, the output noise power also changes and the output noise power of the system compared to the benchmark power can be plotted as seen in figure 7.1 for the unmatched QMA case.

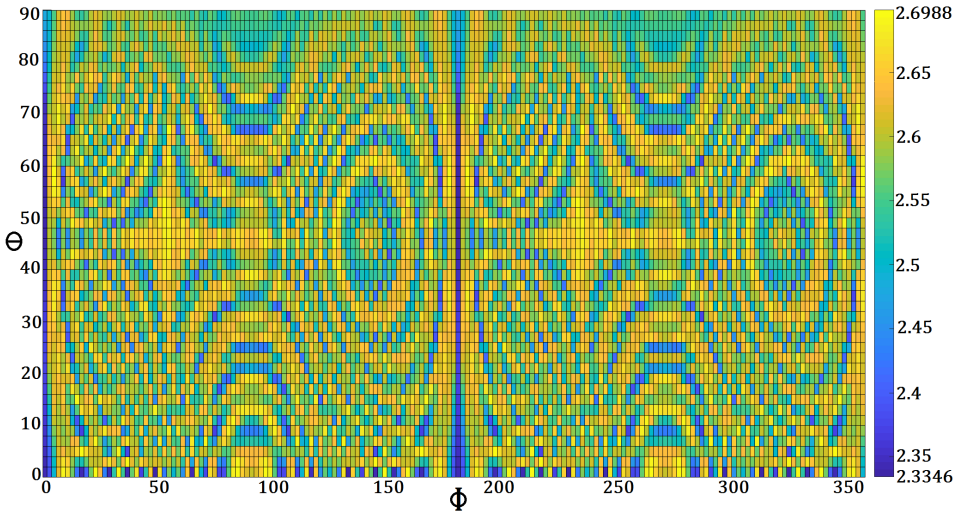

Figure 7.1: dB ratio of $P_{n_{o_{unmatched}}}$ to $P_{n_{o_{benchmark}}}$ at $f = 5.5$ GHz

7.2 Final Selection of Matching Criteria

Figure E.5 of Appendix E shows the dB ratio of $\frac{P_{no}}{P_{n_{o_{benchmark}}}}$ for each criteria for the QMA, while figure E.6 of Appendix E shows the ratio for the FMA for each criteria. At the hand of the primary and secondary considerations, the final matching criteria selected for the QMA is the Shunt-Series Optimized criteria. This selection produces an output SNR over the scan range $\phi = [0°, 358°]$, $\theta = [0°, 90°]$ as shown in figure 7.2 and a dB ratio of $\frac{P_{n_o}(\phi,\theta)}{P_{n_{o_{benchmark}}}}$ as shown in figure 7.3

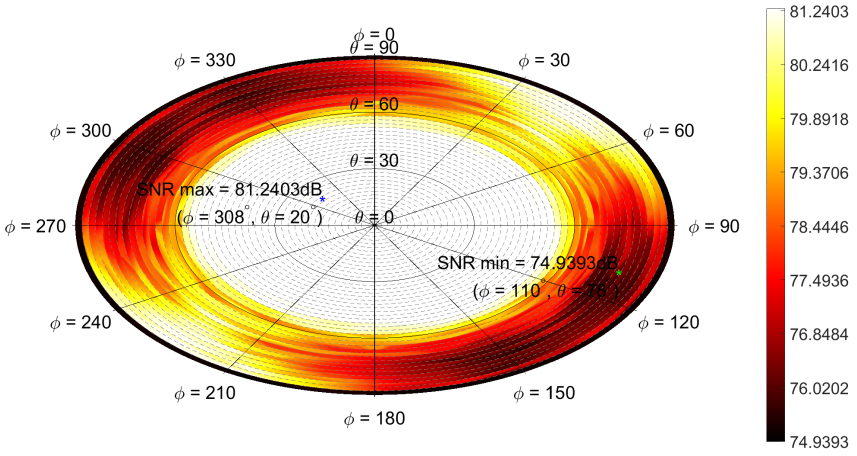

Figure 7.2: QMA $SNR_{o_{Shunt-Series\ Optimized}}(\phi, \theta)$ at $f = 5.5$ GHz

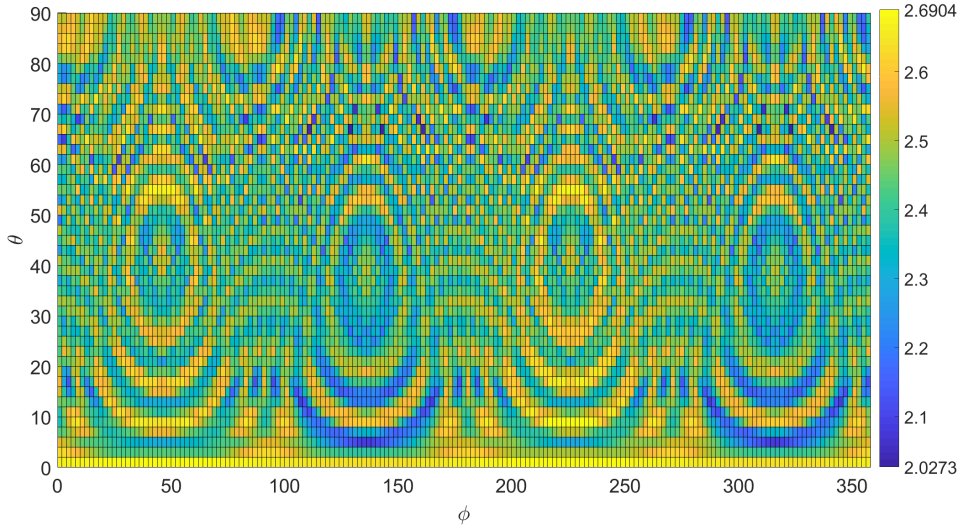

Figure 7.3: QMA dB ratio of $P_{n_{o_{Shunt-Series\ Optimized}}}$ to $P_{n_{o_{benchmark}}}$ at $f = 5.5$ GHz

The SSIM values for the Shunt-Series Optimized criteria at $f = 5.5$ GHz for each receiver channel are given in table 7.1.

$SSIM_{Shunt-Series\ \ Optimized}$

$SSIM_{thresh}$	$SSIM(k=1)$	$SSIM(k=2)$	$SSIM(k=3)$	$SSIM(k=4)$
0.85	0.9089	0.8924	0.9063	0.8913

Table 7.1: SSIM data at $f = 5.5$ GHz for the Shunt-Series Optimized case

Similarly for the FMA, the final matching criteria selected is the $\Gamma'_{s_{opt}} = 0.8\angle 210°$ criteria, which produces an output SNR as seen in figure 7.4 and a dB ratio of $\frac{P_{n_o}(\phi,\theta)}{P_{n_{o_{benchmark}}}}$ as shown in figure 7.5.

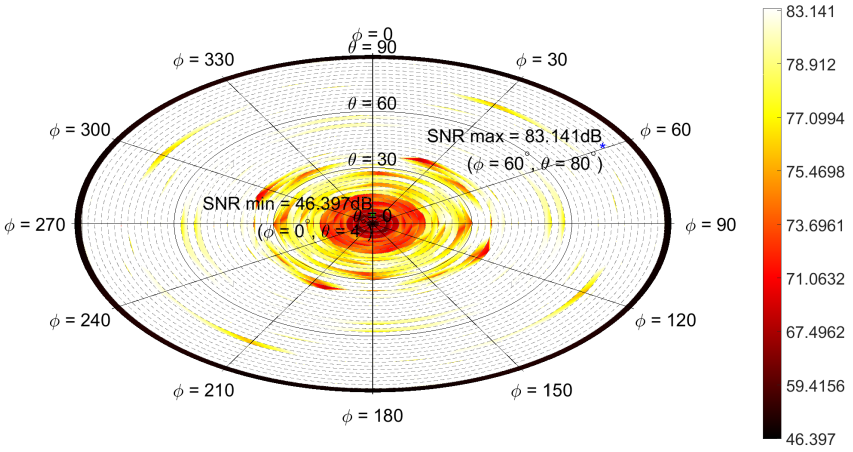

Figure 7.4: FMA $SNR_{o_{\Gamma'_{s_{opt}}=0.8\angle 210°}}(\phi,\theta)$ at $f = 5.5$ GHz

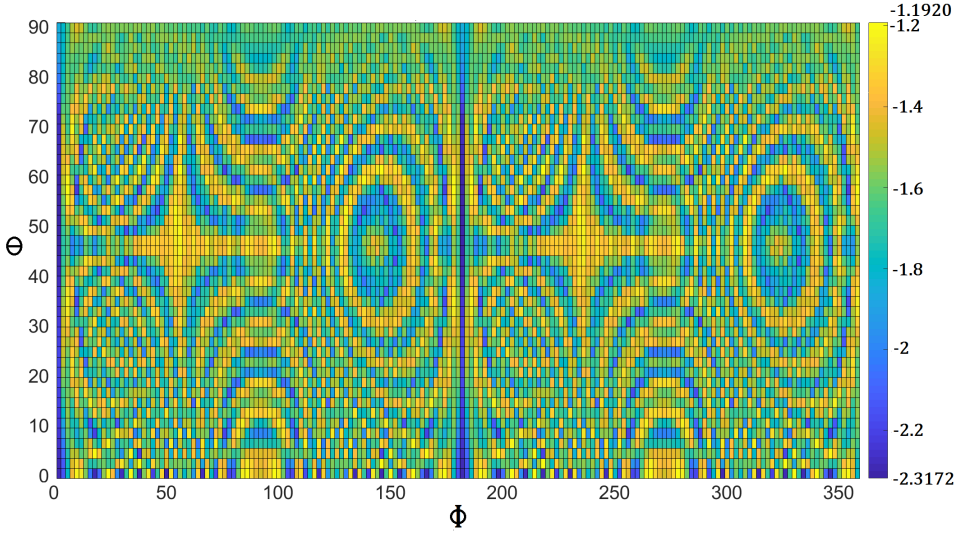

Figure 7.5: FMA dB ratio of $P_{n_{o_{\Gamma'_{s_{opt}}=0.8\angle 210°}}}$ to $P_{n_{o_{benchmark}}}$ at $f = 5.5$ GHz

The SSIM values for the $\Gamma'_{s_{opt}} = 0.8\angle 210°$ criteria at $f = 5.5$ GHz for each receiver channel are given in table 7.2.

	$SSIM_{\Gamma'_{s_{opt}}=0.8\angle 210^\circ}$			
$SSIM_{thresh}$	$SSIM(k=1)$	$SSIM(k=2)$	$SSIM(k=3)$	$SSIM(k=4)$
0.85	0.8906	0.8906	0.8906	0.8906

Table 7.2: SSIM data at $f = 5.5$ GHz for the $\Gamma'_{s_{opt}} = 0.8\angle 210^\circ$ case

7.3 Conclusions Drawn From Criteria Selection

The QMA has a flat radiation pattern in $\theta \in [0^\circ, 60^\circ]$ and then begins to drop off. This flatness makes the QMA lend itself less to optimization methods, as at all angles the signal voltage response per channel will vary little. This however means that optimizing the minimum SNR will also optimize the maximum SNR. The optimizer takes a very long time to run and is very resource heavy in terms of memory and computational power. For the QMA, after 750 iterations, the improvement to the output SNR was almost negligible. Approximation of the signal active impedance produces incremental improvement in the SNR for the QMA. In order to reduce the redundancy by matching to the same impedance value for multiple values of L_{rec_ϕ} and L_{rec_θ}, some preconsideration must be given to how many values will be averaged in each iterative level and whether the set is resorted between iterative levels. For large sets, a lot of redundancy is introduced. There is thus a tradeoff between redundancy and speed and ease of implementation. Matching to the noise active impedance produces marginal improvements for the QMA. For the isotropic noise distribution however, this is a fast implementation. In the case of a non-isotropic noise distribution, the noise active impedance will face similar tradeoffs than the signal active impedance averaging criteria. The iterative point noise figure search is an alternative to the recursive averaging approach which considers every value in the set of impedances. It is a very slow method however, and for the QMA as investigated ran for time in the order of 12 days on a single computer, and as such had to be farmed out to 12 computers to run within a day. After such a long computational time, the active impedance set changes due to the matching network which means that the solution found is still only partly valid and would still have to be subject to other limitations and requirements, such as matching topology for each channel. Selection of the self impedance or multibeam average noise criteria lead to fast computation but the results of these methods are inferior to the more exhaustive methods. A parameter sweep shows that both better and worse output SNR can be achieved and that there is still room for analytical improvement of the criteria. The fact that the variety of matching criteria investigated all produce marginal SNR improvements implies that a practical upper bound of the QMA SNR exists and is achieved to a high degree.

The selected criteria produces output noise power above the benchmark min-

imum noise figure noise power for all values of ϕ and θ. This means that the signal power at the output will be higher than if the LNAs were ideally fed. A drawback however is that the absolute noise power is also higher. It can be seen that the SSIM values for each channel for the QMA are very high. In other words, the set of active impedances before and after impedance matching are very similar. The SSIM in this way also serves as an indicator that the improvements to the SNR will be small as the active impedance, a representation of the ratios between voltages and currents at the antenna ports, are very similar than the ratios before matching.

The FMA has a sharp null at $\theta = 0°$. A null is not desirable to the model as the inverses of matrices can become singular. Singularities can be dealt with using machine precision numbers, but then it must be kept in mind that the solution is not completely accurate at the null coordinates. Considering only SNR improvement outside the null however removes this consideration. The null makes it so that the FMA lends itself more to the improvement of SNR than the QMA. While the null cannot be removed as it is an inherent feature of the radiation pattern of the FMA, the transition from the area around the null to the area over which the radiation pattern magnitude is large can be optimized. It is noted that optimizing the minima of the transition are however does not necessarily produce similar improvements to the maxima of the pattern. It can thus be meaningful to optimize the maximum output SNR and accept the changes to the minimum SNR as given. It must be decided which of the two conditions to optimize. The optimizer still is very slow and memory intensive for the FMA, but a much more meaningful improvement to the minimum SNR can be made through optimization. The improvement to both the maximum and minimum SNR through the recursive averaging of the signal active impedance compared to the unmatched case are much better than in the case of the QMA. The recursive averaging thus has the ability to improve SNR, but only if the antenna lends itself towards improvement. The noise active impedance match produces an improvement again, but not as much as the signal active impedance. The parameter sweep shows that the more the antenna lends itself towards improvement of output SNR, the more susceptible it is to degradation if a poor choice of matching criteria is made.

The selected criteria produces an output noise power which is lower than the ideally fed LNA noise power for all values of ϕ and θ. The lower noise power at the output can be beneficial for some requirements, however this means that the signal power at the output is also lower. The SSIM for each channel is equal and lower than in the QMA case. There is thus more of a change to the antenna active impedance from the unmatched case and thus the output SNR can be optimized to a greater degree.

Chapter 8

Evaluation of Contributions

8.1 Introduction

The main contributions of this study were as follows:

- A design of optimum noise matching networks for the QMA
- Improved noise-matching design approaches for non-ideal, coupled antenna arrays using analytical and numerical optimization methods
- An improved receiver model for coupled arrays which utilizes non-identical amplifiers and non-identical, non-ideal radiating elements that can be numerically optimized
- Construction of a software based receiver model for non-ideal, coupled antenna arrays with non-identical amplifiers

In this chapter, an evaluation of each proposed goal will be set out, that considers the strengths and weaknesses of each contribution in relation to the problem investigated as well other potential areas of use thereof.

8.2 Optimal Noise Matching Networks for the QMA

The QMA is a novel implementation and thus the presented discussions also increase the knowledge of its properties, other than those it was specifically designed for. This work represents the first proposals for optimum noise matching algorithms for the QMA. Algorithms presented include both analytical and numerical approaches. Analysis of the possible SNR improvement of the QMA through noise matching is presented at the hand of a variety of different criteria. It is determined that a choice of matching network will not disturb the flatness of the QMA radiation pattern. While marginal improvements in

output SNR can be made, it is observed that degraded SNR performance can also be obtained for the QMA. The unmatched QMA SNR performance is therefore close to the upper bound for SNR performance. This characteristic of the QMA is not intended in its original design but is a useful property and important to note.

In terms of secondary criteria, it is seen that the output noise power of the QMA, relative to the optimal noise figure benchmark output noise power, can be manipulated to a large extent through the selection of matching criteria. The output signal and noise power are optimized through matching criteria selection without affecting the output SNR to a large degree.

8.3 Improved Noise-Matching Design Approaches Using Analytical and Numerical Optimization Methods

Multiple criteria for the optimal noise match in a receiver with largely varying impedances are presented. Criteria range from theoretical considerations to approximation and numerical optimization. The relative effectiveness in the improvement and possible degradation of SNR per criteria is considered. The criteria are compared to each other, and also across antenna arrays with different radiated field properties. A conclusion is drawn that the efficacy of the criteria is not an isolated metric, but also the degree to which the antenna array lends itself towards improvement of SNR. The degree to which the antenna array lends itself towards improvement is the difference between achieving marginal to no SNR improvement and improvements in the order of multiple dB for the same matching criteria. It is thus an important consideration in the design of the array and SNR improvements cannot be solely left as a post design exercise.

The active impedance recursive approximation considered requires prior calculation to determine which levels are necessary to calculate to remove redundancy. For very large sets of data and sets where the difference in data elements are small, the averages calculated for different levels of recursion can be seen to produce numerically similar results. It can be seen that implementing the recursive average does not shift the coordinates of the maximum output SNR. This method is thus useful for implementation on a directive array as the angle of directivity will not be affected.

The iterative point search and parameter sweep showed that simply calculating approximated theoretically determined values for the optimum match is not necessarily good enough. When the active impedance varies, points other

than the recursive average can still produce better final results. Numerical optimization can then better the produced results even further. It is a drawback that the entire analysis must first be done for all criteria to determine the best performance implementation as a starting point for numerical optimization. Optimization is a slow and intensive process and can produce improvements that are not significant enough to merit the time and resources used to produce them.

8.4 Numerically Optimizable Improved Coupled Array Receiver Model with Non-identical, Non-Ideal Components

In previous implementations of a receiver model, [18], it is seen that the active impedance is dependent on the receiver parameters and beamformer coefficients. Designing the beamformer coefficients in terms of the active impedance therefore becomes circular. The receiver model as investigated removes the circularity by specifying the active impedance only in terms of the receiver circuit parameters. The receiver model is presented in matrix form, which allows for the removal of the explicit dependence of the active impedances of other channels in the calculation of the active impedance for a given channel, as is the case for single channel active impedance calculations using Y or Z-parameters. The active impedances of all N channels of a receiver can thus be calculated simultaneously and in terms of non-varying actual circuit impedances and reactances. The receiver model fully supports non-identicalities in the individual channels of the receiver with regards to the circuit components.

There are two restrictions to the receiver model. Firstly, in order for the matrix formulation to be valid, a decision must be made on the topology implemented, which must be the same for each channel. Though the topologies must match, the specific values for each channel may differ. In the event of a large antenna array, or an antenna array with a relative geometry that is not similar for each antenna element, or non-identical antenna elements, it may be that some elements have widely varying non-similar active impedances over the scan range. The receiver model allows for such an eventuality while enforcing matching topologies through the implementation of non-identical channels. This can, for example, be done by choosing non-identical LNAs for each channel with input impedances such that the matching conditions as shown in equation 4.9 are satisfied.

Secondly, each different implementation of matching section requires a different matrix formulation of the transformation matrices. The general procedure of determining the active impedance in terms of circuit currents through auxil-

iary equations stays the same regardless of the matching section implemented. The complexity of determining the active impedance is thus directly bound to the difficulty of performing a node current analysis for any given implementation.

The introduction of a matching section in the receiver influences the active impedance, but through the use of the SSIM, a quantitative measure of similarity is defined so that a decision on the qualitative similarity of the active impedance can be made. Considerations with regards to implementation and variations are discussed to broaden the scope of the application of the SSIM. The noise correlation matrices are integral to the noise response of the receiver model. It can be seen that previously, transformation matrices that refer open circuit voltages to in circuit voltages have been presented. Previous implementations, however, have implemented transformation matrices in terms of expectations of noise waves through effective amplifier noise temperatures, whereas the presented implementation is directly in terms of circuit impedances and admittances. This direct dependence allows for the use of the transformation matrices directly in the optimizer in order to produce optimized reactances for the matching section.

8.5 Software Receiver Model for Non-ideal, Coupled Antenna Arrays with Non-identical Amplifiers

The theoretical model as implemented in MATLAB is inherently narrowband. It is a simple enough alteration to allow for simulation over a frequency band so that it matches the ADS software model over frequency. The receiver model allows for any array to be considered with only the S,Y or Z-parameters and the open circuit voltage response known. The model as implemented extends the techniques of a wave based design approach [12] to a current based approach. The MATLAB model is directly optimizable in software. The ADS model serves as a control to make sure that the MATLAB calculated values are accurate, but offers the drawback of proprietary software that some information is internally obscured.

Appendices

Appendix A

Impedance Matching Theory

In order to match the source impedance to the amplifier optimal noise impedance at the operating frequency, one of three implementations can be selected, as shown in figure A.1. It is desired to match a given source $Z_s = R_s + jX_s$ to the LNA noise optimal source impedance $Z_{opt} = R_{opt} + jX_{opt}$ so that if Z_s is the impedance of the source to which the LNA is connected, the minimum noise figure F_{min} will be achieved.

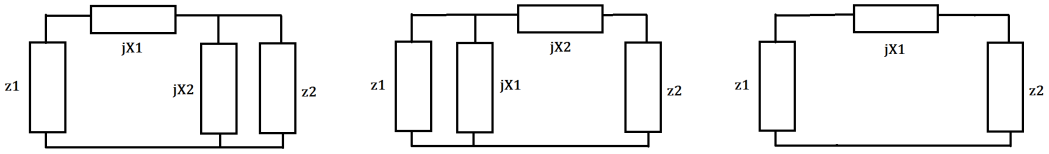

(a) Series-Shunt Match (b) Shunt-Series Match (c) Single-Series Match

Figure A.1: Topologies for impedance matching

The criteria for selection of the matching network topology is then as shown in sections B.2 to B.2.

A.0.1 Series-Shunt Stub Matching Network

This matching topology is used if $R_s < R_{opt}$. The parallel impedance of $Z_{opt} = R_{opt} + jX_{opt}$ and jX_2 is given by

$$\begin{aligned} Z_p &= \frac{jX_2 Z_{opt}}{jX_2 + Z_{opt}} \\ &= \frac{R_{opt}{X_2}^2 + j({R_{opt}}^2 X_2 + {X_2}^2 X_{opt} + {X_{opt}}^2 X_2)}{{R_{opt}}^2 + (X_{opt} + X_2)^2} \end{aligned}$$

Then, for impedance matching, the real part of the parallel load impedance must equal the real part of the source impedance.

$$
\begin{aligned}
R_p &= \Re\{Z_p\} = R_s \\
R_s &= \frac{R_{opt}{X_2}^2}{{R_{opt}}^2 + (X_{opt} + X_2)^2} \\
0 &= {X_2}^2 + \left(\frac{2R_sX_{opt}}{R_s - R_{opt}}\right)X_2 + R_s({R_{opt}}^2 + {X_{opt}}^2) \\
X_2 &= \frac{R_sX_{opt}}{R_{opt} - R_s} \pm \frac{1}{2}\sqrt{\left(\frac{2R_sX_{opt}}{R_s - R_{opt}}\right)^2 - 4R_s\left(\frac{{R_{opt}}^2 + {X_{opt}}^2}{R_s - R_{opt}}\right)}
\end{aligned} \tag{A.1}
$$

The sum of the imaginary parts of the source impedance, the series stub and the parellel load impedance must equal zero.

$$
\begin{aligned}
X_p &= \Im\{Z_p\} = -(X_s + X_1) \\
-(X_s + X_1) &= \frac{{R_{opt}}^2X_2 + {X_2}^2X_{opt} + {X_{opt}}^2X_2}{{R_{opt}}^2 + (X_{opt} + X_2)^2} \\
X_1 &= -\left(\frac{{R_{opt}}^2X_2 + {X_2}^2X_{opt} + {X_{opt}}^2X_2}{{R_{opt}}^2 + (X_{opt} + X_2)^2} + X_s\right)
\end{aligned} \tag{A.2}
$$

The LNA input impedance $Z_{in_{a_m}}$ is then transformed through the matching network stubs jX_{1_m} and jX_{2_m} to ${Z_{in_{a_m}}}'$ as shown in equation A.3.

$$
\begin{aligned}
{Z_{in_{a_m}}}' &= jX_{1_m} + (jX_{2_m} // Z_{in_{a_m}}) \\
&= jX_{1_m} + \frac{-X_{2_m}X_{in_{a_m}} + jX_{2_m}R_{in_{a_m}}}{jX_{2_m} + Z_{in_{a_m}}} \\
&= jX_{1_m} + \frac{R_{in_{a_m}}{X_{2_m}}^2 + jX_{2_m}\left(({R_{in_{a_m}}}^2 + {X_{in_{a_m}}}^2) + X_{in_{a_m}}X_{2_m}\right)}{{R_{in_{a_m}}}^2 + (X_{2_m} + X_{in_{a_m}})^2} \\
&= \frac{R_{in_{a_m}}X_{2_m}^2 + j\left((R_{in_{a_m}}^2 + X_{in_{a_m}}^2)(X_{1_m} + X_{2_m}) + X_{2_m}(X_{2_m}(X_{in_{a_m}} + X_{1_m}) + 2X_{in_{a_m}}X_{1_m})\right)}{{R_{in_{a_m}}}^2 + (X_{2_m} + X_{in_{a_m}})^2}
\end{aligned} \tag{A.3}
$$

A.0.2 Shunt-Series Stub Matching Network

This matching topology is used if $R_s > R_{opt}$. The stub reactance values of the impedance matching sections are determined similarly than in equations A.1 and A.2 as

$$
X_1 = \frac{R_{opt}X_s}{R_s - R_{opt}} \pm \frac{1}{2}\sqrt{\left(\frac{2R_{opt}X_s}{R_{opt} - R_s}\right)^2 - 4R_{opt}\left(\frac{{R_s}^2 + {X_s}^2}{R_{opt} - R_s}\right)} \tag{A.4}
$$

$$X_2 = -\left(\frac{{R_s}^2 X_1 + {X_1}^2 X_s + {X_s}^2 X_1}{{R_s}^2 + (X_s + X_1)^2} + X_{opt}\right) \tag{A.5}$$

The LNA input impedance $Z_{in_{a_m}}$ is then transformed through the matching network stubs jX_{1_m} and jX_{2_m} to ${Z_{in_{a_m}}}'$ as shown in equation A.6.

$$\begin{aligned}
{Z_{in_{a_m}}}' &= jX_{1_m} // (jX_{2_m} + Z_{in_{a_m}}) \\
&= \frac{jX_{1_m}(jX_{2_m} + Z_{in_{a_m}})}{jX_{1_m} + jX_{2_m} + Z_{in_{a_m}}} \\
&= \frac{-(X_{1_m}X_{2_m} + X_{1_m}X_{in_{a_m}}) + jX_{1_m}R_{in_{a_m}}}{R_{in_{a_m}} + j(X_{1_m} + X_{2_m} + X_{in_{a_m}})} \\
&= \frac{R_{in_{a_m}}X_{1_m}^2 + jX_{1_m}\left((R_{in_{a_m}}^2 + (X_{in_{a_m}} + X_{2_m})^2) + (X_{in_{a_m}} + X_{2_m})X_{1_m}\right)}{{R_{in_{a_m}}}^2 + (X_{1_m} + X_{2_m} + X_{in_{a_m}})^2}
\end{aligned} \tag{A.6}$$

A.0.3 Single-Series Stub Matching Network

This impedance matching case will only occur when $R_s = R_{opt}$, but $X_s \neq X_{opt}$. The sum of the imaginary parts of the source impedance, series stub and load impedance must then equal zero.

$$\begin{aligned}
0 &= X_s + X_1 + X_{opt} \\
X_1 &= -(X_s + X_{opt})
\end{aligned} \tag{A.7}$$

The LNA input impedance $Z_{in_{a_m}}$ is then transformed through the matching network stub jX_{1_m} to ${Z_{in_{a_m}}}'$ as shown in equation A.8.

$$\begin{aligned}
{Z_{in_{a_m}}}' &= jX_{1_m} + Z_{in_{a_m}} \\
&= R_{in_{a_m}} + j(X_{in_{a_m}} + X_{1_m})
\end{aligned} \tag{A.8}$$

In the event that $R_s = R_{opt}$ and $X_s = X_{opt}$ or that an unmatched circuit is desired, no matching network is implemented.

Appendix B

Signal and Noise Transformation Matrix Derivations for Matched Case

B.1 Signal Transformation Matrices

Series-Shunt Stub Matching Network For the circuit diagram for the receiver model of a Series-Shunt matching network as shown in figure B.1, similarly than in section 3.1.1, the Series-Shunt signal-no-noise case auxiliary equations B.1 are used to determine the LNA input signal voltage at the post matching node as shown, with jX_{1_m} the reactance of the series stub, jX_{2_m} the reactance of the shunt stub and jB_{1_m} and jB_{2_m} their respective corresponding susceptances for the m-th channel.

$$i_{s_m}{}' = -Y_{in_{a_m}} v_{s_m}{}' \tag{B.1a}$$

$$i_{s_m} = \sum_{k=1}^{N} y_{mk} v_{s_k} \tag{B.1b}$$

$$= i_{s_m}{}' - jB_{2_m} v_{s_m}{}' \tag{B.1c}$$

$$v_{s_m}{}' = v_{s_m} + e_m + jX_{1_m} i_{s_m} \tag{B.1d}$$

$$\tag{B.1e}$$

After rewriting the auxiliary equations into matrix form and manipulation, the source port node signal voltage can be written as

$$\begin{aligned}[\tilde{\boldsymbol{v}}_{\boldsymbol{s}}] &= -\Big[\big[j[B_{2_d}] + [Y_{in_{a_d}}]\big]\big[[I] + j[X_{1_d}][Y]\big] + [Y]\Big]^{-1}\big[[Y_{in_{a_d}}] + j[B_{2_d}]\big][\tilde{\boldsymbol{e}}_{\boldsymbol{s}}] \\ &= [T_x][\tilde{\boldsymbol{e}}_{\boldsymbol{s}}]\end{aligned} \tag{B.2}$$

At the post matching section node, the input signal voltage vector to the LNAs is given by

$$\begin{aligned}[\tilde{\boldsymbol{v}}_{\boldsymbol{s}}{}'] &= [\tilde{\boldsymbol{v}}_{\boldsymbol{s}}] + [\tilde{\boldsymbol{e}}_{\boldsymbol{s}}] + j[X_{1_d}][Y][\tilde{\boldsymbol{v}}_{\boldsymbol{s}}] \\ &= \Big[[I] + \big[[I] + j[X_{1_d}][Y]\big][T_x]\Big][\tilde{\boldsymbol{e}}_{\boldsymbol{s}}] \\ &= [T_x{}'][\tilde{\boldsymbol{e}}_{\boldsymbol{s}}] \end{aligned} \tag{B.3}$$

Shunt-Series Stub Matching Network For the circuit diagram for the receiver model of a Shunt-Series matching network as shown in figure B.2, similarly than in section 3.1.1, the Shunt-Series signal-no-noise case auxiliary equations B.4 are used to determine the LNA input signal voltage at the post matching node as shown. For the m-th channel of the Shunt-Series case, jX_{1_m} is the reactance of the shunt stub, jX_{2_m} the reactance of the series stub and jB_{1_m} and jB_{2_m} their respective corresponding susceptances.

$$i_{s_m}{}' = -Y_{in_{am}} v_{s_m}{}' \tag{B.4a}$$

$$i_{s_m} = \sum_{k=1}^{N} y_{mk} v_{s_k} \tag{B.4b}$$

$$= i_{s_m}{}' - jB_{1_m}(v_{s_m} + e_m) \tag{B.4c}$$

$$v_{s_m}{}' = \frac{Z_{in_{am}}}{jX_{2_m} + Z_{in_{am}}}(v_{s_m} + e_m) \tag{B.4d}$$

The auxiliary equations can be rewritten into matrix form and manipulated to solve simultaneously the signal source port node voltages.

$$\begin{aligned}[\tilde{\boldsymbol{v}}_{\boldsymbol{s}}] &= -\Big[\big[j[X_{2_d}]+[Z_{in_{a_d}}]\big]^{-1}+[Y]+j[B_{1_d}]\Big]^{-1}\Big[j[B_{1_d}]+\big[[Z_{in_{a_d}}]+j[X_{2_d}]\big]^{-1}\Big][\tilde{\boldsymbol{e}}_{\boldsymbol{s}}] \\ &= [T_x][\tilde{\boldsymbol{e}}_{\boldsymbol{s}}] \end{aligned} \tag{B.5}$$

The post matching section node signal voltage is then given by

$$\begin{aligned}[\tilde{\boldsymbol{v}}_{\boldsymbol{s}}{}'] &= [Z_{in_{a_d}}]\big[j[X_{2_d}] + [Z_{in_{a_d}}]\big]^{-1}\big[[\tilde{\boldsymbol{v}}_{\boldsymbol{s}}] + [\tilde{\boldsymbol{e}}_{\boldsymbol{s}}]\big] \\ &= [Z_{in_{a_d}}]\big[j[X_{2_d}] + [Z_{in_{a_d}}]\big]^{-1}\big[[T_x] + [I]\big][\tilde{\boldsymbol{e}}_{\boldsymbol{s}}] \\ &= [T_x{}'][\tilde{\boldsymbol{e}}_{\boldsymbol{s}}] \end{aligned} \tag{B.6}$$

Single-Series Stub Matching Network For the circuit diagram for the receiver model of a Single-Series stub matching network as shown in figure B.3, similarly than in section 3.1.1, the Single-Series signal-no-noise case auxiliary

equations B.7 are used to determine the LNA input signal voltage at the post matching node as shown. For the m-th channel of the Single-Series case, jX_{1_m} is the reactance of the series stub and jB_{1_m} its corresponding susceptance.

$$i_{s_m} = -Y_{in_{a_m}} {v_{s_m}}' \tag{B.7a}$$

$$= \sum_{k=1}^{N} y_{mk} v_{s_k} \tag{B.7b}$$

$${v_{s_m}}' = v_{s_m} + jX_{1_m} i_{s_m} + e_m \tag{B.7c}$$

The auxiliary equations can be rewritten into matrix form and manipulated to solve simultaneously the signal source port voltages.

$$\begin{aligned}[\tilde{\boldsymbol{v}}_{\boldsymbol{s}}] &= -\Big[[Y_{in_{a_d}}]\big[[I] + j[X_{1_d}][Y]\big] + [Y]\Big]^{-1}[Y_{in_{a_d}}][\tilde{\boldsymbol{e}}_{\boldsymbol{s}}] \\ &= [T_x][\tilde{\boldsymbol{e}}_{\boldsymbol{s}}]\end{aligned} \tag{B.8}$$

At the post matching section node, the input signal voltage vector to the LNAs is given by

$$\begin{aligned}[\tilde{\boldsymbol{v}}_{\boldsymbol{s}}{}'] &= [\tilde{\boldsymbol{v}}_{\boldsymbol{s}}] + [\tilde{\boldsymbol{e}}_{\boldsymbol{s}}] + j[X_{1_d}][Y][\tilde{\boldsymbol{v}}_{\boldsymbol{s}}] \\ &= \Big[[I] + \big[[I] + j[X_{1_d}][Y]\big][T_x]\Big][\tilde{\boldsymbol{e}}_{\boldsymbol{s}}] \\ &= [T_x{}'][\tilde{\boldsymbol{e}}_{\boldsymbol{s}}]\end{aligned} \tag{B.9}$$

B.2 Noise Transformation Matrices

Series-Shunt Stub Matching Network The circuit diagram for the receiver model if a Series-Shunt matching network is used is shown in figure B.1.

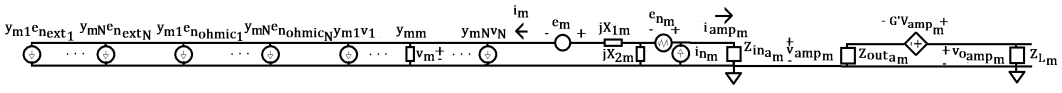

Figure B.1: Channel m of receiver with noisy source and Series-Shunt match

Similarly than in section 3.1.2, the Series-Shunt auxiliary equations B.10 are used to determine the noise voltage at the post matching node as shown, with jX_{1_m} the reactance of the series stub, jX_{2_m} the reactance of the shunt stub and jB_{1_m} and jB_{2_m} their respective corresponding susceptances.

$$
\begin{aligned}
{i_{n_m}}' &= i_{n_m} - Y_{in_{a_m}} e_{n_m} - Y_{in_{a_m}} {v_{n_m}}' && \text{(B.10a)}\\
&= \sum_{k=1}^{N} y_{mk}(v_{n_k} + e_{n_{ohmic_k}} + e_{n_{ext_k}}) + jB_{2_m}{v_{n_m}}' && \text{(B.10b)}\\
{v_{n_m}}' &= v_{amp_{n_m}} - e_{n_m} && \text{(B.10c)}\\
i_{n_m} &= {i_{n_m}}' - jB_{2_m}{v_{n_m}}' && \text{(B.10d)}
\end{aligned}
$$

After rewriting the auxiliary equations into matrix form and manipulation, the post matching node noise voltage can be written as

$$
\begin{aligned}
[\tilde{\boldsymbol{v}}_{\boldsymbol{n}}'] =& \Big[j[Y][X_{1_d}]\big[[Y_{in_{a_d}}]+j[B_{2_d}]+j[B_{1_d}]\big]+j[B_{2_d}]+[y_{in_{a_d}}]\Big]^{-1}\Big[[I]+j[Y][X_{1_d}]\Big]\\
&[\boldsymbol{i_n} - \tilde{\boldsymbol{y}}_{\boldsymbol{in_a}}\boldsymbol{e_n}] - \Big[j[Y][X_{1_d}]\big[[Y_{in_{a_d}}]+j[B_{2_d}]+j[B_{1_d}]\big]+j[B_{2_d}]+[Y_{in_{a_d}}]\Big]^{-1}[Y]\\
&\big[[\tilde{\boldsymbol{e}}_{\boldsymbol{n_{ohmic}}}]+[\tilde{\boldsymbol{e}}_{\boldsymbol{n_{ext}}}]\big]\\
=& [T_z'][\tilde{\boldsymbol{i}}_{\boldsymbol{x}}] + [T_s']\big[[\tilde{\boldsymbol{e}}_{\boldsymbol{n_{ohmic}}}]+[\tilde{\boldsymbol{e}}_{\boldsymbol{n_{ext}}}]\big]
\end{aligned}
\qquad \text{(B.11)}
$$

The noise voltage correlation matrix at the post matching node can be determined as in equation 3.19, substituting $[T_z']$ and $[T_s']$ for $[T_z]$ and $[T_s]$. The noise voltage at the source ports can be calculated by equation B.12 with $[Z]$ the array impedance parameter matrix.

$$
\begin{aligned}
[\tilde{\boldsymbol{v}}_{\boldsymbol{n}}] =& -[Z]\Big[[Y_{in_{a_d}}] + j[B_{2_d}]\Big][\tilde{\boldsymbol{v}}_{\boldsymbol{n}}'] + [Z][\tilde{\boldsymbol{i}}_{\boldsymbol{x}}] - \big[[\tilde{\boldsymbol{e}}_{\boldsymbol{n_{ohmic}}}]+[\tilde{\boldsymbol{e}}_{\boldsymbol{n_{ext}}}]\big]\\
=& [Z]\Big[[I]-\big[[Y_{in_{a_d}}]+j[B_{2_d}]\big][T_z']\Big][\tilde{\boldsymbol{i}}_{\boldsymbol{x}}] - \Big[[Z]\big[[Y_{in_{a_d}}]+j[B_{2_d}]\big][T_s']+[I]\Big]\\
&\big[[\tilde{\boldsymbol{e}}_{\boldsymbol{n_{ohmic}}}]+[\tilde{\boldsymbol{e}}_{\boldsymbol{n_{ext}}}]\big]\\
=& [T_z][\tilde{\boldsymbol{i}}_{\boldsymbol{x}}] + [T_s]\big[[\tilde{\boldsymbol{e}}_{\boldsymbol{n_{ohmic}}}] + [\tilde{\boldsymbol{e}}_{\boldsymbol{n_{ext}}}]\big]
\end{aligned}
\qquad \text{(B.12)}
$$

Shunt-Series Stub Matching Network The circuit diagram for the receiver model if a Shunt-Series matching network is used is shown in figure B.2.

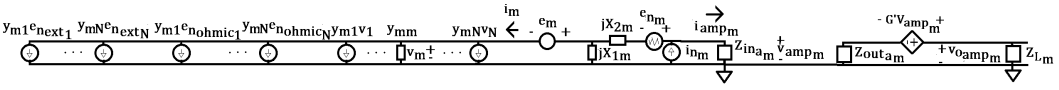

Figure B.2: Channel m of receiver with noisy source and Shunt-Series match

The auxiliary equations for the Shunt-Series case to determine the noise voltage at the post matching node are as shown in equations B.13, with jX_{1_m}

the reactance of the shunt stub, jX_{2_m} the reactance of the series stub and jB_{1_m} and jB_{2_m} their respective corresponding susceptances.

$$i_{n_m}{}' = i_{n_m} - Y_{in_{a_m}} e_{n_m} - Y_{in_{a_m}} v_{n_m}{}' \tag{B.13a}$$

$$= \sum_{k=1}^{N} y_{mk}(v_{n_k} + e_{n_{ohmic_k}} + e_{n_{ext_k}}) + jB_{1_m} v_{n_m} \tag{B.13b}$$

$$v_{n_m}{}' = v_{amp_{n_m}} - e_{n_m} \tag{B.13c}$$

$$i_{n_m} = i_{n_m}{}' - jB_{1_m} v_{n_m} \tag{B.13d}$$

The auxiliary equations can be rewritten into matrix form and manipulated to solve simultaneously the noise voltages.

$$\begin{aligned}[\tilde{\boldsymbol{v}}_{\boldsymbol{n}}{}'] =& \Big[\big[[Y]+j[B_{1_d}]\big]\big[[I]+j[X_{2_d}][Y_{in_{a_d}}]\big]+[Y_{in_{a_d}}]\Big]^{-1}\Big[[I]+\big[[Y]+j[B_{1_d}]\big]j[X_{2_d}]\Big] \\ & [\boldsymbol{i}_{\boldsymbol{n}} - \tilde{\boldsymbol{y}}_{\boldsymbol{in_a}} \boldsymbol{e}_{\boldsymbol{n}}] - \Big[\big[[Y]+j[B_{1_d}]\big]\big[[I]+j[X_{2_d}][Y_{in_{a_d}}]\big]+[Y_{in_{a_d}}]\Big]^{-1}[Y] \\ & \big[[\tilde{\boldsymbol{e}}_{\boldsymbol{n_{ohmic}}}] + [\tilde{\boldsymbol{e}}_{\boldsymbol{n_{ext}}}]\big] \\ =& [T_z{}'][\tilde{\boldsymbol{i}}_{\boldsymbol{x}}] + [T_s{}']\big[[\tilde{\boldsymbol{e}}_{\boldsymbol{n_{ohmic}}}] + [\tilde{\boldsymbol{e}}_{\boldsymbol{n_{ext}}}]\big]\end{aligned} \tag{B.14}$$

The noise correlation matrix can be determined according to equation 3.19, substituting $[T_z{}']$ and $[T_s{}']$ for $[T_z]$ and $[T_s]$. The noise voltages at the source ports are given by

$$\begin{aligned}[\tilde{\boldsymbol{v}}_{\boldsymbol{n}}] =& -\big[[Y]+j[B_{1_d}]\big]^{-1}[y_{in_{a_d}}][\tilde{\boldsymbol{v}}_{\boldsymbol{n}}{}'] + \big[[Y]+j[B_{1_d}]\big]^{-1}[\tilde{\boldsymbol{i}}_{\boldsymbol{x}}] \\ & - \big[[Y]+j[B_{1_d}]\big]^{-1}[Y]\big[[\tilde{\boldsymbol{e}}_{\boldsymbol{n_{ohmic}}}] + [\tilde{\boldsymbol{e}}_{\boldsymbol{n_{ext}}}]\big] \\ =& \big[[Y]+j[B_{1_d}]\big]^{-1}\big[[I]-[y_{in_{a_d}}][T_z{}']\big][\tilde{\boldsymbol{i}}_{\boldsymbol{x}}] - \big[[Y]+j[B_{1_d}]\big]^{-1}\big[[Y]+[y_{in_{a_d}}][T_s{}']\big] \\ & \big[[\tilde{\boldsymbol{e}}_{\boldsymbol{n_{ohmic}}}] + [\tilde{\boldsymbol{e}}_{\boldsymbol{n_{ext}}}]\big] \\ =& [T_z][\tilde{\boldsymbol{i}}_{\boldsymbol{x}}] + [T_s]\big[[\tilde{\boldsymbol{e}}_{\boldsymbol{n_{ohmic}}}] + [\tilde{\boldsymbol{e}}_{\boldsymbol{n_{ext}}}]\big]\end{aligned} \tag{B.15}$$

Single-Series Stub Matching Network The circuit diagram for the receiver model if a Single-Series matching network is used is shown in figure B.3.

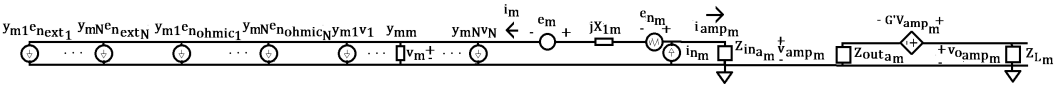

Figure B.3: Channel m of receiver with noisy source and Single-Series match

The auxiliary equations for the Single-Series case to determine the noise voltage at the post matching node are as shown in equations B.16, with jX_{1_m} the reactance of the series stub and jB_{1_m} its corresponding susceptances.

$$i_{n_m} = i_{n_m} - Y_{in_{a_m}} e_{n_m} - Y_{in_{a_m}} v_{n_m}{}' \tag{B.16a}$$

$$= \sum_{k=1}^{N} y_{mk}(v_{n_k} + e_{n_{ohmic_k}} + e_{n_{ext_k}}) \tag{B.16b}$$

$$v_{n_m}{}' = v_{amp_{n_m}} - e_{n_m} \tag{B.16c}$$

$$v_{n_m} = V_{n_m}{}' - jX_{1_m} i_{n_m} \tag{B.16d}$$

The auxiliary equations can be rewritten into matrix form and manipulated to solve simultaneously the noise voltages.

$$\begin{aligned}[\tilde{\boldsymbol{v}}_{\boldsymbol{n}}{}'] &= \Big[[Y]\big[j[X_{1_d}][Y_{in_{a_d}}] + [I]\big] + [Y_{in_{a_d}}]\Big]^{-1}\Big[[I] + j[Y][X_{1_d}]\Big][\boldsymbol{i_n} - \tilde{\boldsymbol{y}}_{\boldsymbol{in_a}}\boldsymbol{e_n}] \\ &\quad - \Big[[Y]\big[j[X_{1_d}][Y_{in_{a_d}}] + [I]\big] + [Y_{in_{a_d}}]\Big]^{-1}[Y]\big[[\tilde{\boldsymbol{e}}_{\boldsymbol{n_{ohmic}}}] + [\tilde{\boldsymbol{e}}_{\boldsymbol{n_{ext}}}]\big] \\ &= [T_z{}'][\tilde{\boldsymbol{i}}_{\boldsymbol{x}}] + [T_s{}']\big[[\tilde{\boldsymbol{e}}_{\boldsymbol{n_{ohmic}}}] + [\tilde{\boldsymbol{e}}_{\boldsymbol{n_{ext}}}]\big]\end{aligned} \tag{B.17}$$

The noise correlation matrix can be determined according to equation 3.19, substituting $[T_z{}']$ and $[T_s{}']$ for $[T_z]$ and $[T_s]$. The noise voltages at the source ports are given by

$$\begin{aligned}[\tilde{\boldsymbol{v}}_{\boldsymbol{n}}] &= -[Z][Y_{in_{a_d}}][\tilde{\boldsymbol{v}}_{\boldsymbol{n}}{}'] + [Z][\tilde{\boldsymbol{i}}_{\boldsymbol{x}}] - \big[[\tilde{\boldsymbol{e}}_{\boldsymbol{n_{ohmic}}}] + [\tilde{\boldsymbol{e}}_{\boldsymbol{n_{ext}}}]\big] \\ &= [Z]\big[[I] - [Y_{in_{a_d}}][T_z{}']\big][\tilde{\boldsymbol{i}}_{\boldsymbol{x}}] - \Big[[Z][Y_{in_{a_d}}][T_s{}'] + [I]\Big]\big[[\tilde{\boldsymbol{e}}_{\boldsymbol{n_{ohmic}}}] + [\tilde{\boldsymbol{e}}_{\boldsymbol{n_{ext}}}]\big] \\ &= [T_z][\tilde{\boldsymbol{i}}_{\boldsymbol{x}}] + [T_s]\big[[\tilde{\boldsymbol{e}}_{\boldsymbol{n_{ohmic}}}] + [\tilde{\boldsymbol{e}}_{\boldsymbol{n_{ext}}}]\big]\end{aligned} \tag{B.18}$$

Appendix C

Example of Recursive Averaging to Illustrate Workings and Properties of Algorithm

Let A be the unsorted set of $N = 7$ complex impedances

$$A = [a_1, a_2, a_3, a_4, a_5, a_6, a_7]$$

The possible values that the level of the recursive averaging can take are then given by

$$L_{rec} \in [0, 1, 2, 3]$$

After sorting A in ascending order, let us assume that the sorted set B is given by

$$B = [a_2, a_7, a_1, a_4, a_3, a_5, a_6]$$

For each value that L_{rec} can take, with the set not being resorted between recursive levels, the recursive average impedance can then be calculated as follows:

$L_{rec} = 0$:

$$A_{avg_{recursive}} = \frac{a_1 + a_2 + a_3 + a_4 + a_5 + a_6 + a_7}{7}$$

$L_{rec} = 1$:

$$B' = \left[\frac{a_2 + a_6}{2}, \frac{a_5 + a_7}{2}, \frac{a_1 + a_3}{2}, a_4\right]$$

$$\begin{aligned} A_{avg_{recursive}} &= \frac{1}{4}\sum_{n=1}^{4} b'_n \\ &= \frac{a_1 + a_2 + a_3 + a_5 + a_6 + a_7}{8} + \frac{a_4}{4} \end{aligned}$$

$L_{rec} = 2$:

$$B'' = \left[\frac{\frac{a_2+a_6}{2} + a_4}{2}, \frac{\frac{a_5+a_7}{2} + \frac{a_1+a_3}{2}}{2}\right]$$

$$\begin{aligned} A_{avg_{recursive}} &= \frac{1}{2}\sum_{n=1}^{2} b''_n \\ &= \frac{a_1 + a_2 + a_3 + a_5 + a_6 + a_7}{8} + \frac{a_4}{4} \end{aligned}$$

$L_{rec} = 3$:

$$B''' = \left[\frac{a_1 + a_2 + a_3 + a_5 + a_6 + a_7}{8} + \frac{a_4}{4}\right]$$

$$\begin{aligned} A_{avg_{recursive}} &= \frac{1}{1}\sum_{n=1}^{1} b'''_n \\ &= \frac{a_1 + a_2 + a_3 + a_5 + a_6 + a_7}{8} + \frac{a_4}{4} \end{aligned}$$

Appendix D

Proof of Total Active Reflection Coefficient Magnitude

Let the total active reflection coefficient of an N-port array, [50], be defined as

$$\Gamma_{act_{tot}} = \sqrt{\frac{\sum_{i=1}^{N} |b_i|^2}{\sum_{i=1}^{N} |a_i|^2}} \tag{D.1}$$

Where $[\tilde{\boldsymbol{b}}] = [S][\tilde{\boldsymbol{a}}]$. The total active reflection coefficient relates the total power going into each port of the multiport array with the power reflected out of each port. The total active reflection coefficient is a real number between 0 and 1, corresponding to no reflected power at 0 and total reflected power at 1. Using $b_m = \sum_{i=1}^{N} s_{mi} a_i$, it can then be seen that

$$\begin{aligned} |\Gamma_{act_{tot}}|^2 &= \frac{\sum_{m=1}^{N} |b_m|^2}{\sum_{k=1}^{N} |a_k|^2} \\ &= \frac{\sum_{m=1}^{N} \left| \sum_{i=1}^{N} s_{mi} a_i \right|^2}{\sum_{k=1}^{N} |a_k|^2} \end{aligned}$$

Using the Cauchy-Schwarz inequality, [51], the numerator can then be rewritten and the equality becomes an inequality.

$$
\begin{aligned}
|\Gamma_{act_{tot}}|^2 &\leq \frac{\sum_{m=1}^{N}\left(\sum_{n=1}^{N}|s_{mn}|^2\sum_{k=1}^{N}|a_k|^2\right)}{\sum_{k=1}^{N}|a_k|^2} \\
&\leq \frac{\sum_{k=1}^{N}|a_k|^2\left(\sum_{m=1}^{N}\sum_{n=1}^{N}|s_{mn}|^2\right)}{\sum_{k=1}^{N}|a_k|^2} \\
&\leq \sum_{m=1}^{N}\sum_{n=1}^{N}|s_{mn}|^2 \qquad \text{(D.2)}
\end{aligned}
$$

For a lossless, reciprocal system, $s_{mn} = s_{nm}^*$ so that the passivity condition $[I] - [S][S]^\dagger = 0$ becomes

$$\sum_{n=1}^{N}|s_{mn}|^2 = 1$$

Substituting into equation D.2 then leads to the form

$$|\Gamma_{act_{tot}}|^2 \leq N \qquad \text{(D.3)}$$

Appendix E

Maximum and Minimum Output SNR per Criteria Plots

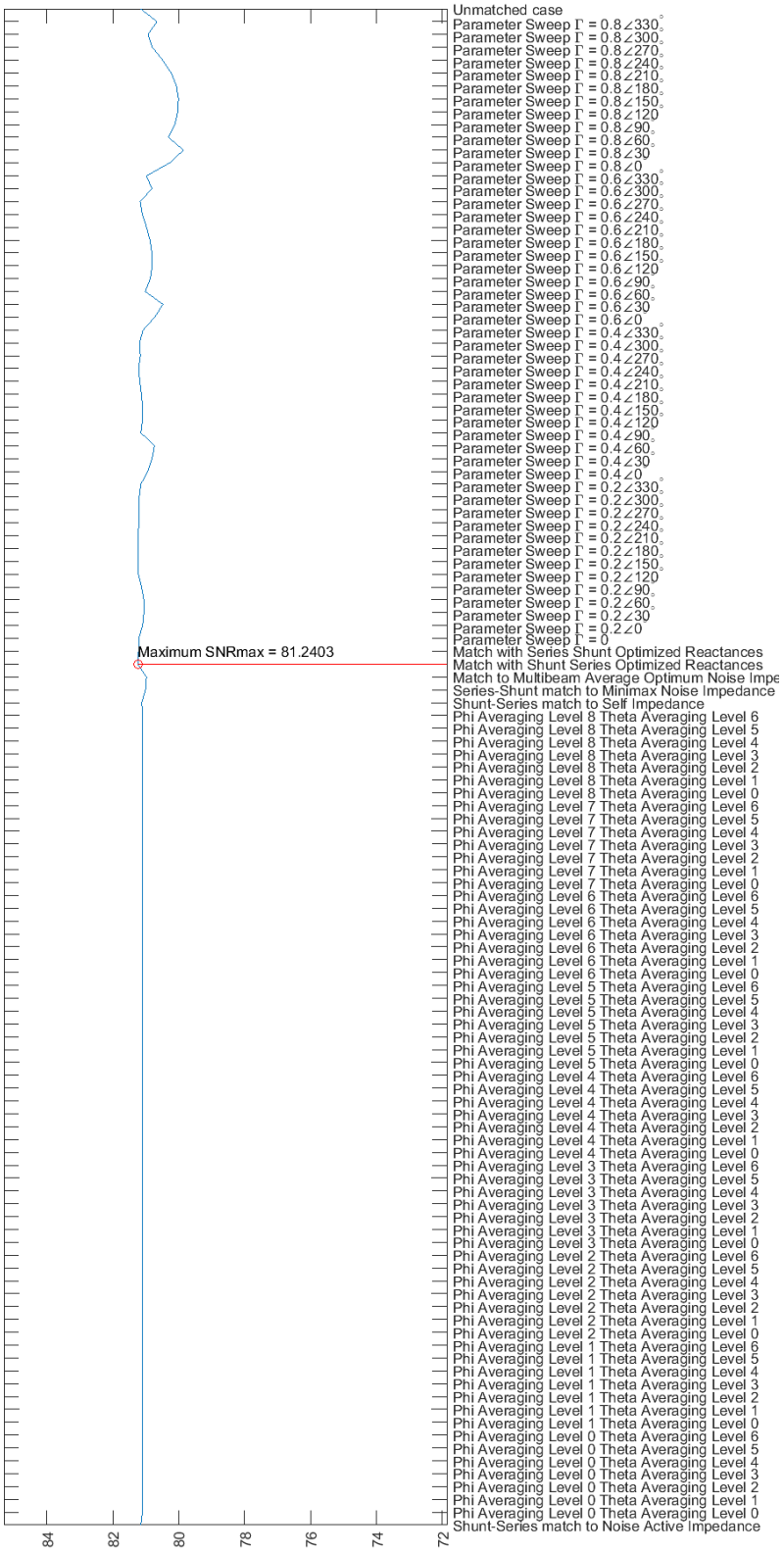

Figure E.1: QMA $SNR_{o_{max}}$ for each matching criteria

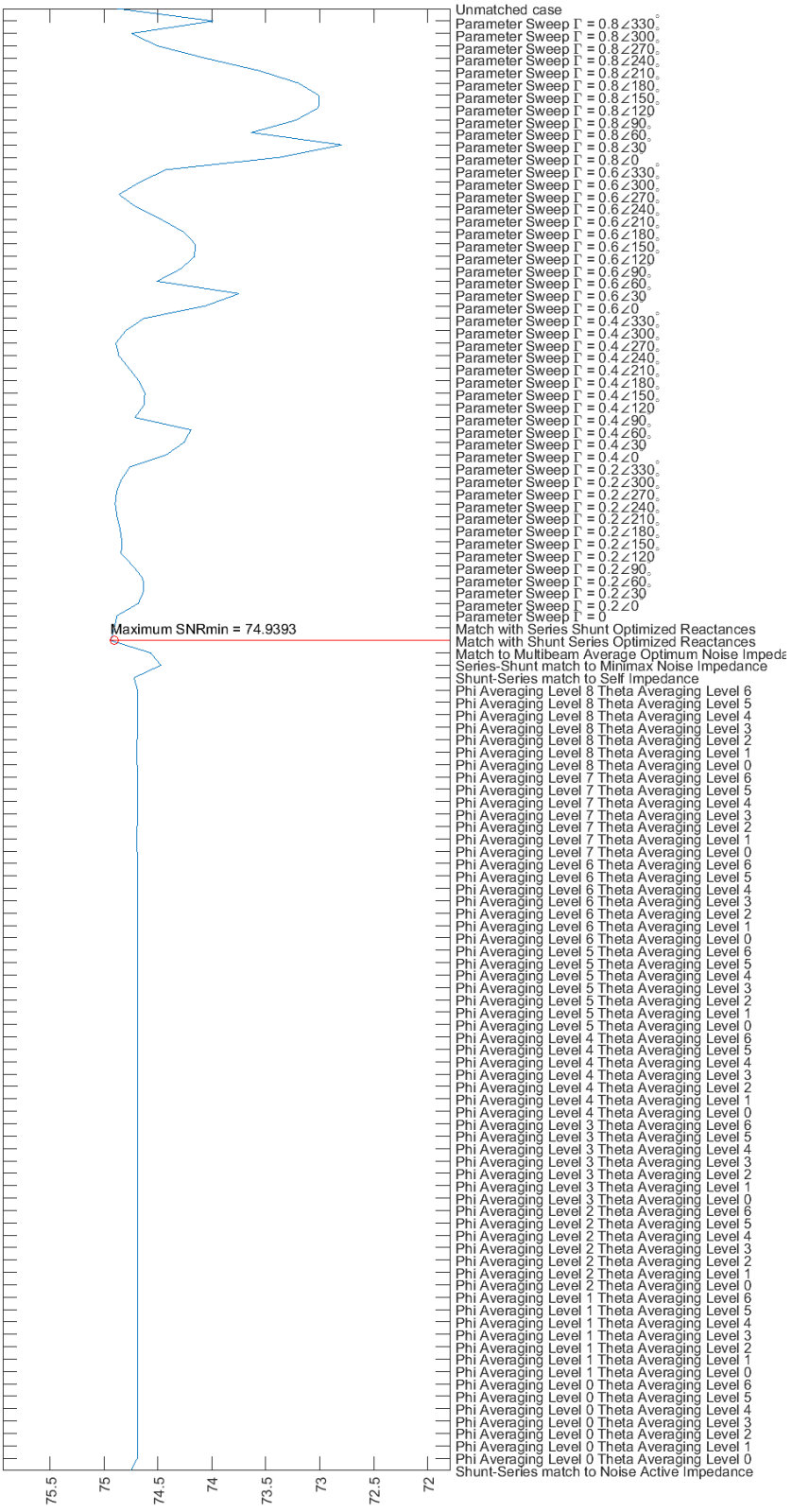

Figure E.2: QMA $SNR_{o_{min}}$ for each matching criteria

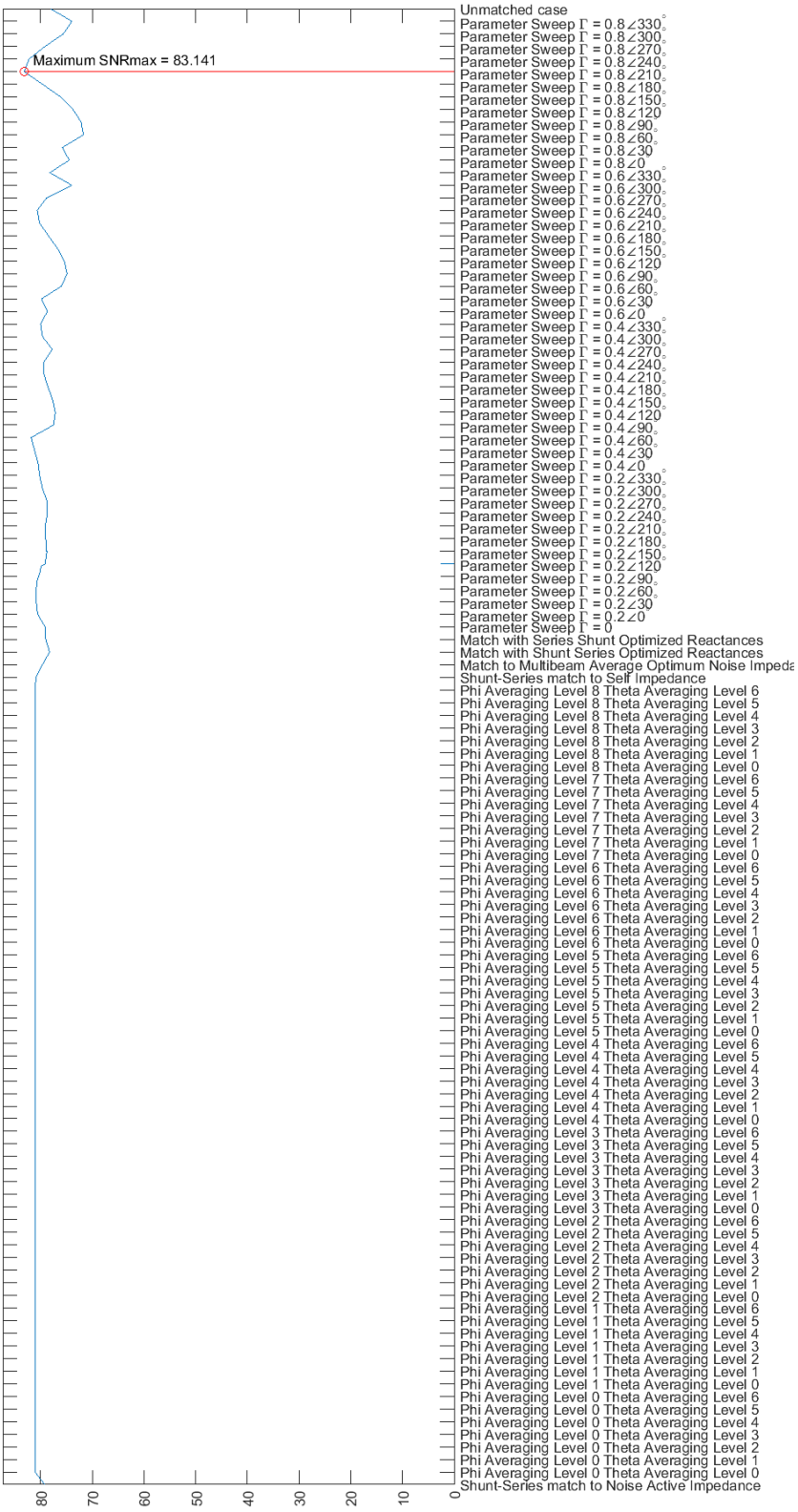

Figure E.3: FMA $SNR_{o_{max}}$ for each matching criteria

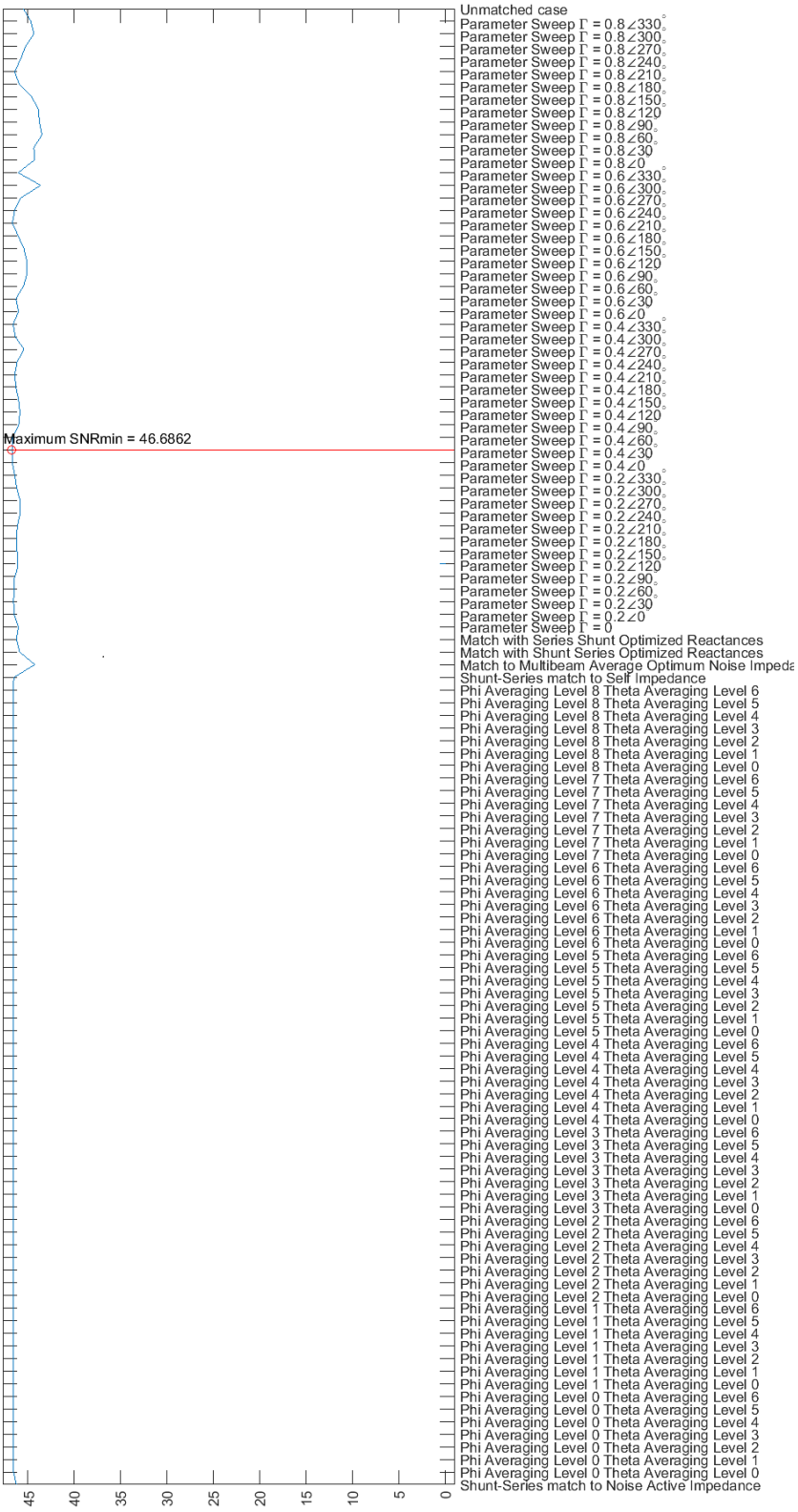

Figure E.4: FMA $SNR_{o_{min}}$ for each matching criteria

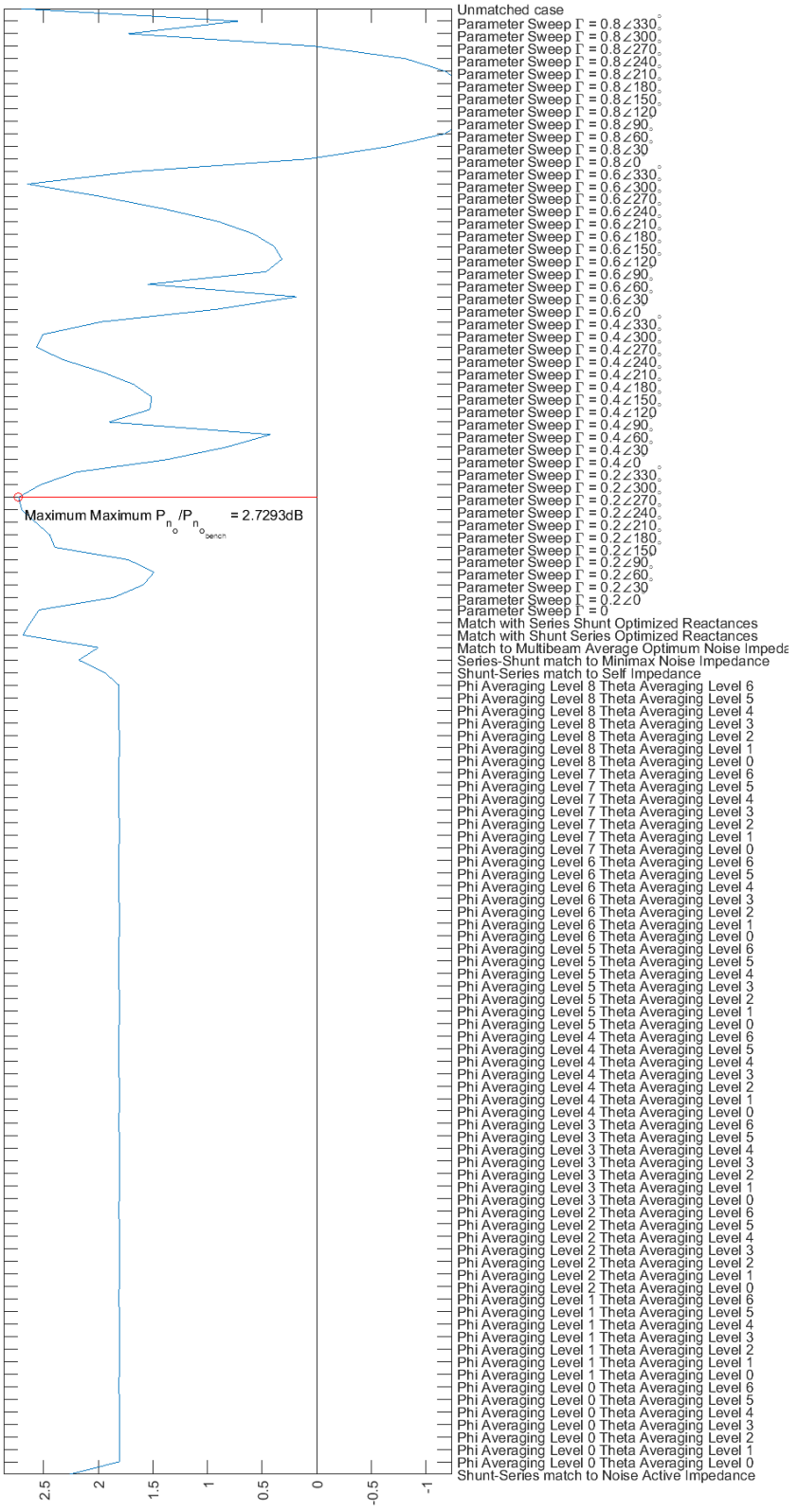

Figure E.5: QMA maximum $\frac{P_{no}}{P_{no_{benchmark}}}$ for each matching criteria

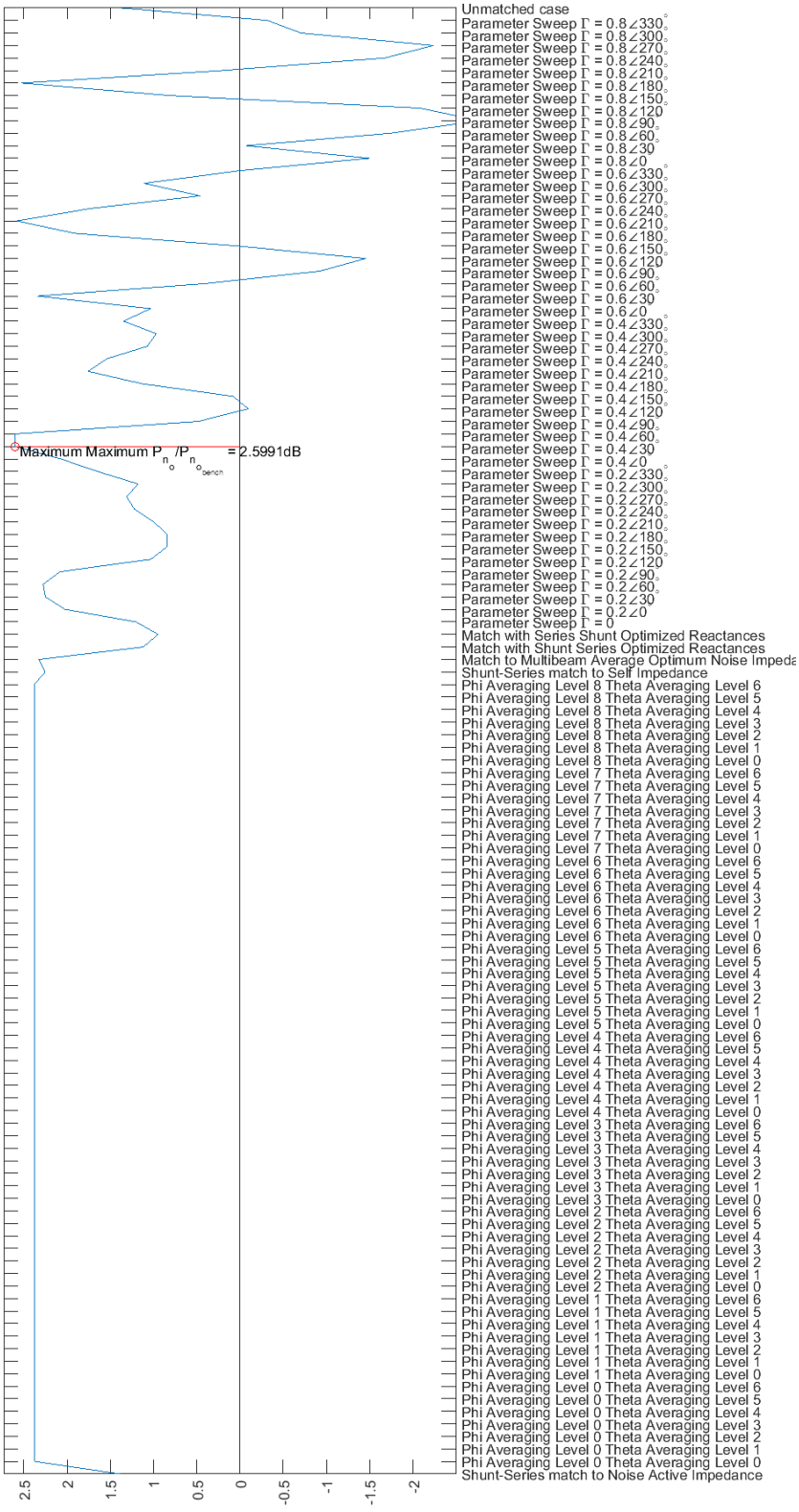

Figure E.6: FMA maximum $\frac{P_{no}}{P_{no_{benchmark}}}$ for each matching criteria

List of References

[1] Dehghanian, V. and Nielsen, J.: On the capacity of densely packed arrays with mutual coupling. *International Journal of Antennas and Propagation*, vol. 2015, 2015.

[2] Krusevac, S.M., Kennedy, R.A. and Rapajic, P.B.: Effects of signal and noise mutual coupling on mimo channel capacity. *Wireless Personal Communications*, vol. 40, pp. 317–328, 2006.

[3] Pozar, D.M.: The active element pattern. *IEEE Transactions on Antennas and Propagation*, vol. 42, no. 8, pp. 1176–1178, August 1994.

[4] Wallace, J.W. and Jensen, M.A.: Mutual coupling in mimo wireless systems: A rigorous network theory analysis. *IEEE Transactions on Wireless Communications*, vol. 3, no. 4, pp. 1317–1325, July 2004.

[5] Morris, M.L. and Jensen, M.A.: Network model for mimo systems with coupled antennas and noisy amplifiers. *IEEE Transactions on Antennas and Propagation*, vol. 53, no. 1, pp. 545–552, January 2005.

[6] Straumann, T. and Mönich, G.: Effects of mutual antenna coupling on sair performance. In: *Antennas and Propagation, 1993, Eighth International Conference on*, vol. 1, pp. 532–535. IET, 1993. ISBN 0-85296-572-9.

[7] Preston Geren, W. and Curry, C.R.: A practical technique for designing multiport coupling networks. *IEEE Transactions on Microwave Theory and Techniques*, vol. 44, no. 3, pp. 364–371, March 1996.

[8] Dossche, S., Blanch, S. and Romeu, J.: Three different ways to decorrelate closely spaced monopoles for mimo applications. In: *IEEE/ACES International Conference on Wireless Comumunications and Applied Computational Electromagnetics, 2005*, pp. 849–852. IEEE, 2005. ISBN 0-7803-9068-7.

[9] Moura, L., Monteiro, P.P. and Darwazeh, I.: Generalized noise analysis technique for four-port linear networks. *IEEE Transactions on Circuits and Systems - I: Regular Papers*, vol. 52, no. 3, pp. 631–640, March 2005.

[10] Beng, Y.C.: *Effects of Mutual Coupling in Small Dipole Array Antennas*. Master's thesis, Naval Postgraduate School, Monterey, California, March 2002.

[11] Haus, H.A. and Adler, R.B.: *Circuit Theory of Linear Noisy Networks*. New York: Wiley, New York, May 1959. ISBN 9780-2625-8232-2.

[12] Wedge, S.W.: Wave techniques for noise modeling and measurement. *IEEE Transactions on Microwave Theory and Techniques*, vol. 40, no. 11, pp. 2004–2012, November 1992.

[13] Randa, J.: Noise characterization of multiport amplifiers. *IEEE Transactions on Microwave Theory and Techniques*, vol. 49, no. 10, pp. 1757–1763, October 2001.

[14] Weem, J.P. and Popović, Z.: A method for determining noise coupling in a phased array antenna. In: *Microwave Symposium Digest, 2001 IEEE MTT-S International*, vol. 1, pp. 271–274. IEEE, May 2001. ISBN 0-7803-6538-0.

[15] Warnick, K.F. and Jensen, M.A.: Effects of mutual coupling on interference mitigation with a focal plane array. *IEEE Transactions on Antennas and Propagation*, vol. 53, no. 8, pp. 2490–2498, August 2005.

[16] Warnick, K.F. and Jensen, M.A.: Optimal noise matching for mutually coupled arrays. *IEEE Transactions on Antennas and Propagation*, vol. 55, no. 6, pp. 1726–1731, June 2007.

[17] Maaskant, R. and Woestenburg, E.E.M.: Applying the active antenna impedance to achieve noise match in receiving array antennas. In: *2007 IEEE Antennas and Propagation Society International Symposium*, pp. 5889–5892. IEEE, 2007. ISBN 978-1-4244-0877-1.

[18] Warnick, K.F., Woestenburg, B., Belostotski, L. and Russer, P.: Minimizing the noise penalty due to mutual coupling for a receiving array. *IEEE Transactions on Antennas and Propagation*, vol. 57, no. 6, pp. 1634–1644, June 2009.

[19] Prinsloo, D.S.: *Multi-Mode Antennas for Hemispherical Field-of-View Coverage*. Ph.D. thesis, Electronic Engineering, University of Stellenbosch, Stellenbosch, South Africa, 2015.

[20] Prinsloo, D.S., Meyer, P., Maaskant, R. and Ivashina, M.: Quad-mode antenna for wide-scan sparse arrays. In: *IEEE AP-S Symposium on Antennas and Propagation and URSI CNC/USNC Joint Meeting*. July 2015.

[21] Ivashina, M., Redkina, E., Maaskant, R. and Prinsloo, D.S.: Capabilities and fundamental limitations of multi-mode antennas in an array environment. In: *The 10th European Conference on Antennas and Propagation*. Davos, Switzerland, April 2016.

[22] Dobrowolski, J.A.: Noise analysis of differential multiport networks - the wave approach. *International Journal of Electronics and Telecommunications*, vol. 60, no. 4, pp. 281–286, 2014.

[23] Dobrowolski, J.A.: Noise characterization of differential multi-element multiport networks - the wave approach. *International Journal of Electronics and Telecommunications*, vol. 61, no. 4, pp. 395–401, 2015.

[24] Vaezi, A., Abdipour, A., Mohammadi, A. and Ghannouchi, F.M.: On the modeling and compensation of backward crosstalk in mimo transmitters. *IEEE Microwave and Wireless Components Letters*, vol. 27, no. 9, pp. 842–844, September 2017.

[25] Hausmair, K., Landin, P.N., Gustavsson, U., Fager, C. and Eriksson, T.: Digital predistortion for multi-antenna transmitters affected by antenna crosstalk. *IEEE Transactions on Microwave Theory and Techniques*, vol. 66, no. 3, pp. 1524–1535, March 2018.

[26] da Silva, E.: *High Frequency and Microwave Engineering*. Elsevier Science, New York City, NY, 2001. ISBN 9780080508023.
Available at: `https://books.google.co.za/books?id=sY53KEhtTZEC`

[27] Fukui, H.: The noise performance of microwave transistors. *IEEE Transactions on Electron Devices*, vol. ED-13, no. 3, pp. 329–341, March 1966. ISSN 0018-9383.

[28] Krusevac, S., Rapajic, P.B., Kennedy, R.A. and Sadeghi, P.: Mutual coupling effect on thermal noise in multi-antenna wireless communication systems. In: *2005 Australian Communications Theory Workshop*, pp. 209–214. Feb 2005.

[29] Engberg, J. and Larsen, T.: *Noise Theory of Linear and Nonlinear Circuits*. Wiley, 1995. ISBN 047194825x.

[30] H. Singh, H. L. Sneha, R.M.J.: Mutual coupling in phased arrays: A review. *International Journal of Antennas and Propagation*, vol. 2013, 2013.

[31] Balanis, C.: *Antenna theory: Analysis and Design*. 3rd edn. Wiley, 1982. ISBN 9780471603528.

[32] Ivashina, M.V., Woestenburg, E.E.M. and Redkina, E.A.: Effects of the element separation on the noise performance of receiving antenna arrays. In: *International Conference on Antenna Theory and Techniques,*, pp. 82–86. IEEE, Sevastopol, Ukraine, 2007. ISBN 978-1-4244-1584-7.

[33] Van Trees, H.: *Optimum Array Processing: Part IV of Detection, Estimation, and Modulation Theory*. Wiley, 2004. ISBN 9780471463832.

[34] Warnick, K.F. and Jensen, M.A.: ECEn 665: Antennas and Propagation for Wireless Communications, February 2015. Course notes ECEn 665.
Available at: `https://ecen665web.groups.et.byu.net/index.html`

[35] Twiss, R.Q.: Nyquist's and Thevenin's Theorems Generalized for Nonreciprocal Linear Networks. *Journal of Applied Physics*, vol. 26, pp. 599–602, May 1955.

[36] Neamen, D.: *Microelectronics: Circuit Analysis and Design*. Connect learn succeed. McGraw-Hill, 2010. ISBN 9780071289474.

[37] Van Der Merwe, J.: *The Effect of Mutual Coupling on the Noise Performance of Large Antenna Arrays*. Master's thesis, Electrical and Electronic Engineering, University of Stellenbosch, Stellenbosch, South Africa, 2010.

[38] Filatrella, G., Pierro, V., Pedersen, N.F. and SÃ¸rensen, M.P.: Negative differential resistance due to nonlinearities in single and stacked josephson junctions. *IEEE Transactions on Applied Superconductivity*, vol. 24, no. 6, pp. 1–7, Dec 2014. ISSN 1051-8223.

[39] Li, T., Yu, Z., Wang, Y., Huang, L. and Xiang, C.: Numerical simulation of negative differential resistance characteristics in si/$Si_{1-x}ge_x$rtd at room temperature. In: *2005 IEEE Conference on Electron Devices and Solid-State Circuits*, pp. 409–412. Dec 2005.

[40] Lin, J.-C., Wang, S.-J., Liou, W.-R., Luo, Y.-C. and Cheng, C.-Y.: The study of negative differential resistance phenomenon in a two-step barrier diode. In: *ICSE '96. 1996 IEEE International Conference on Semiconductor Electronics. Proceedings*, pp. 140–143. Nov 1996.

[41] Chen, S., Griffin, P.B. and Plummer, J.D.: Negative differential resistance circuit design and memory applications. *IEEE Transactions on Electron Devices*, vol. 56, no. 4, pp. 634–640, April 2009. ISSN 0018-9383.

[42] Zhou, J., Han, G., Li, J., Liu, Y., Peng, Y., Zhang, J., Sun, Q., Zhang, D.W. and Hao, Y.: Negative differential resistance in negative capacitance fets. *IEEE Electron Device Letters*, vol. 39, no. 4, pp. 622–625, April 2018. ISSN 0741-3106.

[43] Jensen, M.A. and Lau, B.K.: Uncoupled matching for active and passive impedances of coupled arrays in mimo systems. *IEEE Transactions on Antennas and Propagation*, vol. 58, no. 10, pp. 3336–3343, Oct 2010. ISSN 0018-926X.

[44] Andersen, J. and Rasmussen, H.: Decoupling and descattering networks for antennas. *IEEE Transactions on Antennas and Propagation*, vol. 24, no. 6, pp. 841–846, November 1976. ISSN 0018-926X.

[45] Pozar, D.M.: *Microwave Engineering*. 4th edn. Wiley, Hoboken, NJ, 2012. ISBN 0470631554, 9780470631553.

[46] Meyer, P.: Multi-conductor transmission line analysis using the generalized multi-mode s-parameter transformation. In: *2015 IEEE 19th Workshop on Signal and Power Integrity (SPI)*, pp. 1–4. May 2015.

[47] Collin, R.: *Antennas and radiowave propagation*. McGraw-Hill series in electrical and computer engineering. McGraw-Hill Higher Education, 1985. ISBN 9780070118089.
Available at: `https://books.google.co.za/books?id=pgJTAAAAMAAJ`

[48] Lagarias, J., Reeds, J., Wright, M. and Wright, P.: Convergence properties of the nelder–mead simplex method in low dimensions. *SIAM Journal on Optimization*, vol. 9, no. 1, pp. 112–147, 1998.

[49] Wang, Z., Bovik, A.C., Sheikh, H.R. and Simoncelli, E.P.: Image quality assessment: from error visibility to structural similarity. *IEEE Transactions on Image Processing*, vol. 13, no. 4, pp. 600–612, April 2004. ISSN 1057-7149.

[50] Manteghi, M. and Rahmat-Samii, Y.: Broadband characterization of the total active reflection coefficient of multiport antennas. In: *IEEE Antennas and Propagation Society International Symposium. Digest. Held in conjunction with: USNC/CNC/URSI North American Radio Sci. Meeting (Cat. No.03CH37450)*, vol. 3, pp. 20–23 vol.3. June 2003.

[51] Tuo, L.: Generalizations of cauchy-schwarz inequality in unitary spaces. *Journal of Inequalities and Applications*, vol. 2015, no. 1, p. 201, June 2015. ISSN 1029-242X.